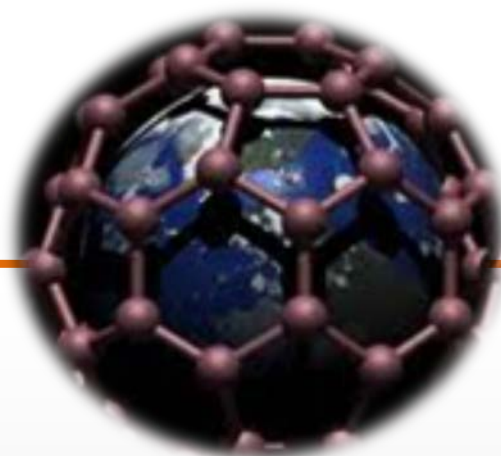
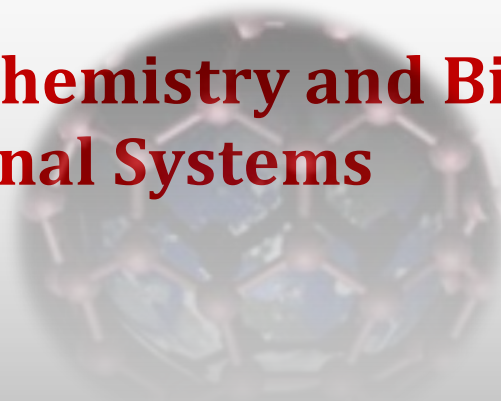




**JOURNAL OF LOW
DIMENSIONAL
SYSTEMS**



**Physics, Chemistry and Biology of Low
Dimensional Systems**



Aims and scope

The *Journal of Low Dimensional Systems* is co-edited by Baku State University.

It publishes papers and review articles on the fundamental and applied aspects of physics, chemistry and biology. General areas of interest are the electronic, spectroscopic and structural properties of low dimensional systems, including perfect and defect lattices, surfaces, two-dimensional electron systems, interfaces, thin films and multilayers, amorphous materials, micro- and nanostructures, and layered structures. Papers dealing with biomaterials for medical purposes are accepted.

Typical examples include the preparation and structural characterization of novel and advanced low dimensional materials, especially in relation to the measurement and interpretation of their electrical, magnetic, optical, thermal and mechanical properties, phase transitions, electronic structure and defect properties, and the application of appropriate experimental and theoretical techniques in these studies. Articles are encouraged in all the above areas, but especially those which emphasize fundamental aspects of materials science.

Address:

Az1148, Z.Khalilov str. 23,
Baku State University, BSU publication, Baku, Azerbaijan

E-mail: mhhuseyng@bsu.edu.az



Journal of LDS



Published by the Baku State University and devoted to original papers in experimental and theoretical physics, chemistry and biology

Editor in Chief:

academician Abel Maharramov (Baku State University, Azerbaijan)

Deputy Editors in chief:

prof. Aydin Kazimzade (Baku State University, Azerbaijan)

prof. Mahammadali Ramazanov (Baku State University, Azerbaijan)

prof. Olgun Güven (Hacettepe University, Turkey)

Editorial board:

prof. Ronald Caple (University of Minnesota, USA)

prof. Eden Mamut (Ovidius University of Constanza, Romania)

prof. Akiko Kimura (Hiroshima University, Japan)

prof. Angelo Chianese (Sapienza University of Rome, Italy)

prof. Zoltan Konya (Szeged University, Hungarian)

prof. Ktiszstian Kordas (Oulu University, Finland)

prof. Pulickel Ajayan (Rice University, USA)

prof. Hiroshi Yamamoto (Komatsu University, Japan)

prof. Irada Aliyeva (Baku State University, Azerbaijan)

academician Valeriy Lunin (Moscow State University, Russia)

prof. Rasit Turan (Middle East Technical University, Turkey)

prof. S. Ismat Shah (University of Delaware, USA)

prof. Mahammad Babanlı (Baku State University, Azerbaijan)

prof. Evgueni Chulkov (Donostia International Physics, Spain)

prof. Jean-Claude Tedenac (Universite Montpellier, France)

prof. Igor Yaminskiy (Moscow State University, Russia)

prof. Ralfrid Hasanov (Baku State University, Azerbaijan)

prof. Metin Balci (Middle East Technical University, Turkey)

prof. Adil Garibov (Nuclear Centre, Azerbaijan)

dr. Akos Kukevech (Szeged University, Hungarian)

dr. A. M. Panich (Ben-Gurion University of the Negev, Israel)

prof. Archil Chirakadze (Georgian Technical University, Georgia)

Executive editors:

prof. Huseyn Mamedov (Baku State University, Azerbaijan)

dr. Laman Abdullayeva (Institute for Physical Problems Baku State University, Azerbaijan)

Table of Contents

PHYSICAL SCIENCES

Definition refractive index of proton waves in the thin films	4
S.G. Abdulvahabova, N.Sh. Barkhalova, T.O. Bayramova	
Breast cancer therapy via chrysin loaded iron oxide nanoparticles.....	8
S. Huseynli, M.A.Ramazanov, D.Cimen	
Properties of ZnSTe:Cr nanocrystalline thin films.....	12
M.A. Jafarov, E.F. Nasirov, I.S.Hasanov, H.M. Mamedov, Syed I. Shah, E.A.Khanmaedova	
Dielectric-conductor transition in a mixture of zeolite and graphite powders.....	16
G.M. Eyvazova, V.I. Orbukh, N.N. Lebedeva	

CHEMICAL SCIENCES

Racemic and enantioselective diels-alldercycloaddition of 2,4-pentadienol to diethyldiazodicarboxylate.....	21
F.N.Axundova, M.J.Alves, M.M.Kurbanova	
Synthesis of dihalogendiazadiene and farmazan derivatives in the catalytic olefinization reaction.....	24
N.G.Shikhaliyev, G.T.Suleymanova, Kh.N.Bagirova, U.F.Asgerova, Kh.A.Garazadeh, G.V.Babayeva, N.E.Ahmedova, V.G.Nenajdenko	
New three-component condensation in the presence of benzylidene acetophenones.....	30
A.I. Ismiyev, K.E. Hajiyeva	

BIOLOGICAL (ECOLOGICAL) SCIENCES

Construction of the pharmacophore models of biologically active molecules based on a theoretical approach.....	34
G.Akverdieva, N.M.Godjajev	
Transfer of nanoparticles in a simplified aquatic food chain: from water plant elodea canadensis to molluscs lymnaea auricularia.....	41
I.S.Ahmadov, E.K.Gasimov, N.A. Sadiqova, N. J. Agayeva, F.H.Rzayev, A.A. Manafov	
Influence of additives organic and mineral substances on nitrification ability grey forest soilsof acinohur cadastre region.....	46
K.A.Huseynov	
Appraisal mapping soil cover of the region.....	52
K.A.Rahimova, G.A.Huseynova	
Improving the photocatalytic activity of different modification of TiO ₂	57
S.A.Hasanova	

DEFINITION REFRACTIVE INDEX OF PROTON WAVES IN THE THIN FILMS

S.G. ABDULVAHABOVA*, N.Sh. BARKHALOVA, T.O. BAYRAMOVA

Faculty of Physics, Baku State University, Az1148, Z.Khalilov str., 23, Baku, Azerbaijan

The refractive index for scattering proton on the density of fluctuations of the thin films is obtained in the framework of the quantum theory of multiple scattering in the quasielastic approximation. The formulas have been obtained under the assumption that the optical potential is nonlocal operator. It was determined that the scattering does not contribute to the attenuation of the coherent proton wave. The results are shown, that if the wavelength of the incident particles becomes much greater than the thickness d of the target and the total cross section for scattering by the complete target becomes universal and does not depend on cross section for scattering by one nucleus. The discussion applies to the case where there is only one isotope of the element. Studies the analytic properties of the scattering amplitude allow to translate the results of the axiomatic study of scattering by a simple physical language.

PACS numbers: 25.40-Ep

Key words: cross section, multiple scattering, proton wave, thin films, refractive index.

*E-mail: sajida.gafar@gmail.com

1. INTRODUCTION

Details of the interaction between fast particles and nucleus in "distant" collisions, when the impact parameter approximately $1f$, are of considerable interest in the physics of passage of particles through solids. Information on the nature of the nuclear field at these relative large distances can be obtained by investigating the scattering of particles in very thin films through small angles. A convenient projectile for this purpose is the proton, because the probability of it capturing electrons is negligible.

Protons interact with matter differently than X-rays. A major difference with X-rays is that the scattering is mostly due to the nuclei of the atoms. That means that there is no need for an atomic form factor to describe the shape of the electron cloud of the atom and the scattering power of an atom does not fall off with the scattering angle as it does for X-rays.

When protons interact with matter, two basic kinds of interaction can be distinguished, which are normally designated as elastic and inelastic. We refer to elastic interactions when the collision leads to essentially zero energy transfer and the protons are only deflected in the field of the nuclei. As protons possess wave properties, a phase relationship exists between incident and scattered beams, and interference may occur between the scattered protons.

In a crystalline substance atoms are arranged in an orderly manner in space. Proton waves add up the point of observation in accordance with the laws of interference if the phase difference between the scattered waves is constant (coherent scattering), we can observe the pattern of alternating in the space diffraction minima and maxima. If the order in the arrangement of atoms is broken, scattering will not be coherent.

At this work the interaction potential is nonlocal. Nonlocal potential allows obtaining clear and closed-form analytical expressions for the scattering amplitude.

2. PASSAGE OF THE PROTONS THROUGH THIN FILMS

Let a stationary flux of protons be incident on target thin films. Our problem is to find the cross section and refractive index. We shall use the method of multiple scattering.

In fact collisional processes are described quantitatively in terms of cross sections and to study them one need the quantum mechanics. One can distinguish between elastic and no elastic collisions depending on whether or not translational momentum and energy are conserved. Among the many processes of the interaction of protons with nuclei, which occur multiple scattering effects most important is the elastic scattering.

Refractive indices for proton is close to unity and difficult to measure its. If the plate has a thickness d and

refractive index n the proton wave undergoes a phase shift and exits in the form of

$$\Psi_k(z > d) = e^{ik(z-d) + nkd} \quad (1)$$

here k momentum of proton after scattering.

Now suppose that the plate substance contains of N localized impurity - scatters and these centres scatters spherically symmetric wave with the scattering length a_l [1]

$$a_l = \frac{1}{kctg\delta_l} = \begin{cases} (\delta_l - \pi)/k & \text{for } |\delta_l - \pi| \ll 1, \\ \delta_l/k & \text{for } |\delta_l| \ll 1, \end{cases} \quad (2)$$

where δ_l scattering phase.

Then, for the $z > d$ the wave can be expressed as

$$\Psi_k(z > d) = e^{ikz} - 2\pi a_l N d \frac{e^{ikz}}{k^2} \quad (3)$$

If (1) submit in the form

$$\Psi_k(z > d) \approx e^{ikz} [1 + ik(n-1)d] \quad (4)$$

and compare with (3), we obtain

$$n - 1 = -2\pi a_l N \frac{1}{k^2} \quad (5)$$

Now suppose that there are two different types of randomly distributed scattering centres scattering lengths a_1 and a_2 . Let there be a first type centres N_1 and N_2 - the second type, with the relative concentrations. In such an analysis the relation (1) should be replaced by

$$|\Psi_k|^2 = b^2 \left| a_1 \sum_{i=1}^{N_1} \frac{\exp[ik(z_i + d_i)]}{d_i} + a_2 \sum_{i=1}^{N_2} \frac{\exp[ik(z_i + d_i)]}{d_i} \right|^2 \quad (6)$$

When disclosed the square of the ratio (6), the sums of the squares of each contribute to the coherent and incoherent parts, while the mixed terms contribute only to the coherent strength.

For slow particles, when the wavelength is much greater than the separation a between centers, it is possible to go over in Eqs. (6) from a sum over centers to integration over the coordinates. The integral can be easily calculated using the coefficient convergence $\exp(-kr)$ ($k > 0$)

$$\int_z^\infty e^{ikr} dr = \lim_{\omega \rightarrow 0} \int_z^\infty e^{(ik-\omega)r} dr = -\frac{e^{ikz}}{ik}, \quad (7)$$

After solving the Schrödinger equation and Fourier transform in some great period T we obtain the amplitude [2]

$$f(r, \omega') = \frac{i}{T} \left(\frac{m}{2\pi\hbar} \right)^{1/2} \int_0^\infty \frac{dt}{t^{3/2}} \int dt_0 e^{-i\omega t_0} e^{i\omega' t} \times \sum_n d_n \int dr \delta[r - r_n] \quad (8)$$

Where $\hbar\omega'$ - the proton energy after scattering, r_n - the distance from the centre to the point where there is the proton wave.

In this section we recall the main steps of the quantum collision theory in the case of two elastic interacting particles. The corresponding section is associated with this amplitude follows. The number of protons passing through the area $r'd\Omega$, there is the ratio incident flux to the scattered flux. Then double differential scattering cross section is equal to

$$\frac{d^2\sigma}{d\Omega dE} = \frac{v}{v_0} \cdot \frac{1}{2\pi\hbar} \int d\tau e^{-i\omega\tau} \sum_{i,j} d_i d_j e^{iq(r_i - r_j)}, \quad (9)$$

where $\tau = t - t_0$, $\omega = \omega_0 - \omega'$, v velocity proton after scattering, v_0 initial velocity of proton and $q = k_0 - k$.

The discussion applies to the case where there is only one isotope of the element. In those cases where the proton wavelength is large compared to the size of the impurity following model can be used [3]

$$\delta\eta(r) = \sum_{i=1}^N \delta\eta_0(r - R_i), \quad (10)$$

where $\delta\eta$ - random density fluctuations, R_i the radius vector of the centre of gravity of i impurity, and $\delta\eta_0$ describes the action of one of the scattering centre.

Proton scattering wave can be taken into account by choosing the real part of the optical potential in the form of:

$$\delta U_R = (2\pi\hbar^2 / \mu) \langle \delta\eta \rangle \text{Re} f(0). \quad (11)$$

Here brackets $\langle \dots \rangle$ denote averaging over the distribution of static states of the scattering system. Averaging over configurations of the scattering nuclei, ie, at the equilibrium position is an independent operation only in case of the crystal.

Similar to (11), can select the imaginary part of the optical potential

$$\delta U_I = (2\pi\hbar^2 / \mu) \langle \delta\eta \rangle \text{Im} f(0). \quad (12)$$

The imaginary part of the potential is models the inelastic processes related to elastic scattering and determines the weakening of the coherent wave in the entrance channel. In general, optical potential is nonlocal and depends of proton's energy. For proton the dependence of energy and no localness of the optical potential is very little effect on the propagation of a proton wave in the thin films.

According to the optical theorem

$$\text{Im } f(0) = -k(\sigma_{abs} + \sigma_{inel})/4\pi \quad (13)$$

where

$$\sigma_{abs.} = NV \left\langle (\delta\eta_0)^2 \right\rangle, \quad (14)$$

$$\sigma_{inel.} = N\sigma_{el.} NV \langle (\delta\eta)^2 \rangle, \quad (15)$$

σ_{abs} cross section of absorption and σ_{inel} cross section of inelastic scattering. Elastic scattering related unitarily condition with all inelastic processes. Since the cross section of inelastic scattering in the approximation of a heavy target is proportional to the cross section of elastic scattering [4].

Elastic scattering cross section is equal to

$$\sigma_{el.}(k) = \int |f(k, \theta)|^2 d\Omega, \quad (16)$$

and expression (17) can be represented as a series expansion in the multiplicity of elastic scattering

$$\begin{aligned} \sigma_{el.}(k) = & N_1 \int |f(k, \theta)|^2 d\Omega + \\ & + \frac{N_2}{k^2} \int dk' |f(k')f(k-k')|^2 d\Omega + \dots \end{aligned} \quad (17)$$

where

$$N_i = \frac{1}{\sigma_i!} \int \exp(-\sigma_i \delta\eta r)^i dr, \quad (18)$$

here σ_i a total scattering cross section, related to the scattering center:

$$\sigma_i = 4\pi \frac{V}{V_0} \left\langle \left(\frac{\delta\eta}{\eta_0} \right)^2 \right\rangle, \quad (19)$$

where V_0 - the volume per one scattering nucleus, and i - the number of scattering nuclei per unit volume of the crystal.

If the scattering is not spherically symmetric, which corresponds to the amplitude $f(\theta)$, we obtain [5]:

$$n - 1 = -2\pi N \frac{1}{k^2} f(0), \quad (20)$$

where $f(0)$ forward scattering amplitude because the refractive index describes the propagation of proton waves in the forward direction. If the refractive index contains an imaginary part, it is necessary to divided (21) into two parts: real and imaginary:

$$\begin{aligned} \text{Re}(n - 1) = & -2\pi N \frac{1}{k^2} \text{Re } f_x(0) \\ \text{Re}(n - 1) = & \frac{2\pi N}{k^2} \text{Re } f_x(0) \end{aligned}, \quad (21)$$

Imaginary part of the refractive index determined by the condition of the decreasing the particle in the channel of elastic scattering.

Determining the effective cross section by the optical theorem for the imaginary part of the refractive index obtain the following expression

$$\text{Im } n = \frac{2\pi N^2}{k} \left\langle \left(\frac{\delta\eta}{\eta_0} \right)^2 \right\rangle \quad (22)$$

At $kf_k(0) \ll 1$ the imaginary part of the scattering amplitude is small and the refractive index can be considered real. Thus, in this case, scattering in density fluctuations does not contribute to the attenuation of the coherent proton wave. If the wavelength is much larger than the thickness of the film, then the amplitude is a constant and the difference of the angular dependence of n from that in the case of rigidly fixed nuclei is determined by the form factor.

3. CONCLUSION

These formulas have been obtained under the assumption that the optical potential is a non-local operator. The effective potential was conceived as a straightforward generalization of the theory of two-particle interaction potential in the relativistic case, the existence of inelastic processes. The application range of the effective potential for non-relativistic case shows that it is not only a good method of accounting for kinematic features of scattering, but also allows entering a theoretical approach the dynamics of interaction. If do not resort to this hypothesis, have to deal with the time-consuming calculation of the sum of the vectors of the crystal lattice.

The mechanism of these processes is of interest in connection with existing concepts of the surface bond. Transfer of much smaller energies to the adsorbate can lead to vibrational excitation. If the energy transferred in the inelastic collision is high enough to excitation low-lying levels of the nuclei, radiation less reordering of the nucleon configuration can occur subsequently. The scattering protons of characteristic energy emitted in these processes can be used for qualitative analysis of the levels. The above discussion applies to the case where there is only one isotope of one element present (especially an element with zero nuclear spin), however practically all real systems will have a distribution of both elements and isotopes of those elements.

Moreover for protons due to the shallow depth of penetration into the wall of the crystal must carefully consider the effect of the surface structure. The crystal

surface is two-dimensional defect, distorting the frequency spectrum of vibrations of atoms located in the surface layer of the lattice.

The results are shown also, that if the wavelength of the incident particles becomes much greater than the thickness d of the target and the total cross section for scattering by the complete target becomes universal and does not depend on cross section for scattering by one nucleus.

It was the aim of this paper to show that the specific processes brought about by scattering of the proton wave by the density fluctuation of the nuclear are well suited for the investigation of nuclei. The characteristics of the interaction depend on the parameters of the nucleus, it may be expected that a better understanding of these processes will improve our theoretical concepts of the physical entities "density fluctuation of the nuclear". An indirect confirmation of this conclusion may be provided by experiments on the determination

of the coefficient of transmission of protons through films. The exact experimental definition of the fluctuation the nuclear density is a very important prerequisite.

4. REFERENCES

1. Calogero F. Variable phase approach to potential scattering. Academic Press, New York and London, 1967, p. 292.
2. Abdulvahobova S.G., Barkhalova N. Sh, Bayramova T.O./ BSU news, Physics series, 2015, N1, p.150-156.
3. Stepanov A.V. /PEPA, 1996, v.7, N.4, p. 989-993.
4. Gurevich A. I. and Lomonosov V. V. / JETP, 1996, v.82, N3, p. 493-496.
5. Abdulvahobova S. G., Masti D./ Russian Journal, Physics, 2008, v.11, p.235-239

BREAST CANCER THERAPY VIA CHRYSINLOADED IRON OXIDE NANOPARTICLES

S. HUSEYNLI^{1*}, M.A.RAMAZANOV¹, D.CIMEN²

¹Baku State University, Z. Khalilov Street 23, Baku AZ1148, Azerbaijan

²Hacettepe University, Department of chemistry, Ankara, Turkey

In the field of biomedical applications of magnetic nanoparticles it has been recently increasingly widespread. Magnetic nanoparticles (MNP) have attracted much attention due to their unique physical properties, magnetic susceptibility, biocompatibility and stability. In this study, controlled synthesis and characterization of chrysin loaded biocompatible polymer coated iron oxide nanoparticles (Fe_3O_4) were performed. In the following steps, we investigated the controlled synthesis of biocompatible polymer coated magnetic nanoparticles loaded with chrysin and evaluation for their drug loading, releasing behavior. The structure, morphology and the magnetic properties of the prepared materials were studied by using scanning electronic microscopy (SEM), Fourier transform infrared spectroscopy (FTIR), X-ray diffraction analysis (XRD). FTIR analysis confirmed that the chrysin molecules were conjugated with PEG coated iron oxide nanoparticles. X-ray diffraction pattern indicated that the magnetic nanoparticles were highly pure with a spinel structure.

PACS numbers: 87.19.xj; 61.46.+w

Key Words: Magnetic nanoparticle (MNP), Flavanoids, Chrysin, Cancer treatment, Drug delivery.

*E-mail:sabinalarss@gmail.com

1. INTRODUCTION

Cancer is a complex disease that is caused by uncontrolled division and proliferation of cells, under the influence of genetic and environmental conditions. Cancer is one of the biggest problems of our era and leading causes of death [1]. There are more than 100 types of cancers and because it is a personal disease, people have different responses to similar treatments [2,3]. With the advancement of technology, new treatment methods are being developed in addition to current treatments [4,5]. In addition to standard methods as chemotherapy, radiotherapy and surgery considered biological, hormonal, targeted, and gene therapies are increasingly being used [6]. One of the methods used in biomedical systems is controlled drug delivery systems with modified release system. Controlled release is the release of active substance at a predetermined rate within a certain period of time [7]. Since the drugs used in chemotherapy are not specific to cancerous cells, they damage both cancerous and healthy cells. To suspend this problem, magnetic nanoparticles can be used to deliver therapeutic agents to the desired target site and these particles can be retained in this specific region during drug release using an external magnetic field [8] (Fig. 1).

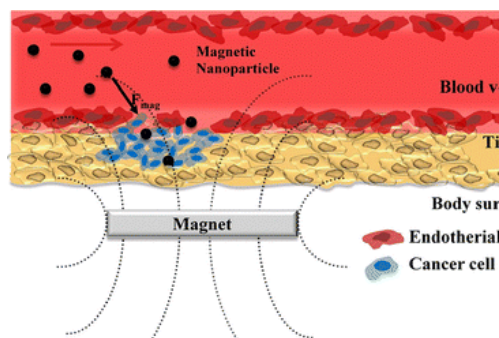


Figure 1. Magnetic nanoparticles as therapeutic agents.

Magnetic drug delivery systems are usually formed by binding the therapeutic agent to the MNP surface or encapsulating the polymer in a mixture of nanocomposites containing the polymer and MNPs. This approach protects the cytotoxic drug until it reaches the cancer cells, which will provide its therapeutic effect [9].

Successful applications of MNPs are particularly dependent on their magnetic properties, i.e., controlled distribution by the application of an external magnetic field and the degree of aggregation [10]. Therefore, in order to increase the stability of the molecule, a biocompatible polymer is used either during the synthesis or after the synthesis. Various polymers approved by Food and Drug Administration

(FDA) have been used to coat MNPs. Examples of these polymers are polyethylene glycol (PEG), polycaprolactone (PCL), polylactic acid (PLA), polylactic-co-glycolic acid (PLGA), dextran and chitosan [11].

Flavonoids have recently been used in drug delivery systems to treat the cancer. Flavonoids are polyphenolic compounds found in fruits, vegetables and beverages. Chrysin belongs to a class of flavonoids (Fig. 2). It occurs naturally in plants such as the passionflower, silver linden, and some geranium species; and in honey and bee propolis (glue). Chrysin, found in high levels of honey and propolis, is a competitive inhibitor of aromatase. Chrysin is used for bodybuilding; for treating anxiety, inflammation, gout, HIV, AIDS, erectile dysfunction (ED), and baldness; and for preventing cancer [12-16]

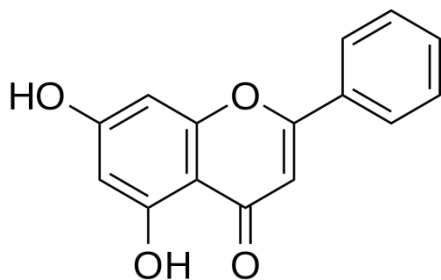


Figure 2. Chemical formula of chrysin (C₁₅H₁₀O₄).

In this review, we summarize the synthesis and characterization of chrysin-coated magnetite nanoparticles. Several methods have been investigated by researchers to obtain Fe₃O₄ nanoparticles, but we used co-precipitation method [17]. The synthesis of chrysin coated magnetic nanoparticles was carried out in three steps: The first step; synthesis of nanoparticles, the second step involves the coating of these particles with the chrysin layer, and the third step involves the characterization of chrysin-coated and non-coated nanoparticles.

2. EXPERIMENTAL

Materials

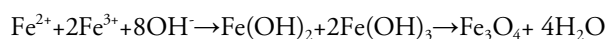
Reagents and chemicals were purchased from Merck (Darmstadt, Germany). Iron(II) sulphate (FeSO₄·x7H₂O) and Iron (III) chloride (FeCl₃·x6H₂O) was obtained from Merck (Darmstadt, Germany). Polyethylene glycol (PEG) was also obtained from Merck (Darmstadt, Germany). Chrysin (C₁₅H₁₀O₄)

97% and ammonium hydroxide (NH₄OH) were investigated from Sigma (St. Louis, MO).

Synthesis of Fe₃O₄ Nanoparticles

Iron oxides (Fe₃O₄) can be synthesized through the co-precipitation of Fe²⁺ and Fe³⁺ aqueous salt solutions by addition of a base. The control of size, shape and composition of nanoparticles depends on the type of salts used (e.g. chlorides, sulphates, nitrates, perchlorates, etc.). Also polyethylene glycol (PEG) used as stabilizer and to prevent agglomeration.

Conventionally, magnetite is prepared by adding a base to an aqueous mixture of Fe²⁺ and Fe³⁺ at a 1:2 molar ratio. The precipitated magnetite is black in color. The chemical reaction of Fe₃O₄ precipitation may be written as below:



Synthesis of PEG coated Fe₃O₄ Nanoparticles

PEG-coated nanoparticles were also synthesized. To a solution of 10 ml of iron oxide nanoparticle (1 mg/ml concentration) was added 5 ml of a 1mM PEG concentration. For the activation of the process, pH should be 7-9. The NHS-ester group results in the formation of stable, irreversible amide bonds. The amide bond formed is physiologically very stable. The solution was then sonicated for 3 hours at 30°C for dispersion and separation of the particles. The solution was centrifuged and washed several times with ethanol and dried under vacuum overnight. The sample thus prepared was heated at 200°C for 24 hours.

Preparation of chrysin loaded Fe₃O₄ nanoparticles

Chrysin conjugated iron oxide nanoparticles were prepared by co-precipitation method. In general, chrysin is soluble in organic solvents such as DMSO and dimethyl formamide, which should be purged with an inert gas. Chrysin were dissolved in 3ml of dimethyl sulfoxide (DMSO). Then, 100mg of PEG coated iron oxide nanoparticles were dissolved in 30ml of dimethyl sulfoxide (DMSO) and deionised water under ultrasonication. Then, chrysin solution was added to the above mixture, and ultrasound was continued and allowed to stir at room temperature for 24 hours. The pH of the solution was adjusted to 10 by adding KOH solution. A resultant black precipitate was washed with distilled water to remove any unbound drug or other organic impurities. The drug loaded iron oxide nanoparticles were collected using lyophilisers.

Subsequently, chrysin solution was added to the above mixture, and ultrasound was continued and allowed to stir at room temperature for 24 hours. The pH of the solution was adjusted to 10 by adding KOH solution. A resultant black precipitate was washed with distilled water to remove any unbound drug or other organic impurities. The drug loaded iron oxide nanoparticles were collected using lyophilisers.

FT-IR characterization

Fourier transforms infrared (FT-IR) spectroscopy of iron oxide was conducted by using Fourier Spectrophotometer Varian 3600 with KBr pellet method. Each KBr disk was scanned over a wave number region of 500-4000 cm^{-1} .

X-Ray Diffraction analysis

The XRD analysis was performed with MiniFlex 600, Rigaku Corporation. The method of X-ray diffraction (XRD) was used to investigate the crystalline structure of Fe_3O_4 nanoparticles. The power of X-ray diffractometer was 40kVx25mA.

Scanning Electron Microscope (SEM) Analysis

The samples were placed on polycarbonate substrate and the excess water was left to dry at room temperature. They were then dried in a critical point dryer using carbon dioxide, and sputter coated with gold in a metallizer, and examined under a scanning electron microscope (JEOL JSM 7600F, Japan) operating at an accelerating voltage of 20kV.

3. RESULTS AND DISCUSSION

FT-IR

FTIR is generally used to identify the functional groups found on the nanoparticles. Fig. 3(a,b) shows the FTIR spectra for pure, PEG coated, chrysin conjugated Fe_3O_4 nanoparticles. The broad absorption peak at 577 cm^{-1} represents the Fe-O bond of spinel structure validates the formation of Fe_3O_4 nanoparticles as shown in Fig. 3b. The peak at Fig. 3b for the Fe-O bond was slightly shifted from 679 to 751 cm^{-1} which may be due to the surface interaction between PEG and Fe_3O_4 nanoparticles.

The absorption bands at 1056 cm^{-1} represent the characteristic stretching vibration of alcoholic hydroxyl C-OH bond. These results strongly reveal that PEG was successfully grafted onto the Fe_3O_4 nanoparticles. Fig.

3a shows the FTIR spectrum for the pure chrysin molecule. The major peaks of chrysin at fig.3b were present in the range of 786 -1298 cm^{-1} . All the peaks represent the hydroxyl, carboxylic and aromatic groups present in the chrysin molecule. The broad peaks at 3116 and 1168 cm^{-1} were assigned to stretching and bending vibration of hydroxyl group.

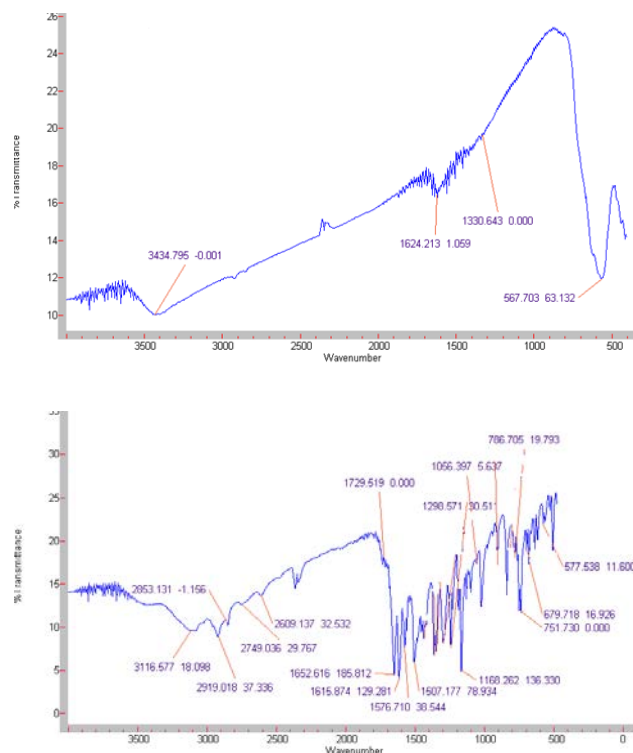


Figure 3. FT-IR peaks of pure chrysin (a) and chrysin coated Fe_3O_4 nanoparticles (b).

XRD

XRD patterns of the Fe_3O_4 were obtained. Six characteristic peaks at 30,081, 35,487, 42,983, 56,526, 57,110 and 62,808 were corresponding to the crystal planes of a pure Fe_3O_4 with a spinel structure. The peaks indicating that Fe_3O_4 with a spinel structure and no characteristic peak of impurities are detected in the XRD pattern.

Scanning Electron Microscopic Analysis

SEM analysis was used to confirm the morphology of the synthesized particles. The scanning electron microscopy (SEM) micrograph for synthesized Fe_3O_4 nanoparticles is shown in Fig. 4 a-b. SEM images revealed that the particles surface was roughness and the particles get aggregated to a varied extent that might be due to the magnetic dipole moment interaction between the particles. The particles had a narrow size distribution

were within 6-13 nm diameter.

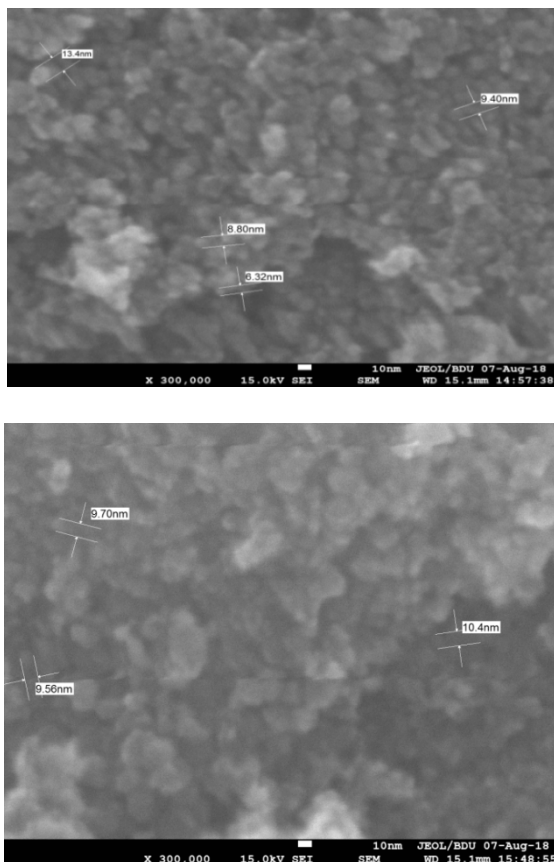


Figure 4. SEM photographs of Fe_3O_4 nanoparticles (a) and chrysin coated nanoparticles (b).

4. CONCLUSION

Uncoated and chrysin coated Fe_3O_4 nanoparticles were prepared using coprecipitation method. Slightly modified co-precipitation method shows that both coated and uncoated iron oxide nanoparticles has an inverse spinel structure with oxygen forming a face-centered cubic crystal system. Chrysin was chosen as a potent anticancer model drug and it was loaded with PEG coated Fe_3O_4 nanoparticles. The successful conjugation of chrysin on the surface of Fe_3O_4 nanoparticles was confirmed by FT-IR analysis. The crystalline, monodispersed spherical shape was obtained with from SEM analysis. As this is a comprehensive study, we have not completed the studies and the research is continuing. In the following steps, we investigated the controlled synthesis of biocompatible polymer coated magnetic nanoparticles loaded with chrysin and evaluation for their drug loading, releasing behavior.

5. REFERENCES

1. Davis E.M. & Heath R.J./The Annual Review of Medicine, 2008, v.59, p.251–65
2. Vogelstein B.&Kinzler K/Nature Medicine, 2004, v.10, p.789-799
3. Hanahan S. &Weinberg R.A./Cell, 2000, v.100, p.57-70
4. Fitzmaurice C. Dicker D. Pain A. Hamavid H.Moradi-Lakeh M. MacIntyre M.F. Allen C./The Global Burden of Cancer, JAMA Oncol. 2015, 2013, v.1, p.505-27
5. Pavlopoulou A.Spandidos D.A., Michalopoulos I./Human cancer databases (review) Oncol Rep., 2015, v.33, p.3-18
6. Jemal A.&Siegel R./CA: a cancer journal for clinicians, 2008, v.58, p.71-96
7. Kumar B.P. Puvvada N. Rajput S. Sarkar S. Das S.K. Emdad L. Sarkar D.Venkatesan P. Pal I. Dey G./Journal of Materials Chemistry B, 2015, v.3, p.90–101
8. Shakeri-Zadeh A. Khoei S. Shiran M.B. Sharifi A.M. Khoei S./Journal of Materials Chemistry B, 2015, v.3, p. 1879–1887
9. Hałupka-Bryl M. Asai K.Thangavel S.Bednarowicz M.Krzyminiewski R. Nagasaki Y./Colloids and Surfaces B: Biointerfaces, 2014, v.118, p.140–147
- 10.Filippousi M. Papadimitriou S.A. Bikiaris D.N. Pavlidou E. Angelakeris M. Zamboulis D. Tian H. Van Tendeloo G./International journal of pharmaceuticals, 2013, v.448, p.221–230
- 11.Weissleder R. Nahrendorf M. Pittet M.J./ Nature materials, 2014,v.13, p.125
- 12.Walle U.K. Galijatovic A. Walle T./Biochem. Pharmacol, 1999, v.58, p.431–438
- 13.Hertog M.G. Feskens E.J. Hollman P.C. Katan M.B. Kromhout D./Lancet, 1993, v.342, p.1007–1011
- 14.Keli S.O.Hertog M.G.Feskens E.J. Kromhout D./Arch Intern Med, 1996, v.156, p.637–642
- 15.Le Marchand L. Murphy S.P. Hankin J.H. Wilkens L.R. Kolonel L.N./J Natl. Cancer Inst, 2000, v.92, p.154–160
- 16.Ishige K. Schubert D. Sagara Y./Free Radic.Biol Med, 2001, v.30, p.433–446
- 17.Chen F. Xie S. Zhang J. Liu R./J. Mater Lett., 2013, v.112, p.177-179

PROPERTIES OF ZnSTe:Cr NANOCRYSTALLINE THIN FILMS

M.A. JAFAROV^{1*}, E.F. NASIROV¹, I.S.HASANOV², H.M. MAMEDOV¹,
SYED I. SHAH³, E.A.KHANMAEDOVA²¹Faculty of Physics, Baku State University, Az1148, Z.Khalilov str., 23, Baku, Azerbaijan²Azerbaijan Academy of Science, Institute of Physics, AZ0143 Baku, Azerbaijan³University of Delaware, 208 DuPont Hall, Newark, DE 19716, USA

Thin films of ZnSTe and Cr doped ZnSTe have been deposited on glass substrates by chemical bath deposition (CBD) method taking ammonia as complexing agent. The pH of the solution was maintained at 8–9 at a temperature of 70 °C. Characterization of the ZnSTe and Cr-doped ZnSTe films were carried out using X-ray diffraction (XRD) and Atomic force microscopy (AFM). Structural properties and optical absorption has been observed for both doped and undoped films. Parameters like crystallite size, lattice constant, microstrain, dislocation density; and optical constants such as extinction coefficient, absorption coefficient for both types of films were measured from XRD and absorbance spectra respectively. Studies show that there is an increase of crystallite size and good optical properties in visible region from 420 nm in Cr-doped ZnS thin film.

PACS numbers: 54.72.Hj; 34.34. Mn; 42.30. Ht**Keywords:** chemical bath deposition, crystallite size, thin film, nanoparticles***E-mail:** maarif.jafarov@mail.ru

1. INTRODUCTION

Studying the size quantum phenomena in the little-studied and promising semiconductors of the type A^2B^6 opens up many prospects for the elaboration of new devices on their basis with different functional abilities. Among the wide range of nanomaterials, nanostructure materials for nanoelectronics occupy a special place. Nanostructuring allows one to tune the physicochemical properties of the substance. It caused the emergence of the definition “programmable matter” in the literature, which can strictly be understood as the elaboration of materials with a defined set of characteristics via nanostructuring.

Interest in the synthesis of small particles and nanocrystals of various substances has noticeably increased when a decrease in the crystallite size below a certain threshold value is found to cause a pronounced change in the crystal structure and the emergence of quantum properties. The quantum effects are manifested at a particle size below 10 nm. The spherical shape of nanocrystals is also of great importance to attain the optimum discrete spectrum of the energy levels of quantum dots. Chemical deposition from aqueous solutions allows the acquisition of semiconductor nanocrystals with much smaller dimensions in contrast to molecular-beam epitaxiation and lithography. The incipience of nuclei and their growth upon chemical deposition results in a quasi-spherical shape of the nanocrystallites, whereas the synthesis of films via molecular-beam epitaxiation or electrochemical deposition leads to a nonspherical shape. On the other hand, a

small amount of the broken bounds on the cleavage surface (below 10^{10} cm⁻²) allows the layered semiconductors to be used as solid substrates for quantum-dot formation [1], growing fullerenes, and the acquisition of van der Waals epitaxy [2–4] in the production of solar elements [5]. The X-ray detectors [6], optical converters [7], and luminophores [8], as well as photodetectors operating in the UV–visible–near-IR spectrum range of the electromagnetic radiation on the basis of A^2B^6 compounds are favorably different from the others by high radiation resistance and photosensitivity [9]. The ZnS-based luminophores exhibit high brightness and light output in the visible spectrum range. Doping ZnS with the activators results in blue luminescence for ZnS:Ag crystals, while it is green for ZnS:Cu and orange for ZnS:Mn. In this work we report the experimental results for nanoparticles synthesized on the basis of ZnS:Mn, combined with an analysis of their structure and electrical, optical, and photoluminescent characteristics.

2. EXPERIMENTAL AND RESULTS

The ZnSTe:Cr nanoparticles were obtained via chemical vapor deposition (CVD). The preparation of substrates and compounds, as well as the synthesis, play important role. The glass substrates were previously cleaned in the potassium dichromate/sulfuric acid solution. Deposition of ZnS films was based on the reaction between zinc chloride ($ZnCl_2$) as the source of Zn^{2+} , TeO_2 and thiourea ($SC(NH_2)_2$) providing S^{2-} and ammonium (NH_4OH) that was used as the complex-

forming agent varying pH in the solution and enabling us to control the Zn^{2+} concentration.

Afterwards the mixed solution was stirred for 15 minutes. To improve homogeneity and the growth rate 15 ml of 1M hydrazine hydrate $\{(NH_2)_2\}$ was used. Then ammonia solution was added drop wise to form the complex and to raise the pH of the solution. The pH value was maintained between 8-9; keeping the temperature constant at 70 °C. For the Cr doping ZnSTe thin film, 0.05 M and 0.1 M solutions of CrO_3 were prepared separately. 20 ml of CrO_3 of each molarity was mixed in two separate beakers containing chemical solution of zinc acetate, thiourea and hydrazine hydrate of same molarities as described above in the deposition of pure ZnS thin film and then the CrO_3 mixed solution was stirred for 45 minutes. After some chemical reaction, deposition of films started slowly on the substrates. Keeping bath temperature maintained for 30–45 minutes, the whole solutions were kept undisturbed at room temperature for further deposition of the films. All the films were kept deposited for 24 hours. Then the glass slides covered with a white layer were taken out, washed with distilled water and dried out in air. However Cr-doped films were yellowish white in colour. Thus we prepared three different types of thin films namely undoped ZnSTe, 0.05M CrO_3 doped ZnSTe (Cr-ZnSTe1) and 0.1 M CrO_3 doped ZnSTe (Cr-ZnSTe2) separately. Some films were covered in both sides of the substrates. One side of these substrates was then cleaned by nitric acid. These films were kept to study the optical absorption. Other deposited films were kept “as it were” for the other characterization like XRD, AFM and XRF. Thickness of the films was measured by gravity method. Thickness for ZnSTe, Cr-ZnSTe films was varied from 84 – 85.26 nm.

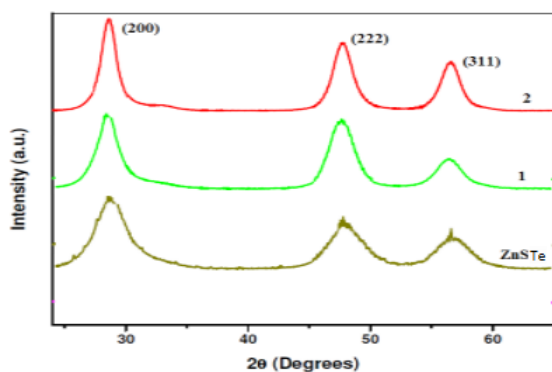


Fig. 1. XRD spectra of ZnSTe and Cr-doped ZnSTe films

Atomic force microscopy (AFM) is one of the effective ways for the surface analysis of thin films due to its high resolution and powerful analysis software. The

ZnSTe and Cr-ZnSTe thin films were morphologically characterized using AFM technique. Fig. 2 shows the 2D and 3D image of undoped and doped ZnSTe film (Cr-ZnSTe2) in scanned area of 5×5 and $10 \times 10 \mu m^2$. In both the films the surface is rough and fully covered in the substrate. Clusters of particles are observed over the surface in undoped ZnSTe film. While formation of unregulated grains of different sizes are observed clearly with pinhole free in Cr-ZnSTe2 film. From the AFM images average grain size in Cr-ZnSTe2 film is found to be 250 nm and the RMS (Root Mean Square) roughness is 210 nm as obtained by using the software WSxM 4.0 Beta7.0 version (14). RMS roughness is larger in doped film than that obtained from the undoped ZnSTe film which is 145 nm. Again we have found that grain size obtained from AFM image is quit larger than the crystallite size obtained from XRD. This may be because of small crystallites combine to form larger grain.

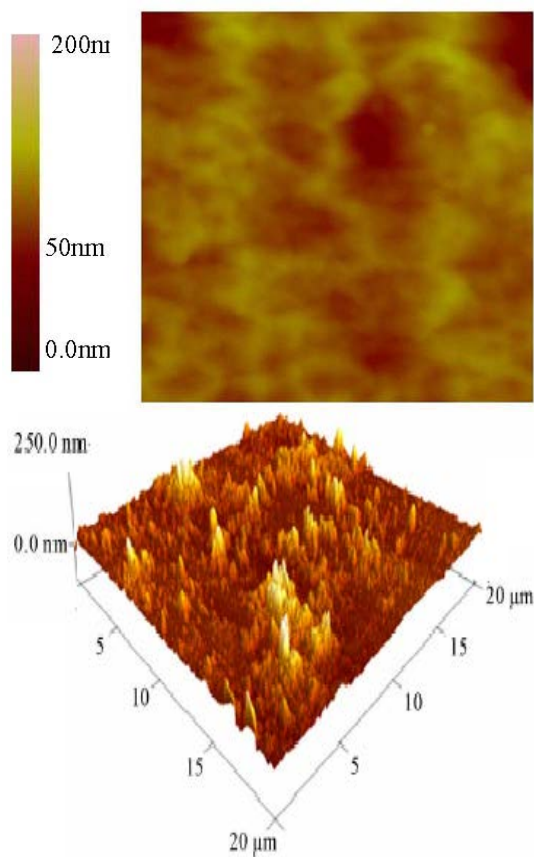


Fig. 2. The 2D and 3D image of undoped and doped ZnSTe film (Cr-ZnSTe2)

Optical absorption of ZnS and Cr-ZnS films have been studied in the wave length range 340-800 nm. Optical absorption studies of semiconducting materials

give some information related to band structure. Optical absorption spectra of typical undoped ZnSTe and Cr-ZnSTe thin films have been shown in Fig. 3. At higher wavelength i.e. at lower energy side, absorption is low towards visible region. However, an increase of absorption is seen in lower wave length (higher energy) side for both types of films. Higher absorbance has been observed in Cr doped ZnSTe films. This may due to the presence of extra states created by Cr impurity in the doped films that absorbs more photon energy than that of the undoped film.

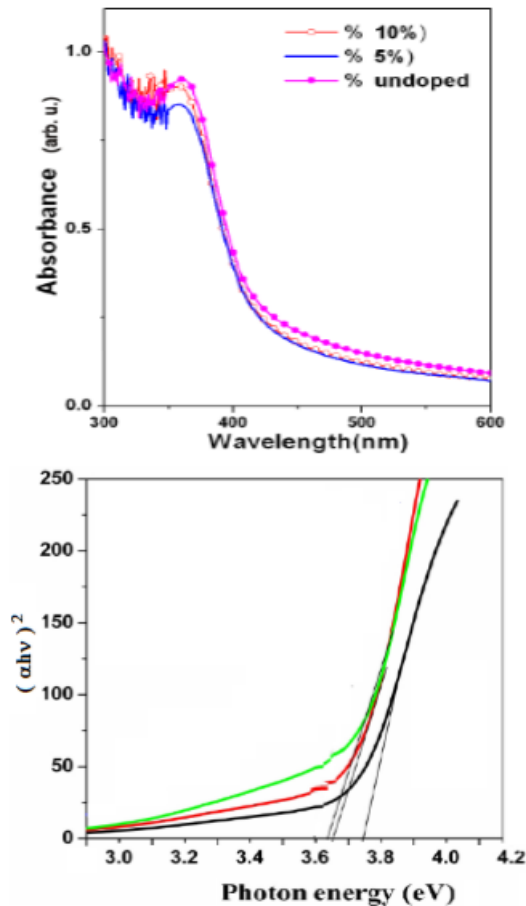


Fig. 3. Absorbance spectra of ZnSTe and Cr-doped ZnSTe films

For direct transition the n value is $\frac{1}{2}$ whereas for indirect transition the n value is 2.

Fig. 4 shows a typical plot of $(\alpha h\nu)^2$ versus $h\nu$ for doped and undoped ZnSTe film from which extrapolation of data to the $(\alpha h\nu)^2 \rightarrow 0$ axis gives the band gap energy $E_g = 3.84$ eV and for Cr-ZnSTe1 and Cr-ZnSTe2 film, this value is 3.76 eV and 3.74 eV respectively. Thus band gap decreases in case of Cr doped ZnSTe film. This is due to the extra electronic states associated with Cr located below the conduction band.

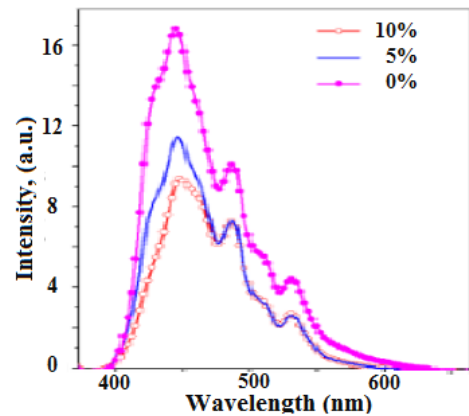


Fig. 4. Luminescence spectra of ZnSTe:Cr

Figure 4 shows the PL spectra and absorption spectra of a series of samples with different doping concentration. The PL spectra (Fig. 4a) of the nanocrystal samples show three peaks, at 444, 478, and 530 nm, which are attributed to the band edge, shallow and deep traps, respectively. We see that undoped nanocrystals have a narrower size distribution than the 5% and 10% doping nanocrystals.

From the comparison it is seen that value of extinction coefficient is higher in Cr-ZnSTe films than that of the undoped ZnSTe film which indicates more efficiency of Cr-ZnSTe film in electrical conduction than ZnSTe film.

3. CONCLUSION

Thin films of ZnSTe and Cr-doped ZnSTe have been prepared by the CBD method. XRD results reveal the polycrystalline nature of the films with preferred orientation along (200) plane. Different structural parameters such as crystallite size, lattice constant, internal strain and dislocation density were calculated from their XRD spectra. AFM images show the rough surface of the films with increasing grain size and RMS roughness with doping. Optical studies confirm the direct band gap nature of the films and also the decrease of band gap energy in case of doped films. Higher value of extinction coefficient in Cr-ZnSTe films may enhance the efficiency of Cr-ZnSTe film in electrical conduction than that of ZnSTe film.

4. REFERENCES

1. Aamodt, T.I. Characterization of ZnS:Cr films for Intermediate Band Solar Cells, MSc Thesis

- (unpublished), Norwegian University of Science and Technology, Norway, 2011.
2. Allouche N.K., Nasr T.B. et al. / Materials Chemistry and Physics, 2010, v.123, N 2-3, p.620-624.
3. Girija, K., Thirumalairajan, S., et al. / Chalcogenide Letters, 2009. v. 6 (9), p. 351-357.
4. Hai-Qing, X., Yuan, et al. / Chinese Phys Letters, 2011, v. 28 (2), p.027806-9.
5. R.N. Bhargava, D. Gallagher and T. Welker, /J. Lumin. 1994, v. 60, No. 61, p. 275-278.
6. H. Lu and S.Y.S. Chu /J. Cryst. Growth., 2004, v. 265, p. 476-480.
7. Arai T., Senda S. et al. /Chem. Mater., 2008, v. 20, p. 1997-2000.
8. Bhattacharya S. and Chakravorty D. /Chem. Phys. Lett., 2007, v. 444, p. 319-323.

DIELECTRIC- CONDUCTOR TRANSITION IN A MIXTURE OF ZEOLITE AND GRAPHITE POWDERS

G.M. EYVAZOVA*, V.I. ORBUKH, N.N. LEBEDEVA

Institute for Physical Problems, Baku State University, Z. Khalilov str.23, Baku, AZ1148

*Nano Centre, BSU, Z. Khalilov str.23, Baku, AZ1148

We reviewed the results of experimental studies of bulk specific conductivity and dielectric permittivity in a mixture of a dielectric (zeolite) and a conductor (graphite) as a function of the volume content of graphite at different frequencies. It was observed a dielectric-conductor transition (an increase in conductivity by 400 times with a change in the concentration of graphite by 2%) We have proposed a qualitative model that explains the obtained dependencies on the basis of percolation theory with the involvement of the concept of fractals.

PACS numbers: 77.84.lf;72.80.Tm;84.37+q

Keywords: zeolite, graphite, temperature dependence, resistance.

***E-mail:** nnlebedeva@gmail.com

1. INTRODUCTION

The electrical conductivity of composites formed by a complex network of conducting and insulating phases is determined by percolation mechanisms (flowing) in a continuous network of conducting particles and/or tunneling between conducting particles in the insulating phase. The dielectric-conductor transition in disordered heterogeneous systems is one of the varieties of percolation processes that attract the attention of researchers. For example, in the two-component static mixtures [1,2] and ferroelectric ceramics [3] with strongly differing dielectric permittivity (DP) and specific conductivity of the components, the increase in the percolation threshold of the static permittivity due to the Maxwell-Wagner relaxation was repeatedly observed and studied. No less interesting is the effect of the giant increase in the effective conductivity of the composite, which is undeservedly poorly represented in publications [4]. At present, not only the physical mechanism, but even the possibility of obtaining giant conductivities in disordered heterogeneous systems, has not been studied. In [4], a statistical mixture of PCR-8 ferroelectric ceramics ($\epsilon=1200$, with a conductivity of 10^{-10} Ohm $^{-1}\cdot$ m $^{-1}$) and polyethylene ($\epsilon=2.5$, with conductivity of 10^{-6} Ohm $^{-1}\cdot$ m $^{-1}$) was studied and the effect of a gigantic increase in the effective conductivity of the statistical mixture at the percolation threshold was observed for the first time. The authors of this work assume that an infinite ceramic cluster with very thin interlayers of a conductive component with a small DP arises near the percolation threshold. In these layers,

very strong electric fields arise, and their high conductivity leads to an increase in the effective conductivity of the statistical mixture.

In work [8], based on theoretical studies of the dielectric properties of inhomogeneous media [5-7], an effective medium method was developed. This method was widely used in describing the physical properties of inhomogeneous media, but did not allow us to predict the behavior of the system during the metal-dielectric transition near the percolation threshold [9-13].

Detailed information on the metal-dielectric transition was obtained in [14], where the frequency dependencies of the dielectric properties of a metal-dielectric composite typical for fractal structures were determined on the basis of a fractal model of a heterogeneous medium with a chaotic structure. Recently, the use of the ideas of fractal geometry [15] has made it possible to reveal new regularities in the physics of disordered media [14]. It turned out that near the percolation threshold, the conducting channels in the mixtures of a metal with a dielectric have the structure of a stochastic fractal [15, 17-19]. That is, the geometrically current-carrying framework is a loose object that has its own fractal dimension, and the physical processes on them are described by power functions [15]. The effective conductivity of a mixture of metal with a dielectric at the percolation threshold is the similar function. We denote the conductivity of the metal by g_1 , and the dielectric- g_2 . At a concentration corresponding to the percolation threshold p_c , the mixed

conductivity regime [19] is realized: the effective conductivity g_e depends only on the ratio $h=g_2/g_1$. In the two-dimensional case ($p_c=0.5$), the dependence of the effective conductivity on h is determined by the $g_e = g_1 h^{1/2}$ expression, first obtained in [20], where it is also shown that the electric field can experience enormous spatial fluctuations in the mixed conductivity regime. In our previous studies [21,22], in the study of the electrical properties of a mixture of zeolite with conducting metals (Cu, Si), we did not observe a dielectric-metal transition. In this paper, we chose graphite as a conductive component in a zeolite-conductor mixture, since graphite, being a fairly soft material, has a high conductivity. In this paper we have studied the conductivity and dielectric constant, as a function of the concentration at different frequencies.

2. EXPERIMENTAL

As a model for studying the conductivity of macro-disordered systems, the following systems were chosen: a non-conducting dielectric (zeolite) and a conductor (graphite). As conductors, graphite particles were used.

For this we chose thermo graphite. It is a colloidal graphite preparation, dry C-1, with a basic particle size of $4 \cdot 10^{-6}$ m. The use of graphite as a conductive component has significant advantages over other metals in terms of minimizing the contact resistance between graphite particles and zeolite crystallites. 1) Due to the scaly structure, graphite tightly covers the surface of the zeolite crystallite; 2) graphite has a resistivity close to metallic; 3) since carbon oxides are gases, irrespective of the occurrence of graphite, one can not consider the formation of an oxide film on graphite particles.

The dielectric matrix was a natural zeolite. On the basis of X-ray and spectral chemical analyzes, the affiliation of natural zeolite to high-silica zeolites of the type clinoptilolite was established [21]. Crystalline structure is composed of an alternating negatively charged tetrahedra AlO_4 and SiO_4 , which are interconnected by nodes with a pore- nanochannels [23]. These channels are filled with the extra-framework cations that is, Na^+ , K^+ , Mg^{2+} , Ca^{2+} , which compensate the negative charges of the framework.

Mapping and the characteristic elemental analysis were studied by scanning electron spectroscopy (SEM) using JEOLJSM7600F. Clinoptilolite was processed on a ball mill FRITSCH, and the resulting powder consisted of crystallites of size 0,5-30 μm . The sample for the study was a capacitor filled with a mixture of

graphite of a certain concentration and a zeolite. The concentration of graphite in the mixture varied from 5% to 50%.

The resistivity at constant voltage was determined by the standard method, and the capacitance was measured by impedance spectroscopy. For this purpose, a condenser with a mixture was installed at the input of the device E7-20. The measurements were carried out at room temperature, atmospheric pressure and humidity of 0.85%.

3. THE RESULTS AND DISCUSSION

In this work, we studied the conductivity and dielectric constant of a mixture of zeolite and graphite powders, depending on the percentage of graphite (from 5% to 50%) for different values of the frequency of the external electric field (from 120Hz to 1MHz). Let us formulate the experimental results:

1. As can be seen from Fig. 1, with a change in the concentration of graphite in the range from 23% to 30%, the conductivity of the mixture increases by 10000 times. With a further increase in the graphite content, the conductivity decreases, but at a concentration greater than 40% it is restored.
2. The plot of the dependence of the dielectric constant on the concentration of graphite (Fig. 2) shows a similar behavior at small (about 23%) concentrations of graphite – a maximum with a subsequent minimum, and has no specific features at high concentrations.

In the test mixture, the concentration of one component is several times different from the concentration of the other. That is why an anomalous increase in conductivity is observed with a small change in the concentration of graphite (Fig.1a). We interpret this phenomenon as a dielectric-conductor transition. Such a transition is described as a phenomenon associated with percolation.

The inset in Fig. 1 shows a part of the main plot corresponding to the fastest change in conductivity as a function of the concentration (20-30%), in an enlarged 400 times along the conductivity axis. As can be seen (Fig. 1a), the graph on the insert is topologically equivalent to the main graph. Such invariance in scale allows us to assert that the increase in conductivity indicated in Fig.1b is a percolation process. To explain the nonmonotonic dependence of the conductivity on the concentration of graphite, we note the fact that the measurements were made in a direct electric field. The point is that when studying the dielectric-conductor

transition in a constant electric field, isolated conducting regions only polarize, but do not contribute to the direct current. With increasing concentration of the conductive component (in the course of the dielectric-conductor transition), conductive regions are formed, gradually merging into larger and larger regions. This process ends with the formation of an infinite cluster (which can only be registered by a constant electric field). Conversely, in the case of measurement in an alternating electric field, the local conducting regions contribute to the electrical conductivity.

Therefore, in an alternating field, anomalies with increasing graphite concentration can be observed associated with the merger of conductive regions.

To explain our results, we start with the Shklovskii-De Gennes percolation model [24, 25]. In this model, the static conductivity of a mixture of conducting and nonconducting (or weakly conducting) particles is determined by a set of electrically interconnected conductive particles (the skeleton of an infinite cluster). However, the main mass of an infinite cluster consists of conducting dead-end branches of it. Of course, these branches, by definition, do not contribute to the static conductivity, but they contribute to the conductivity measured in the alternating field. Even more important is the fact that an anomalously large capacitance of the system is associated with these branches when the dielectric-conductor transition occurs. In the Shklovskii-De Gennes model, the dependence of the conductivity of a binary mixture σ on the concentration of a conducting component x has the form:

$$\sigma = \sigma_d (x_c - x)^{-1}, x < x_c \quad (1)$$

$$\sigma = \sigma_h \left(\frac{\sigma_d}{\sigma_h} \right)^{0,62}, x = x_c \quad (2)$$

$$\sigma = \sigma_h (x - x_c)^{1,6}, x > x_c \quad (3)$$

Here σ_h - is the conductivity of the low-resistance component of the mixture (in our case, graphite), σ_d - is the conductivity of the high-resistance component of the mixture (in our case, zeolite), x_c - is the critical concentration.

We use the formulas (1) - (3) to explain the features of the dependence of the conductivity of the mixture on the concentration of graphite (Fig. 1). It is followed by these formulas that when the concentration approaches to the critical value $x = x_c$ from the side of

concentrations less than x_c , the conductivity tends to infinity hyperbolically, as is clear from (1).

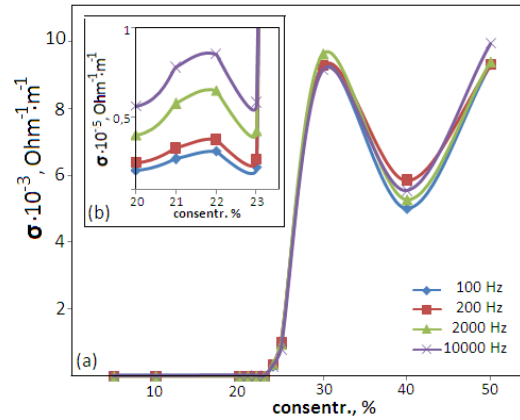


Fig. 1. The dependence of the conductivity of the mixture on the concentration of graphite: (a) - from 5% to 50%; (b) - from 20% to 23%.

When approaching the critical point from the side of concentration greater than x_c , the conductivity tends to zero, as is clear from (3). Such a nonanalyticity of conductivity, as a function of the concentration of the conductive component, means that the experimental data should be compared with formulas (1) - (3).

The feature observed in Fig. 1 is completely described by formulas (1) - (3). The section corresponding to a decrease in conductivity (as a function of concentration), we consider as an instability zone, which includes a critical point. The region of increase of the conductivity located to the left of this zone is in good agreement with formula (1). The same can be said about the behavior of the graph to the right of the instability zone: it agrees with formula (3). Note that formula (3) also predicts concavity down (since the second derivative of (3) is positive), which is observed on the graph. This behavior is observed at different scales at concentrations of the order of 20 and 40%, respectively. In our opinion, this behavior is associated with the formation of conducting local clusters, the combination of which, is completed by the formation of an infinite cluster with an increase in the concentration of the low-resistance component.

Turning to a discussion of the measurement of the dielectric constant should be noted that the conductivity and dielectric constant in homogeneous systems are independent. In contrast, in inhomogeneous systems, such as ours, the measured conductivity and permittivity are dependent on each other. This is due to

redistribution of the field between different parts of the mixture: it is displaced from low-resistance regions to high-resistance regions. Fig. 2 shows the dependence of the dielectric constant on the concentration of the conductive component. It can be seen that at concentrations greater than 25% and at frequencies below 10,000 Hz, measurements are not possible.

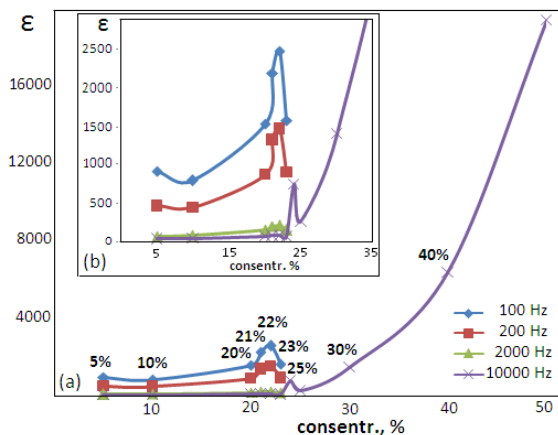


Fig. 2. The dependence of the dielectric constant of the mixture on the concentration of graphite: (a) - from 5% to 50%; (b) – from 5% to 30%.

When measurements are still possible, the values of the dielectric constant are extremely large (of the order of 16,000). When a dielectric-conductor transition occurs, such an anomaly in the dielectric constant has its own explanation [24-25]. This transition itself is explained by the formation of an infinite cluster consisting of a current carrying skeleton and chains of electrically interconnected conductive particles. They are originated in the conducting skeleton and ended with dead-ends (i.e., a chain break). It is these dead-end chains that make up the bulk of the infinite cluster and lead to anomalously large values of the dielectric constant [26]. Since the number of dead-end chains of graphite particles contacting each other increases with the concentration of graphite, the dielectric constant also increases (Fig. 2, frequency 10000 Hz). It can be seen from Fig. 3 that the dielectric constant, beginning at a concentration of 25%, sharply changes the nature of its frequency dependence: measurements at low frequencies (lower 10,000 Hz) become impossible, the dielectric permittivity increases sharply. From the graph of the dependence of the conductivity on the concentration in Fig. 1, it is seen that the concentration of 25% is the concentration of the dielectric-conductor transition, at which an infinite cluster is formed. Therefore, the curves in Fig. 3, corresponding to

concentrations less than 25%, reflect the frequency dependence of the dielectric constant of the dielectric (zeolite). At concentrations greater than 25%, the graphs in Fig. 3 reflect the frequency dependence of the dielectric constant associated with dead-end chains of conductive graphite particles. The impossibility of measuring the dielectric constant at frequencies below 10,000 Hz and concentrations greater than 25% (i.e., in the conducting phase) is attributed to the displacement of the electric field from the volume of the composite to the internal resistance of the current source. At high frequencies, this effect decreases and measurements become possible.

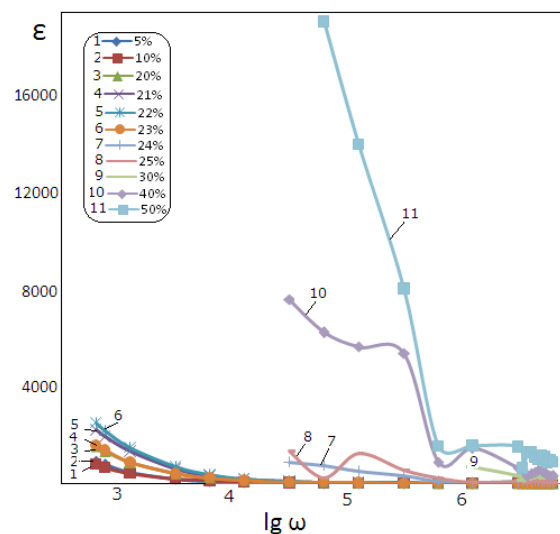


Fig. 3. The dependence of the dielectric constant on the frequency.

4. CONCLUSION

An instability zone has been observed in the range of graphite concentrations from 23% to 30%. Within this zone, the conductivity increases by 10,000 times for the frequency of 100 Hz and 2000 times for the frequency of 1 MHz. The identical behavior of the dependence of the conductivity on the concentration of graphite at different scales (differing by a factor of 400) is observed. In other words, in the form of the dependence of the conductivity on the concentration of graphite, the features of fractal behavior are observed. Therefore, we interpret the observed phenomena as a percolation-induced dielectric-conductor transition. The dependence of the dielectric constant on the graphite concentration for different frequencies demonstrates anomalously large (up to 2500) values, typical of the dielectric-conductor transition. The local peak of the dielectric constant is observed at the same concentration

(23%) at which the dielectric-conductor transition is observed. It is important to note that composites based on zeolite with other conductive powders (copper, silicon) do not exhibit a dielectric-conductor transition at the same concentrations. A possible cause of this difference may be a low density of graphite, which provides direct electrical contact between graphite particles at distances larger than their sizes (due to the formation of traces of graphite on the zeolite during the mixing of the composite).

5. REFERENCES

1. Efros A.L., Shklovskii V.I. / Phys.Stat.Solid B, 1976, v.76, N 2, p.475-485.
2. Yemes Y.P. / J. Experimental and Theoretical Physics , 2002, v.121, N 6, p.1339-135.
3. Lemanov V.V. et al. / FTP, 2002, v.44, N 11, p.1948-1957.
4. Turik S.A. et al. / El. J. Issledovano v Rossii, 2026<http://zh.nol/apl/relarn/ru/art/2004/191/pdf>.
5. Maxwell J.C. et al. Oxford, 1873, 365 p. [Reprint: Dover, 1973, N 4, P. 501]
6. Maxwell Garnett J.C., Phil J.C. / Trans. R. Soc. 1904, 203, p.385-420.
7. Bruggeman A.G. / Ann. Phys., 1935, v.24, p.636.
8. Landauer R., 1st Conf. on the Electrical Transport and optical properties of inhomogeneous media, AIP, Columbus, OH, 7-9 september, 1977, AIP conf. Proc., 1978,v.40,p.2-45.
9. Stauffer D. Introduction to the Percolation Theory. London-Philadelphia, 1985.
10. Sahimi M. Applications of Percolation Theory, Taylor and Francis, London. 1994.
11. Privalko V.P., Novikov V.V. / J. Wiley, New York, 1995, p. 235.
12. Webman I., Jortner J. / Phys. Rev. B, 1975, v.11, N8, p.2885.
13. Webman I., Jortner J. Cohen M.H. / Phys. Rev. B, 1976, v.13, N2, p.713.
14. Satanin A.M., Kharkov S.V., Uqolnikov A.Y. / L. Experimental and Theoretical Physics , 1995, v.62, N4, p.301-304.
15. Feder E. Fraktals, M.; Mir; 1991, 254p.
16. Shklovskiy V.I., Efros A.L., Electronic Properties of Doped Semiconductors, M.;Nauka, 1979, 416p.
17. Halvin S., Nossal R. /J. Phys.A. 1984, v.17, L 427.
18. Havlin S., Nossal R., Trus B. and G H Weiss /J. of Physics A: Mathematical and General, 1984, v.17, N18, L 957.
19. Ohtsuki P., Keyes T. / J. Phys. A, 1984, v.17, L 559.
20. Dixne A.N. / J. Experimental and Theoretical Physics, 1970, v.59, p.110-115.
21. Orbukh V.I., Lebedeva N.N., Ozturk S., Salamov B.G. / Superlattices and Microstructures, 2013, v.54, p.16-25.
22. Ozturk Koc S. et al. /Superlattices and Microstructures, 2016, v.91, p. 269-277.
23. Gollardi G, Galli E, Natural Zeolites, Spriger-Verlager, Berlin, 1985, 409 p.
24. Efros A.L. Physics and Geometry of Disorder, «Nauka», Board edition fiz-mat literature 1982, 174p.
25. Scaling Ideas in Polymer Physics [Russian translation] P de Gennes - 1982 – Moscow. p.312.

RACEMIC AND ENANTIOSELECTIVE DIELS-ALLDERCYCLOADDITION
OF 2,4-PENTADIENOL TO DIETHYLDIAZODICARBOXYLATEF.N.AXUNDOVA*¹, M.J.ALVES², M.M.KURBANOVA¹.¹Baku State University, Z.Khalilov 23 Str., Baku, Azerbaijan²Universidade do Minho Campus de Gualtar4710-057 Braga, Portugal

Racemic cycloadduct was synthesized based on a modified Bols protocol. The optically active (S)-diethyl 3-(hydroxymethyl)pyridazine-1,2(3H,6H)-dicarboxylate were synthesized based on asymmetric Diels-Alder reaction in the presence of (S)-BINOL chiral catalyst. The structures of synthesized cycloadducts were proved by IR, ¹H NMR, ¹³C NMR, HRMS (ESI) spectroscopes, and a specific rotation of optically active cycloadduct was determined by AUTOPOL III polarimeter.

PACS numbers:33.15.Bh , 82.90.+j

Keywords: Diels–Alder cycloaddition, asymmetric synthesis, 1-Azafagomine, Bols protocol.

*E-mail:fidan.axundova.88@mail.ru

1. INTRODUCTION

1-Azasugars are a series of synthetic nitrogen-containing sugar analogues consisting of a monosaccharide structure where the anomeric carbon has been replaced by a nitrogen atom. Interest in these compounds is based on the discovery that 1-azafagomines are very good as α - and β -glucosidase [1,2] inhibitors. A great number of biochemical processes in human biology involve glycoside-cleaving enzymes.

2. EXPERIMENTAL

Solvents were distilled under anhydrous conditions. All reagents were purchased and used without further purification. Glassware was dried prior to use. Compounds were purified by dry flash chromatography using silica 60, <0063 mm and water pump vacuum or by flash-chromatography using silica 60 Å 230–400 mesh as stationary phases. TLC plates (silica gel 60 F254) were visualized either at a UV lamp or in I2. ¹H NMR and ¹³C NMR were run on a Bruker Avance III 400 spectrometers (measuring frequency: ¹H NMR = 400 MHz, ¹³C NMR = 100.6 MHz). Infrared spectra were recorded on a Bomem MB 104. Samples were run as oils as thin films. Melting points are uncorrected. MS spectra were recorded on a Varian 500-MS LC Ion Trap Mass and VG Autopic M. spectrometer. The specific rotation was determined by AUTOPOL III polarimeter.

Synthesis of racemic diethyl-3-(hydroxymethyl)-3,6-dihydropyridazine-1,2-dicarboxylate (1). To a

There is, therefore, a considerable drug potential in selective inhibitors of glycosidases and similar enzymes. So far glycosidase inhibitors have been investigated as antidiabetic, antiviral or antimetastatic agents, work which has resulted in the antidiabetes drug acarbose [3] and the new anti-influenza drug Zanamivir [4]. Therefore, nowadays the field of azafagomine is a very exciting area of research because of biological activity.

solution of 2,4-pentadienol 1.33 g (16.0 mmol) in dry toluene (10 mL) was added diethyl azodicarboxylate 7.30 mL (40% in toluene, 16.0 mmol) under magnetic stirring at rt. The stirring was continued for 24 h and the solvent removed to give cycloadduct (1) as an orange oil (4.32 g; 99%).

Synthesis of diethyl(S)-3-(hydroxymethyl)-3,6-dihydropyridazine-1,2-dicarboxylate (2). **Solution A:** To a solution of 2,4-pentadienol (0.100 g; 1.19 mmol) in dry toluene (6 ml) was added dimethylzinc(0.991 ml; 1.19 mmol) under magnetic stirring at the 0°C for 5 min.

Solution B: To a solution of (S)-BINOL, (R)-BINOL (0.340 g; 1,19 mmol) in dry toluene (6 ml) was added methyl magnesium bromide (0.849 ml; 1.19 mmol) under magnetic stirring at the 0°C for 5 min. Then, solution A was added to solution B and 10 ml toluene was added as well then left it to stir for 5 min 0°C. After 5 min temperature was decreased -78°C, DEAD (0.543 ml; 1.19 mmol) was added the 10 ml toluene was added after that left it the temperature to

become room temperature. The reaction was stirred for 18 h. The reaction was quenched with saturated solution of NaHCO₃ (1 mL), filtered through a pad of celite, and the celite washed with EtOAc (3×20 mL). The filtrates were combined and concentrated under reduced pressure giving a yellow oil. The crude oil was purified by “dry-flash” chromatography (silica, petroleum ether/diethyl ether). (S)-BINOL,(R)-BINOL were recovered with petroleum ether and product with diethyl ether as a yellow oil. Specific rotation: $[\alpha]_D^{20}$ -23.4° (con. 1.25% in CHCl₃)

Structural analysis of compounds 1-2:

ν_{\max} (neat) 3483, 1707 cm⁻¹. ¹H NMR δ_{H} (400 MHz, CDCl₃) 1.23-1.30 (12H, m, 4CH₃, A+B), 2.58 (1H, s, OH), 3.35 (1H, dd, *J* 12.3, 9.5 Hz, H-3', A), 3.45 (1H, dd, *J* 12.0, 9.8 Hz, H-3', B), 3.56-3.69 (2H, m, 2H-3', A+B), 3.77 (1H, dd, *J* 13.5, 4.3 Hz, H-6, A), 3.91 (1H, s, H-6, B), 4.11-4.26 (8H, m, 4CH₂, A+B), 4.30 (1H, tdd, *J* 6.0, 3.9, 2.2 Hz, H-6, B), 4.34-4.44 (1H, m, H-6, A), 4.72 (2H, s, H-3, A+B), 5.66-5.88 (4H, m, H-4 + H-5, A+B) ppm. ¹³C NMR δ_{C} (100 MHz, CDCl₃) 14.3 (CH₃, A), 14.4 (CH₃, B), 42.2 (C-6, A), 43.6 (C-6, B), 55.9 (C-3, A), 56.9 (C-3, B), 61.9 (C-3', A+B), 62.6, 62.7, 62.8, 62.9 (CH₂, A+B), 123.4, 124.2, 124.6, 125.2 (C-4 or C-5, A+B), 154.9, 155.7, 156.2, 156.3 (C=O, A+B) ppm. HRMS (ESI) calcd for C₁₁H₁₈N₂NaO₅; 281.1108; found: 281.1109.

3.RESULTS AND DISCUSSIONS

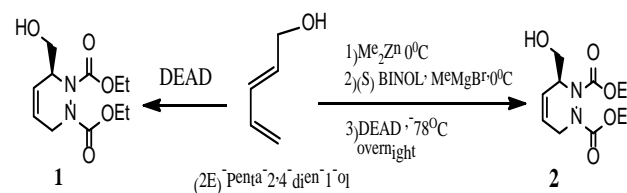
The synthesis of cycloadduct based on Diels–Alder reaction which, plays the main role as an intermediate compound in the synthesis of 1-azasugars. On the other hand, it should be pointed out that, Diels–Alder strategy quite a short route to reach 1-azafagomine. That is why it is a preferable way for the synthesis of cycloadduct.

In the first time, the synthesis of homochiral (-)-1-azafagomine was accomplished by Bols and coworkers based on the Diels–Alder cycloaddition to 4-phenyl-1,2,4-triazole-3,5-dione (PTAD) to achiral dienes: 2,4-pentadienoic acid, methyl 2,4-pentadienoate and 2,4-pentadienol [5].

In this article we have interested, the new synthesis of the racemic and optically active cycloadduct by a modification of Bol's protocol.

Thus, racemic cycloadduct (1) was obtained in a good yield by a modification of Bol's protocol, by changing the diethyl-azodicarboxylate (DEAD) instead of 4-phenyl-1,2,4-triazole-3,5-dione (PTAD). (Scheme

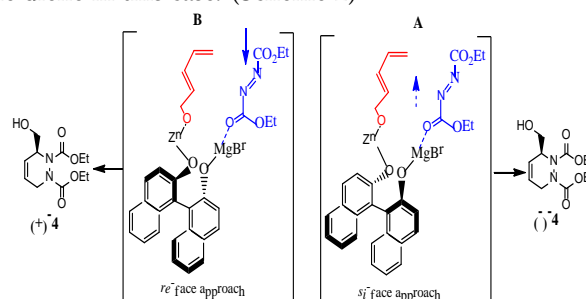
1) 2,4-Pentadienol was obtained by repeating the literature procedure [5].



Scheme 1. The synthesis of racemic and optically active cycloadducts.

Optically active (S)-diethyl 3-(hydroxymethyl)pyridazine-1,2(3H,6H) dicarboxylate (2) were synthesized based on enantioselective Diels–Alder cycloaddition of achiral (2E)-Penta-2,4-diene-1-ol to diethyl azodicarboxylate in the presence of (S)-BINOL chiral catalyst. In order to form chiral center reagent were tethered to (S)-1,1'-binaphthalene-2,2'-diol (BINOL) in a bimetallic complex with magnesium and zinc (Scheme 1). Cycloaddition reactions of Penta-2,4-diene-1-ol with diethyl azodicarboxylate in the presence of (S)-BINOL occur through the attack to the si face of diene. This was confirmed by transformation of the resulting cycloadduct into the known 5-epi-1-azafagomine through oxidation with osmium tetroxide followed by hydrazinolysis. The resulting product had an optical rotation +22.7°, in agreement with the value for chiral 5-epi-1-azafagomine reported in the literature [6].

The reactions with (R)-BINOL gave products with the same ¹H and ¹³C NMR spectra as those obtained with (S)-BINOL, but their optical rotation was opposite, showing that the DEAD attacks the re-face of the diene in this case. (Scheme 2)



Scheme 2. Approaches of DEAD in the presence of (S)-BINOL (A) or (R)-BINOL (B)

At the end of the reaction purification of (S)-BINOL by dry-flash chromatography give a chance to use

catalyst constantly without losing activity. Recycling method of catalyst brings economical and ecological benefits. The structures of synthesized compounds were proved by IR, ^1H NMR, ^{13}C NMR, HRMS (ESI) spectroscopies. ^1H NMR spectrum of compound (1-2) showed 1:1 of rotamers A and B. In some regions of the ^1H NMR spectrum the duplication of peaks. ^{13}C NMR spectrum shows either broad peaks or duplication of signals for all carbons. These phenomena are probably related to the difficulty of nitrogen's inversion due to the two bulky groups attached to them.

4. CONCLUSION

In conclusion, the reaction of diethyl azodicarboxylate with Penta-2,4-diene-1-ol in the presence of a bimetallic complex of zinc and magnesium tethered to BINOL gave the product (2) in high yield and with total enantioselectivity. Synthesized compounds (1-2) were used to obtain racemic 5-epi-1-azafagomines and optical active 1-azafagomines.

5. REFERENCES

1. Bols M. et al. / European Journal of Organic Chemistry 1997, № 6, p. 940–947.
2. Lopez O. L. et al. / Chem. Bio. Chem. 2007, № 8, p. 657–661.
3. Truscheit E. et al. / Chemistry and Biochemistry of Microbial α -Glucosidase Inhibitors Ed. Engl. 1981, v. 20, 8, p. 744–761.
4. Lew W. et al. / Bioorganic & Medicinal Chemistry Letters, 1998, v. 8, 23, p. 3321–3324.
5. Petty P. J. et al. / In Organic Syntheses, Coll, Organic Syntheses. 1988, v. 6, p. 95–98.
6. Costa M. J. et al. / The Journal of Organic Chemistry 2011, v. 76, 23, p. 9584–9592.

SYNTHESIS OF DIHALOGENDIAZADIENE AND FARMAZAN DERIVATIVES
IN THE CATALYTIC OLEFINIZATION REACTIONN.G.SHIKHALIEV^{1*}, G.T.SULEYMANOVA¹, Kh.N.BAGIROVA¹, U.F.ASGEROVA¹,
Kh.A.GARAZADEH¹, G.V.BABAYEVA¹, N.E.AHMEDOVA¹, V.G.NENAJDENKO²¹Baku State University, Z.Khalilov 23 Str., Baku, Azerbaijan²Lomonosov Moscow State University, Leninskiye Gory, Moscow, 119899

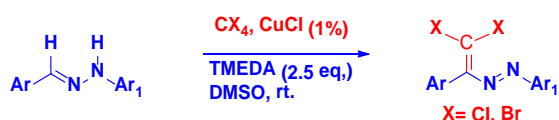
The presence of intermolecular non-covalent π - π^* interactions in the corresponding phenylhydrazon (3) synthesized on reaction of 4-(dimethylamino)benzaldehyde with 4-hydrazinylbenzonitrile have been determined by the X-ray method. Unlike other reactions, π - π^* non-covalent interactions, obtained due to the presence of electron donor dimethylamine group in aldehyde and electron acceptor CN group in hydrazine fragment have a profound effect on the direction of the reaction, the output of the products received, and the design of the crystal. Along with this, it has been established that, in addition to dioxordiazadiene, the phenylhydrazones have been dimerized as a result of their attraction on "head-tail" principle, and this has led to the synthesis of farmazan, the main product in the reaction.

PACS numbers: 61.66.hq, 61.05.c

Key words: Catalytic olefinization reaction, phenylhydrazon, diazabutadiene, π - π^* non-covalent bond, dimeric product*E-mail: namiqst@gmail.com

1. INTRODUCTION

The synthesis reactions of corresponding dichlorodiazadiene derivatives from the catalytic olefinization reaction of N-substituted hydrazons of many aldehydes with polyhalomethanes in the presence of CuCl catalyst were investigated.



Scheme 1. Synthesis of dihalodiazodienes

Unlike other phenylhydrazines, in the same reaction conditions as (E)-4-(2-(4-(dimethylamino)benzylidene)hydrazinyl) benzonitrile synthesized on the basis of 4-cyano-phenylhydrazine and 4-dimethylaminobenzoic aldehyde, it is not appropriate dioxordiazadiene, but farmazan derivative was obtained as a result of dimerization of phenylhydrazone and its structure has been confirmed by X-ray analysis.

The reason for the formation of farmazan derivative is the difference of electron density of benzene rings in (E)-4-(2-(4-(dimethylamino)-benzylidene) hydrazinyl) benzonitrile. As a result of the π - π^* non-covalent interaction between the benzene rings, the distance between the molecules has been reduced, and it is resulted in the crosslinking of hydrazone molecules.

2. EXPERIMENTAL PART

The X-ray analysis of the compounds 1,2,5 and 7 was carried out using of Bruker APEX II CCD diffractometer ($T = 273$ K, λ MoK α -radiation, graphite monochromator, φ - and ω -scanned). The NMR ¹H and ¹³C spectra were obtained by the Bruker Avance 300 (working frequency 300 and 75 MHz solvents CDCl₃ and DMSO-d₆). TMS was used as a standard, and TLC was carried out on the Silufol on UB-254, for visualization of the spots was used the KMnO₄ solution and UB lamp. Column chromatography was carried out using silica gel (Merck 63-200).

The general method of synthesis of hydrazones:

Ethanol (20-50 ml) and 0.820 g of CH₃COONa (10 mmol) are added to phenylhydrazine (5 mmol) in the tripod tubular flask. Then 5 mmol of aldehyde dropwise added and reaction mixture is stirred and heated. When the temperature reaches 78 ° C, the mixture is boiled for 5-10 minutes. Then, the reaction mixture is cooled to room temperature, 50 ml of distilled water is added to reaction mixture. Temperature reaches 60 ° C at intensive stirring. The cooled to room temperature reaction mixture is filtered. If necessary, the residue of the product is washed with distilled water. The resulting hydrazone is dried at ambient temperature (15-20 hours). The NMR ¹H and ¹³C spectra are compatible with the literature, **Substance 1:** yield 90

%, yellow solid substance, ^1H NMR (300 MHz, $\text{DMSO}-d_6$) δ 10.89 (s, 2H), 8.26 (s, 2H), 8.16 (dd, $J = 8.1, 1.6$ Hz, 2H), 8.00 – 7.91 (m, 2H), 7.70 (t, $J = 7.7$ Hz, 2H), 7.48 (s, 1H), 7.47 (dt, $J = 15.5, 1.7$ Hz, 1H), 7.26 (t, $J = 7.8$ Hz, 4H), 7.11 (d, $J = 8.0$ Hz, 4H), 6.82 (t, $J = 7.3$ Hz, 2H). ^{13}C NMR (75 MHz, $\text{DMSO}-d_6$) δ 147.18, 144.98, 133.53, 131.08, 130.38, 129.67, 128.56, 127.41, 124.95, 120.24, 112.88.

Substance 4: yield 85%, brown solid substance, ^1H NMR (300 MHz, $\text{DMSO}-d_6$) δ 7.81 – 7.73 (d, 2H), 7.65 – 7.55 (m, 3H), 7.33 – 7.28 (d, 2H), 7.13 – 7.09 (d, 2H), 6.2 (s, 1H), 3.71 (s, 3H); ^{13}C NMR (75 MHz, $\text{DMSO}-d_6$) δ 168.14, 160.66, 155.74, 138.60, 126.81, 124.71, 120.33, 117.11, 115.21, 111.15, 54.35

Substance 6: yield 74%, white solid substance ^1H NMR (300 MHz, DMSO) δ 10.10 (s, 1H), 7.77 (s, 1H), 7.49–7.46 (d, 2H), 7.22–7.19 (d, 2H), 7.02–6.99 (d, 2H), 6.73–6.70 (d, 2H), 2.93 (s, 6H). ^{13}C NMR (75 MHz, DMSO) δ 150.86, 145.20, 139.06, 129.24, 127.44, 123.77, 121.43, 113.44, 112.50, 40.37

The general preparation method of dichlorodiazabutadienes

1 mmol of starting (E)-4-(2,2-dichloro-1-phenylvinyl) diazenyl)phenyl) methanes is added to the flask, then 10–12 ml of DMSO , and then (290 mg; 1.25 mol / eq) TMEDA are added. Further catalyst CuCl (6 mg; 3 mol%) is added. Finally, CCl_4 (4–5 mol / eq., 1.5 g) is added. The reaction mixture was stirred. Typically, the reaction goes in 1.5–3 hours. At the end of reaction 50–60 ml of water is added. Then the product of reaction is extracted with methylene chloride (3 * 15 ml). After washing with water (3 * 50 ml) organic phase washed once with saturated NaCl solution (1 * 50 ml). Dried with Na_2SO_4 (MgSO_4), filtered and dichloromethane was removed by rotor evaporation in the vacuum. The residue (eluent is dichloromethane / hexane 1: 5) is purified by column chromatography method. Fractions containing the main reaction product identified by TLC

Substance 2: yield 70%, brown solid substance, ^1H NMR (300 MHz, CDCl_3-d_6) δ 9.00 (s, 1H), 7.75 – 7.69 (m, 2H), 7.62 – 7.56 (m, 2H), 7.36 – 7.28 (m, 4H), 7.13 (dt, $J = 7.5, 1.1$ Hz, 2H), 7.02 – 6.96 (m, 2H), 6.75 – 6.69 (m, 2H), 6.60 – 6.54 (m, 2H), 3.79 (s, 1H), 3.02 (s, 12H), 2.69 (s, 1H). ^{13}C NMR (75 MHz, CDCl_3) δ 153.47, 150.55, 145.96, 143.65, 132.02, 130.02, 129.22, 128.34, 125.09, 123.90, 122.33, 120.13, 118.11, 116.75, 112.77, 112.13, 107.37, 54.40, 40.42.

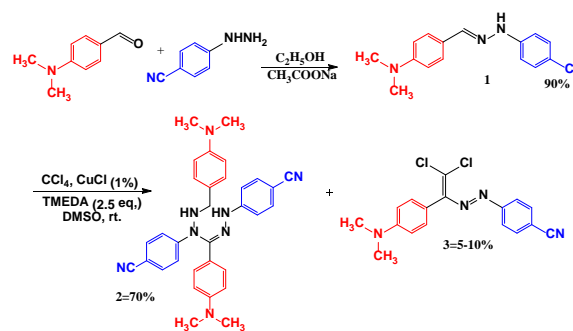
Substance 3: yield 5–10%, red solid substance, ^1H NMR (300 MHz, CDCl_3-d_6) δ 7.89–7.86 (d, 2H, $J = 9$ Hz), 7.77–7.74 (d, 2H, $J = 9$ Hz), 7.09–7.06 (d, 2H, $J = 9$ Hz), 6.79–6.75 (d, 2H, $J = 12$ Hz), 3.04 (s, 6H); ^{13}C NMR (75 MHz, CDCl_3) δ 162.08, 154.31, 152.59, 146.76, 135.98, 132.50, 131.25, 128.75, 120.90, 117.76, 115.52, 38.42.

Substance 5: yield 55%, red solid substance, ^1H NMR (300 MHz, CDCl_3-d_6) δ 7.90 – 7.84 (m, 2H), 7.46 – 7.40 (m, 2H), 7.24 – 7.18 (m, 2H), 6.85 – 6.80 (m, 2H), 3.80 (s, 3H). ^{13}C NMR (75 MHz, CDCl_3) δ 160.00, 152.31, 147.76, 134.98, 133.50, 131.76, 131.31, 122.90, 116.76, 114.52, 114.32, 55.35.

Substance 7: yield 62%, red solid substance, ^1H NMR (300 MHz, CDCl_3) δ 7.81–7.78 (d, 2H), 7.46–7.43 (d, 2H), 7.13–7.10 (d, 2H), 6.80–6.77 (2H), 3.05 (s, 6H). ^{13}C NMR (75 MHz, CDCl_3) δ 152.41, 151.45, 150.29, 137.26, 135.11, 131.08, 129.27, 124.50, 119.11, 111.48, 40.29.

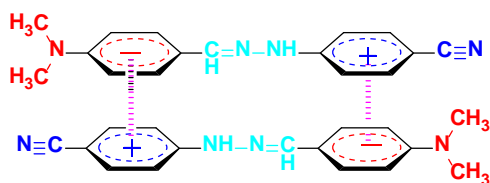
3. RESULTS AND DISCUSSION

In contrast to the reactions carried out with other phenylhydrazones [1–9] during the reaction of the phenylhydrazone (1) synthesized on the basis of 4-dimethylaminobenzaldehyde and 4-cyanophenylhydrazine farmazan derivative (2) was synthesized as a main product (Scheme 2).



Scheme 2. The synthesis of compounds 3–5

The reason for the formation of the dimerization product (2) is related with the difference of electron density of benzene rings in (E)-4-(2-(4-(dimethylamino)-benzylidene)hydrazinyl) benzonitrile. As a result of the $\pi-\pi^*$ non-covalent interaction between the benzene rings, the distance between the molecules has been reduced, and it is resulted in the crosslinking of hydrazone molecules (Scheme 3).



Scheme 3. π - π interactions between benzene rings.

The structure of the synthesized (1) and (2) compounds has been confirmed by the X-ray method.

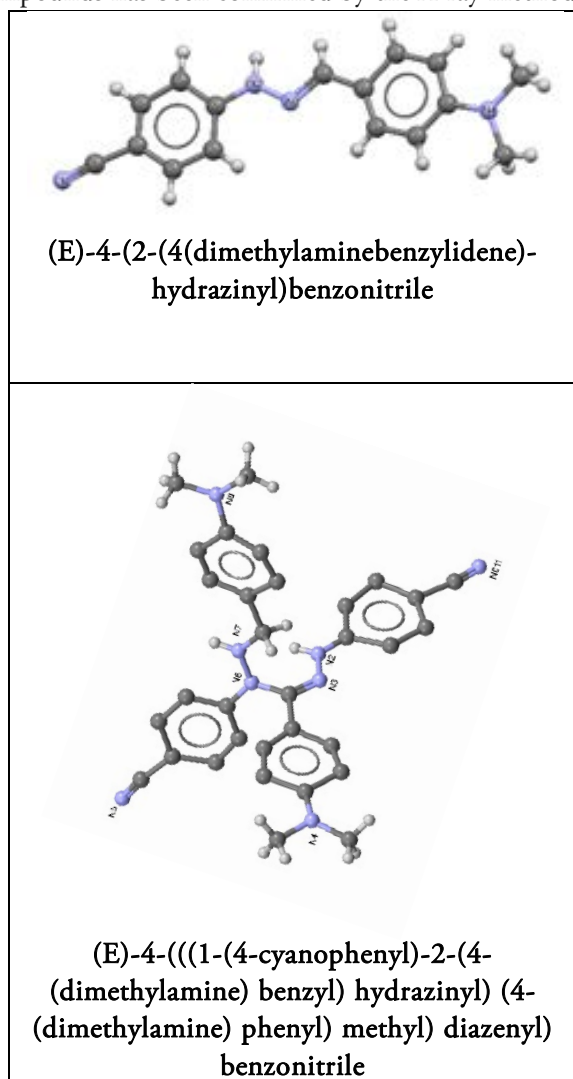


Figure 1. The structure of (E)-4-(2-(4(dimethylamine)benzylidene)hydrazinyl) benzonitrile and (E)-4-(((1-(4-cyanophenyl)-2-(4-(dimethylamine)benzyl)hydrazinyl)(4-(dimethylamine)phenyl)methyl)diazanyl) benzonitrile

The crystallographic and structural data of the compounds obtained are given in the following table.

Table 1. Crystallographic and structural data of compounds 1 and 2

	1	2
Formula	$C_{16}H_{16}N_4$	$C_{32}H_{32}N_8$
Mr	264	528
Crystal cage	Monoclinic	Triclinic
Spacial group	$P2_1/n$	P_1
a, (Å)	6.0325(8)	11.3580(19)
b, (Å)	7.5897(10)	11.732(2)
c, (Å)	30.814(4)	12.428(2)
α , °	90°	108.058(5)°
β , °	90.885(5)°	98.545(5)°
γ , °	90°	99.731(5)°
V, (Å ³)	1410.6(3)	1515.8(5)
ρ (calc.),g/cm ³	1.278	1.009
Z	4	4

It should be noted that the main method of formazan synthesis involves the interaction of bis-diazo salts with methylene-active and methyne compounds, typical yields being within 10-50% [10].

Representatives of the farmazan family are applied for the synthesis of different heterocycles, while the "formazan - tetrazolium salt" system is widely used as a redox-based staining component for different biochemical studies. Moreover, formazans are valuable spectrophotometric analytical agents and ionophors; they can be used for the simultaneous selective determination of several metal cations. Polymers with formazan moieties are known as selective complexing sorbents for the concentration of micro quantities of elements. The high photo- and thermo-resistance of some formazan complexes allow their application as registering components in optical data storage devices [11].

Farmazans can also be used as antiviral agents. Thus, 1-aryl-3-(5-substituted indolyl)-5-(1-naphthylacetyl) farmazans have a negative effect on the Ranikhet Disease Virus (RDV) and Vaccinia Virus (VV) in the vitro system. Some of the compounds have shown promising activity against either one of these or both the viruses in vitro.

Based on these positive characteristics of farmazans, this reaction can be used in a wide range as a new preparation method of these compounds.

It should be noted that the energy of non-covalent bonds is significantly lower than the energy of

corresponding covalent bonds, but their diversity and dissemination may have a general effect on the reaction [12]. This idea, that is, the existence of intermolecular π - π * non-covalent interactions has been confirmed by the X-ray method (Figure 2). As it is seen from the structural formula, due to the π - π * interaction effects (2.852Å) formed as a result of the mutual attraction of the benzene rings and the two hydrogen bonds (2.721Å), (2.571Å) created by the nitrile group with adjacent molecules, molecules are maximally approximated to each other according in horizontal direction to "tail-tail", in parallel - "head-tail" principle [13-17]. It is resulted in the formation of dimerization product 2 ((E)- (4 (((1-(4-cyanophenyl)-2-(4-(dimethylamine)benzyl)hydrazinyl)(4-(dimethyl-amine) phenyl)methyl)diazenyl)benzonitrile). (Figure 2)

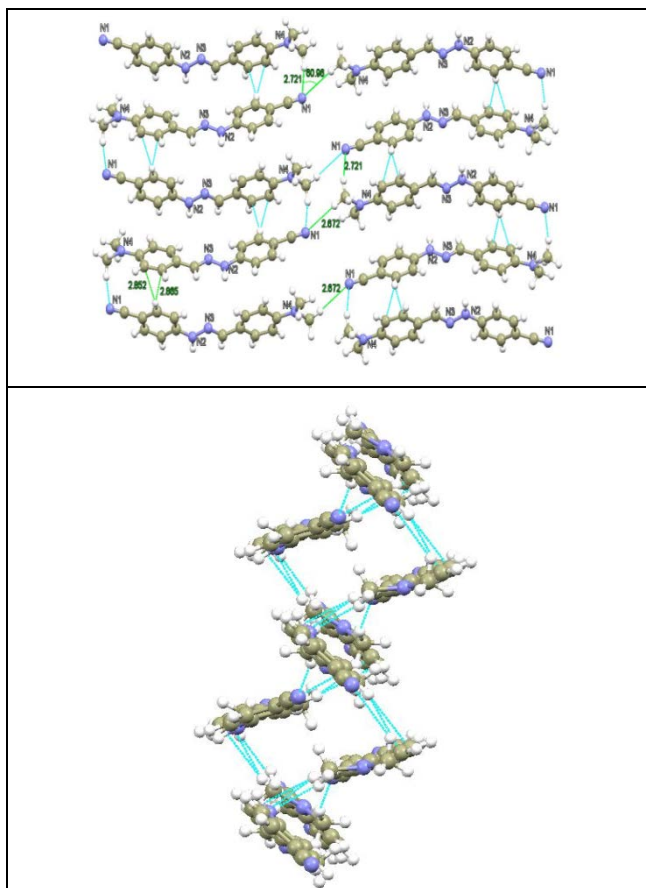


Figure 2. π - π * interactions in the compound 3, hydrogen bonds are shown in broken lines.

While literature has been reported to have information on this type of dimerization reaction of phenylhydrazones [18-20], its structure has never been confirmed by the X-ray method.

For example, the obtaining of dimerization product as intermediate during the oxidation of aldehydes to

appropriate acids based on phenylhydrazones can be confirmed by Mass Spectroscopy and NMR method [18]. Thus, the authors note that the dimerization product is unsustainable, and they could investigate the structure only through these methods. In our case, the monocrystals of the dimerization product have been grown and the structure has been studied by X-ray method. If we look at compound 1, we see that the main reason for the durability of the compound is the presence of two strong intermolecular hydrogen bonds ($\text{NH}\cdots\text{N}\equiv\text{C}$ (2.298Å) and $\text{Ar-H}\cdots\text{N}\equiv\text{C}$ (2.645 Å)).

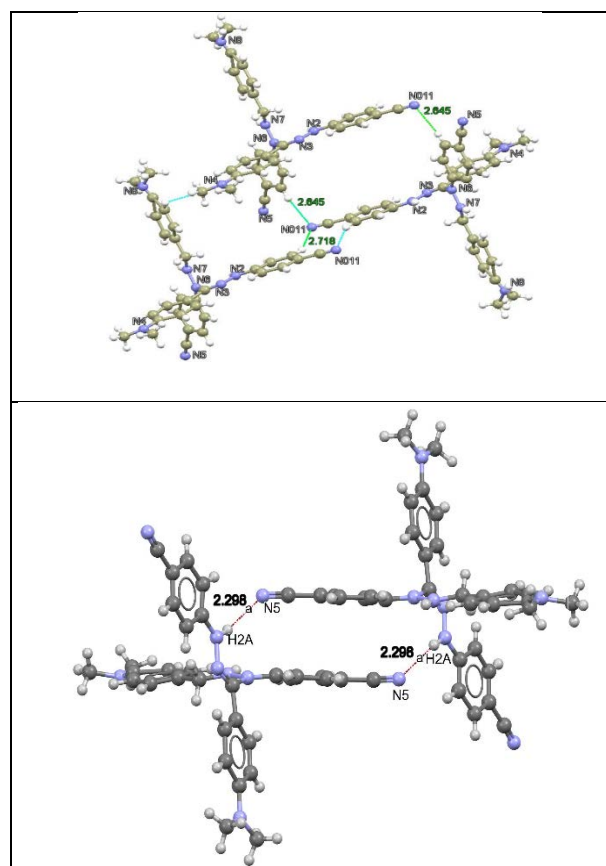
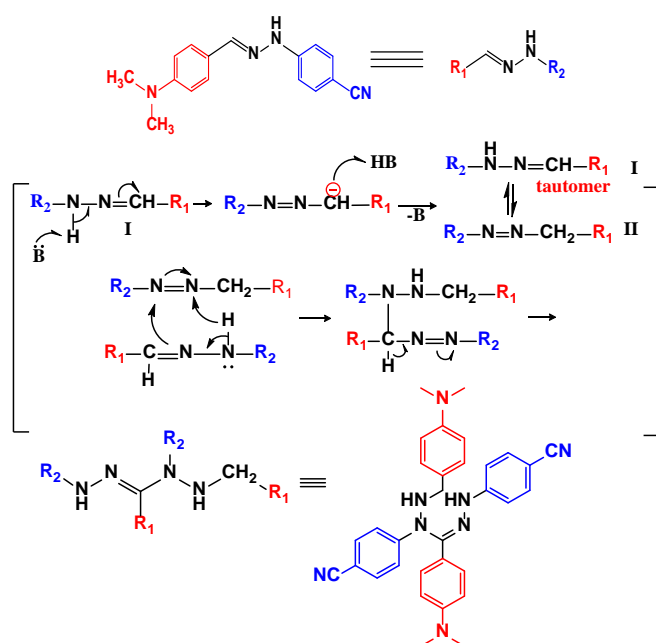


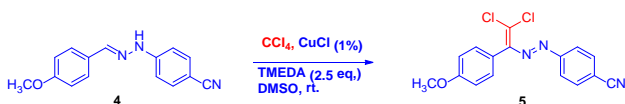
Figure 3. The intermolecular hydrogen bonds in compound 4 are shown in broken lines.

Based on the foregoing, the mechanism to obtain the dimerization product is shown in the following scheme. First, phenylhydrazone transfers into tautomeric form II in the TMEDA environment. Subsequently, as the result of the relative closeness location of the azine to the hydrazone, the intermolecular crosslinking (the formation of C-N bond) and as the result of the corresponding groupings the obtaining of farmazon derivative 2 occur. In general, it is possible to propose the following scheme for the reaction mechanism as these transformations are synchronized:

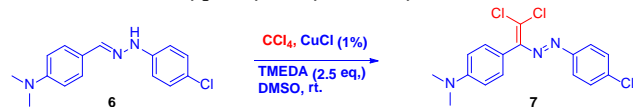


Scheme 4. A general mechanism for obtaining of compound 2

Note that, in the case of electron donor (-OCH₃) methoxy group instead of -N(CH₃)₂ group in para-position, and Cl instead of CN group only dichlorodiazadiene products are obtained. It can be concluded, that the main cause of dimerization is the presence at the same time of p-N(CH₃)₂ and p-CN groups in phenylhydrazone. Scheme 5-6



Scheme 5. The synthesis reaction of (E)-4-((2,2-dichloro-1-(4-methoxyphenyl)vinyl)diazenyl)benzonitrile



Scheme 6. The synthesis reaction of (E)-4-(2,2-dichloro-1-((4-chlorophenyl)diazenyl)vinyl)-N,N-dimethylaniline

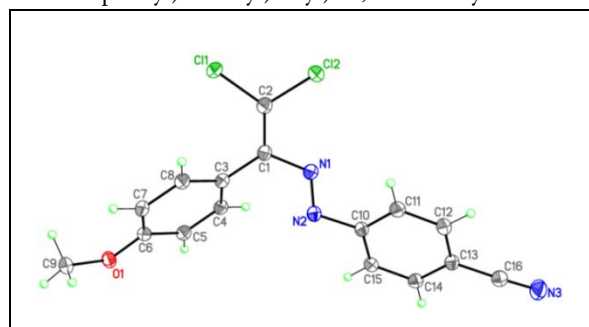


Figure 4. The molecular structure of (E)-4-((2,2-dichloro-1-

(4-methoxyphenyl)vinyl)diazenyl)benzonitrile

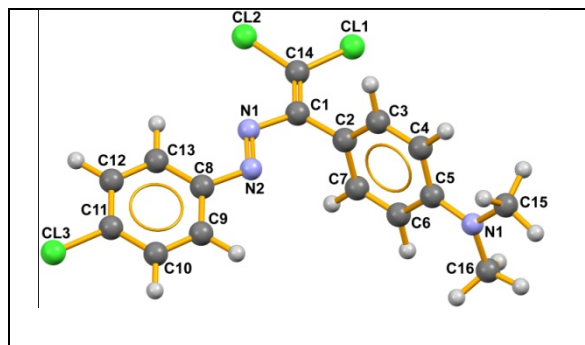


Figure 5. The molecular structure of (E)-4-(2,2-dichloro-1-((4-chlorophenyl)diazenyl)vinyl)-N,N-dimethylaniline

4. CONCLUSION

Thus, the presence of intermolecular non-covalent π - π^* interactions in the corresponding phenylhydrazone (1) synthesized on reaction of 4-(dimethylamino)benzaldehyde with 4-hydrazinylbenzonitrile have been determined by the X-ray method. Unlike other reactions, π - π^* non-covalent interactions, obtained due to the presence of electron donor dimethylamine group in aldehyde and electron acceptor CN group in hydrazine fragment have a profound effect on the direction of the reaction, the output of the products received, and the design of the crystal. Along with this, it has been established that, in addition to dioxidiazadiene, the phenylhydrazones have been dimerized as a result of their attraction on "head to tail" principle, and this has led to the synthesis of farmazan, the main product in the reaction.

5. ACKNOWLEDGMENTS

This work was supported by the Science Development Foundation under the President of the Republic of Azerbaijan- Grant No EIF-BGM-4-RFTF-1/2017-21/13/4

6. REFERENCES

1. Nenajdenko V.G. et al. *IACS Catal*, 2017, vol. 104, 3, p.1-6 – 672
2. Shikhaliyev. N. Q. et al./*Dyes and Pigments*, v. 150, March 2018, p. 377–381
3. A.M.Maharramov. et al./*Dyes and Pigments*/ v. 159, December 2018, p 135-141
4. Shikhaliyev N.Q. et al./ *News of Baku University*, 2016, №1, p.40-49.
5. Shikhaliyev N.Q. et al./ *News of Baku University*, 2016, №3, p.5-12

6. Israyilova A. et al./International Journal of Innovative Research in Science, Engineering and Technology. v.6, 8, August 2017. p.1111-1115
7. Maharramov A.M. et al./Physics, Chemistry and Biology of Low Dimensional Systems. BSU Publication, Journal of Low Dimensional Systems, v.1 (1), 2017. p.4-7
8. A.M.Maharramov. et al.Chemical Problems Journal, 2018, №2, p-230-238.
9. Maharramov A.M. et al./ Physics, Chemistry and Biology of Journal of Low Dimensional Systems,BSU Publication, Journal of Low Dimensional Systems, v. 2 (1), 2018, p-37-44.
- 10.Yauhen Yu., Karabach. et al./Synthesis, application and coordination chemistry of formazans, Nova, 2014, p-249-274
- 11.Murali Manohar Tiwari. et al./ Indian J Pharm/ 1995, 57(3), pp 113-116
- 12.Maharramov A.M. et al./ Non-covalent interactions of water with metal complexes in solution, Antonio romerosa and franco scalambra, non covalent interactions in the synthesis and design of new compounds, Willey,2016, p 85-99
- 13.Hernandez Losada. et al./ Journal of Physical Chemistry A, 2000, v. 104, 3, p. 661 – 672
- 14.Higuchi et al./Bulletin of the Chemical Society of Japan, 2001, v. 74,12, p. 2467 – 2467.
- 15.Socrates et.al./Bulletin of the Chemical Society of Japan, 2001, v.74, p. 179 – 180.
- 16.Hu Xian-Lei. et al./Iron and Steel (Peking), 2007, v. 42, 4, p. 50 – 52.
- 17.Angiolini et al./ Synthetic Metals, 2015, vol. 202, p. 169 – 176
- 18.Kristyna Burglova et al./ European Journal of Organic Chemistry, 2017 (2), 389-396
- 19.Xiaohu Deng et al./ Organic letters, 2008, 10, 6, 1307-1310.
- 20.Fomenko. et al./ Chemistry of Heterocyclic Compounds , 1976, v. 12, p. 527 – 532.

NEW THREE-COMPONENT CONDENSATION IN THE PRESENCE OF
BENZYLIDENE ACETOPHENONES

A.I. ISMIYEV, K.E. HAJIYEVA*

Baku State University, Z.Khalilov 23 Str., Baku, Azerbaijan

A new three-component condensation of benzylidene acetophenones with acetoacetic ether and malonodinitrile in a molar ratio of 1: 1: 1, respectively, in the presence of an equimolecular amount of morpholine and glacial acetic acid as a catalyst, which allows the synthesis of ethyl 4,6-diaryl-2-dicyanomethylenecyclohex-3-en-1-carboxylates was established

PACS numbers:82.39.-k, 87.68.+z

Keywords:three-component condensation, benzylidene acetophenones, ethyl acetoacetate, malononitrile

*E-mail:kushvar.hajiyeva@gmail.com

2. INTRODUCTION

Multicomponent reactions involving simultaneous interaction of at least three compounds, forms one final substance which contains parts of all the starting components, proceed in the smallest number of stages in a single reactor with a good overall yield including the use of accessible and safe substances and solvents, also forms few by-products. These reactions have firmly entered to the synthetic arsenal of modern organic chemistry, by contributing to the formation of new chemo-, regio, stereo- and enantioselective methods for the synthesis of polyfunctional carbo- and heterocycles that have useful properties [1-5]. In all the diversity of reagents of multicomponent reactions, we would like to emphasize ethyl acetate and malonodinitrile, the usefulness of which is due to

- their accessibility;

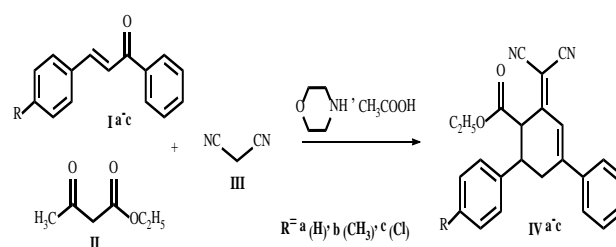
-high reactivity, which allows planning and implementing multicomponent syntheses on their basis, by varying the structures of reactants [6,7].

3. EXPERIMENTAL

A series of ethyl 4, 6-diaryl-2-dicyanomethylenecyclohex-3-en-1-carboxylates (**IVa-c**) were synthesized by one-pot multicomponent reactions of benzylidene acetophenones (**I a-c**), ethyl acetoacetate and malononitrile in the presence of morpholine. As a result, ethyl 4,6-diaryl-2-dicyanomethylenecyclohex-3-en-1-carboxylates (**IVa-c**) were isolated as a reaction products with 63-72% yield (scheme 1)

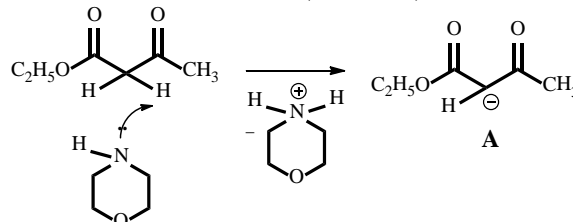
As to the mechanism of reaction, the process is

multi-stepped, though it is one-way. In modern science, such reactions are called cascade or tandem reactions.



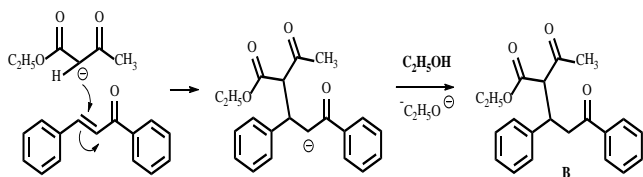
Scheme 1. The synthesis of compound IV a-c

In other words, the new functional group or reaction center that forms in the firststage of the reaction results in the subsequent phase. In our case, it is possible to say that the reactionwas proceed bycascademechanism.First, morpholine, which is the basic catalyst at the first stage, breaks the active methylene hydrogen in the acetate ether and forms carboanion A (scheme 2)



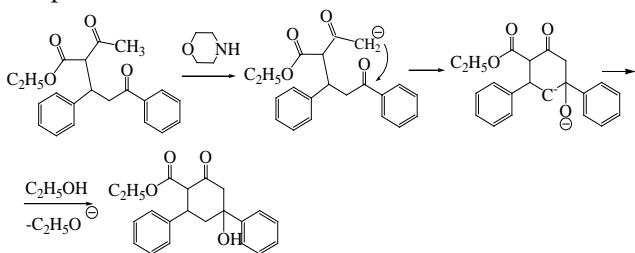
Scheme 2. The formation of carboanion A

The carboanion A obtained from the first phase of the reaction is coupled to the C = C bond activated by carbonyl group's electron-acceptor effect for nucleophilic (**I a-c**) compounds and forms intermediate B (scheme 3)



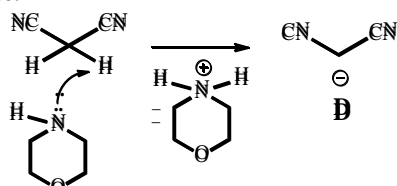
Scheme 3. The formation of intermediate B

It is impossible to predict the pathway of the next stage. From the structures of reaction products (IV a-c), it can be assumed that by the influence of morpholine the methyl group of acetyl group undergoes intramolecular ketolization through formation of carboanion. The carbocyclization results in the formation of thermo-dynamically stable cyclohexane ring (scheme 4). In our view, morpholine's basicity can be enough only for realizing these transformations. It is not possible to claim that the cyclohexene ring formed due to the dehydration, occurs in the presence of morpholine



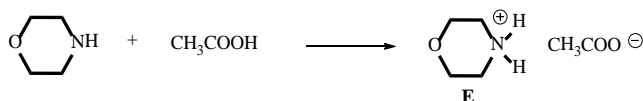
Scheme 4. The formation of cyclohexane ring

Malononitrile is also an active methylene grouped compound. Since the nitrile group is a strong electron-withdrawing group, it results in the increase of acidity of the C-H bonding (scheme 5). Thus, malononitrile can easily be converted to carboanion (D) by the effect of morpholine:



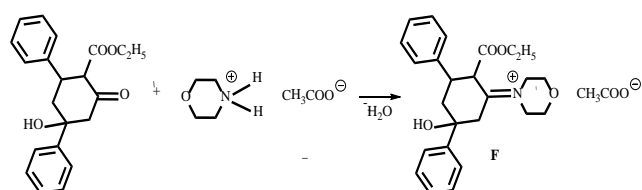
Scheme 5. The formation of carboanion D

After the reaction was carried out at room temperature, morpholine acetate salts (E) are obtained by addition of icy acetic acid to the mixture (scheme 6)



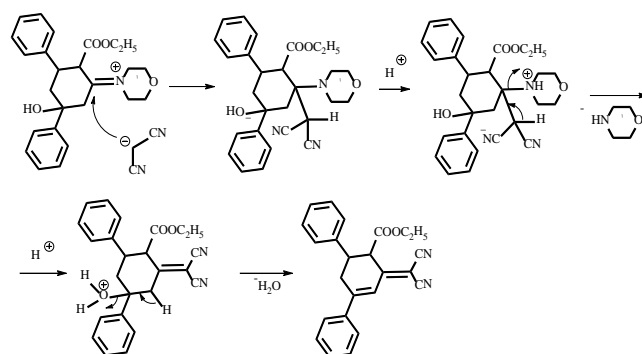
Scheme 6. The formation of morpholine acetate salt (E)

From catalytical point of view obtained morpholine acetate salt plays a crucial role in this reaction. The fact is that, malononitrile easily undergoes Knevenagel condensation with aldehydes. However, as the carbonyl activity of ketones is relatively low compared to aldehydes, when the reactions with malononitriles are carried out in the catalytic presence of amines the result is not achieved. Such reactions are usually carried out in the presence of ammonium acetate. In our case, morpholinacetate causes condensation of malononitrile with the ketone group. First, activated (F) intermediate formed (scheme 7)



Scheme 7. The formation of intermediate F

The formation of C-C bonding by the combination of malononitrile into the iminium salt (F) can be explained by the electron-withdrawing effect of the positively charged nitrogen atom. It is assumed that the intermediate (K) obtained from the combination of malononitrile on C = N bonding can be converted into interval (L) by the separation of morpholine molecule due to the effect of proton. At the last stage, dehydration occurs by the effect of an acidic proton (scheme 8)



Scheme 8. Reaction mechanism for the synthesis of compounds IV a-c

The structure of the synthesized compounds (IVa-c) were determined by IR- and NMR spectroscopy methods.

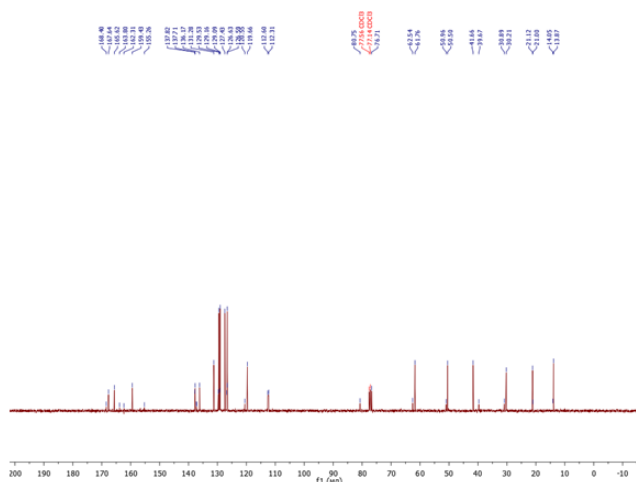


Figure .1 The ^{13}C NMR spectra of ethyl 4-(4-methyl)-6-phenyl-2-dicyano- methylenecyclohex- 3-ene-1-carboxy-late (IV b)

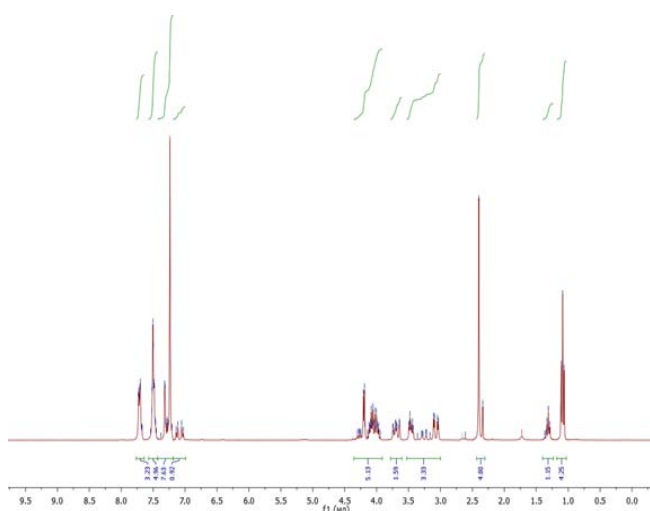


Figure 2. The ^1H NMR spectra of ethyl 4-(4-methyl)-6-phenyl-2-dicyano-methylenecyclohex-3-ene-1-carboxy-late(IV b).

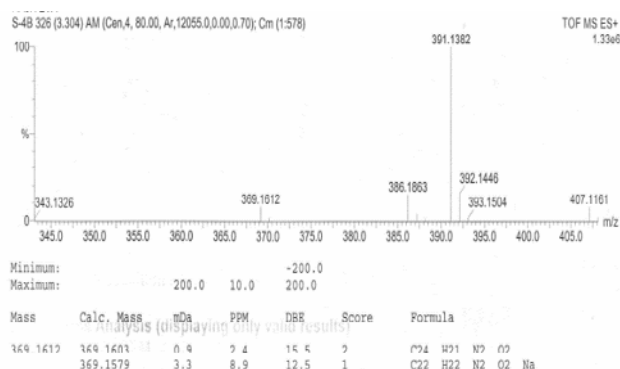


Figure 3. The mass spectra of ethyl 4,6-diphenyl-2-dicyanomethylenecyclohex-3-ene-1-carboxylate (IV a)

4. RESULTS AND DISCUSSION

^1H and ^{13}C NMR spectra recorded on a Bruker AC-300 instrument (300 MHz on ^1H and 75 MHz nuclei at ^{13}C cores) in a CDCl_3 solution, residual signals of the solvent used as the standard. IR spectra recorded on a Varian 3600 FT-IR Excalibur Series IV FTIR spectrometer in KBr tablets. Mass spectra obtained on a Waters Q-TOF Premier (ESI) spectrometer. The melting points were determined on a Kofler's table. TLC monitored the purity of the resulting compounds on Silufol UV-254 plates, eluent acetone-hexane 1: 1, developer-iodine vapor, UV detector

The general method of synthesis of ethyl 4,6-diaryl-2-dicyanomethylenecyclohex-3-en-1-carboxylates (IV a-c)

10-mmol benzylidene acetophenones (1 a-c) and 10-mmol ethyl acetoacetate added to 15 ml ethanol. While mixing 10 mmol morpholine was added to the reaction mixture drop by drop. After keeping for 24h at room condition, 10 mmol malononitrile and 10 mmol glacial acetoacetic acid added and reaction mixture was heated till 70°C and at this condition it was stirred for 6 h. After cooling, bright yellow crystals were precipitated and filtered. The yellow crystals obtained by evaporation of filtrate, was also combined with initial crystals and recrystallized again in ethanol.

Ethyl 4,6-diphenyl-2-dicyanomethylenecyclohex-3-ene-1-carboxylate (IV a), pale yellow solid, $t_{m,p} = 157^\circ\text{C}$, yield: 72%

^1H NMR (300 MHz, CDCl_3 , δ , ppm): 1.18 t (3H, CH_3), 3.0 d (1H, CH), 3.2 d (1H, CH), 3.4-3.6 m (1H, CH), 3.8-4.0 q (2H, CH_2), 4.2 d (1H, CH), 7.20-7.4 m (5H, Ar), 7.40-7.50 m (3H, Ar), 7.4-7.8 m (2H, Ar); ^{13}C NMR (75 MHz, CDCl_3 , δ , ppm): 13.86 (CH_3), 30.22 (CH), 41.64 (CH_2), 50.6 (CH), 61.74 (OCH_2), 112.32 (CN), 112.6 (CN), 119.64 (CH), 126.62 (2CH), 127.42 (2CH), 129.08 (2CH), 129.52 (2CH), 131.26 (CH), 136.16 (C), 137.68 (C), 159.40 (2C), 165.60 (2C), 167.62 (COO); HRMS: calcd for $\text{C}_{24}\text{H}_{21}\text{N}_2\text{O}_2[\text{M}+\text{H}]^+$ 369.1603, found 369.1612

Ethyl 4-(4-methyl)-6-phenyl-2-dicyanomethylenecyclohex-3-ene-1-carboxylate (IV b), pale yellow solid, $t_{m,p} = 185^\circ\text{C}$, yield: 63%

^1H NMR (300 MHz, CDCl_3 , δ , ppm): 1.2 t (3H, CH_3), 2.35 s (3H, CH_3), 3.1 d (1H, CH), 3.4 d (1H, CH), 3.6-3.7 m (1H, CH), 3.9-4.1 q (2H, CH_2), 4.4 d

(1H, CH), 7.25-7.4 m (5H, Ar), 7.45-7.55 m (3H, Ar), 7.6-7.75 m (2H, Ar);

¹³C NMR (75 MHz, CDCl₃, δ, ppm): 13.88 (CH₃), 21.12 (CH₃), 30.21 (CH), 41.66 (CH₂), 50.5 (CH), 61.76 (OCH₂), 112.32 (CN), 112.6 (CN), 119.66 (CH), 126.63 (2CH), 127.43 (2CH), 129.09 (2CH), 129.53 (2CH), 131.28 (CH), 136.17 (C), 137.71(C), 159.43(2C), 165.62(2C), 167.64(COO); HRMS: calcd for C₂₅H₂₂N₂O₂382.45, found 382.17

Ethyl 4-(4-chloro)-6-phenyl-2-dicyanomethylene-cyclohex-3-ene-1-carboxylates (IV c), pale yellow solid, $t_{m,p}=175^{\circ}\text{C}$, yield: 68%

¹H NMR (300 MHz, CDCl₃, δ, ppm): 1.23 t (3H, CH₃), 3.2 d (1H, CH), 3.5 d (1H, CH), 3.6-3.8 m (1H, CH), 3.9-4.2 q (2H, CH₂), 4.6 d (1H, CH), 7.2-7.4 m (5H, Ar), 7.5-7.6 m (3H, Ar), 7.7-7.8 m (2H, Ar)

¹³C NMR (75 MHz, CDCl₃, δ, ppm): 13.86 (CH₃), 30.20 (CH), 41.68 (CH₂), 50.6 (CH), 61.78 (OCH₂), 112.32 (CN), 112.6 (CN), 119.68 (CH), 126.64 (2CH), 127.46 (2CH), 129.1 (2CH), 129.54 (2CH), 131.28 (CH), 136.2 (C), 137.71(C), 159.44(2C), 165.64(2C), 167.66 (COO);HRMS: calcd for C₂₄H₁₉ClN₂O₂402.87 found 402.11

5. CONCLUSION

In conclusion, we can say that multicomponent condensation of benzylidene acetophenones with acetoacetic ether and malonodinitrile in a molar ratio of 1: 1: 1, respectively, in the presence of an equimolecular amount of morpholine and glacial acetic acid as a catalyst allows the synthesis of ethyl 4,6-diaryl-2-dicyanomethylenecyclo-hex-3-en-1-carboxylates

6. REFERENCES

1. Orru R. V. A et al./ Synthesis, 2003. N.10, p.1471.
2. Carlone A et al./ Chem. Int. Ed. 2007. v.46, p. 1101-1104.
3. Hugel H./Microwave Multicomponent Synthesis, Molecules, 2009, v.14, N 12, p 4936-4972.
4. Eckert H. /Molecules, 2012, v.17, N 9. p.1074.
5. Gu Y. /Green chemistry, 2012, 14, p.2091-2128.
6. Simon C. et al. / Eur. J. Org. Chem., 2004. p. 4957-4980.
7. Shestopalov A.M., et al./ Synthesis, 2008. N1. p.1-25

CONSTRUCTION OF THE PHARMACOPHORE MODELS OF BIOLOGICALLY ACTIVE MOLECULES BASED ON A THEORETICAL APPROACH

G.AKVERDIEVA*, N.M.GODJAYEV

Institute for Physical Problems, Baku State University, Z.Khalilov, st.23, AZ-1148 Baku, Azerbaijan

Based on a theoretical approach the conformational-electronic peculiarities, which are important for the functional activity of some biologically active molecules, are revealed. By molecular mechanics, molecular dynamics and quantum chemistry methods with application of modern computer programs the conformational possibilities, electronic structure, and dynamic properties of these molecules have been investigated. Using received results and data of SAR studies the bioactive conformations of investigated molecules were assessed and the pharmacophore models for their interaction with the specific receptors were constructed.

PACS numbers: 36.20.Ey; 36.20.Fz; 36.20 Hb

Keywords: biologically active molecules, structure-function relationships, bioactive conformation, pharmacophore model

*E-mail: hagverdignara@gmail.com

1. INTRODUCTION

The development of the representations on the interaction mechanism of pharmaceutical substance with the receptor and the understanding its electoral ability are possible owing to the structure-functional investigations. Many experimental works are devoted to the structure-functional investigations of the biologically active peptide molecules. Note that none of these used methods led to a sufficient clarity, and even more so to a reasonable quantitative representation of the structure of these molecules. At present, the use of various theoretical calculation methods, the recent achievements of the computer technology, including programs with a graphic representation of spatial structures, allows researchers to construct all possible models of the peptide molecules under study. The research work conducted on the basis of molecular modeling within the framework of the pharmacophore concept is most relevant.

In this paper by molecular mechanics, molecular dynamics, quantum chemistry methods with application of modern computer programs the conformational possibilities, electronic structure, dynamic properties of the biologically active molecules – peptide T, showing therapeutic effect against a HIV, dermorphin, deltorphin I, deltorphin II opioid peptides have been investigated. As result the conformational-electronic peculiarities, which are

important for the functional activity of these peptides are revealed. On the basis of calculation results and the data of structure-activity relationships (SAR) studies the bioactive conformations of investigated molecules were assessed and the models of pharmacophore for their interaction with specific receptors were offered. An estimation of the arrangement of pharmacophore elements of the investigated molecules can be used for design of the peptidomimetics. The results of research create the prospects for the purposeful synthesis of steady medical products.

2. METHODS

Conformational energy calculations were made with an IBM computer using version of ECEPP (Empirical Conformational Energy Program for Peptides) [1,2]. The program was developed from the matrix method principle of Hermans and Ferro [3]. The conformational analysis was carried out within molecular mechanics framework. The nomenclature and conventions adopted are those recommended by IUPAC-IUB [4]. The molecular dynamics of peptide molecules was spent with use of force field AMBER in the temperature interval 293-313K with step 5K during 10 nanoseconds by means [5]. The solvation procedure with application of model of water in the set spherical volume TIP4P [6] has been used. The electronic structure of the molecules was investigated by quantum-chemistry methods [7], used the demonstration version of

software package HyperChem (<http://www.hyper.com>).

3. RESULTS AND DISCUSSION

I. Modeling of the bioactive conformation of peptide T and of the pharmacophore for its binding to the CD4 receptor

The results of the study of peptide T (H-Ala1-Ser2-Thr3-Thr4-Thr5-Asn6-Tyr7-Thr8-OH), showing the therapeutic effect against a HIV, revealed the important role of the residues of the physiologically active fragment Thr4-Thr8 in the formation of the regular structure and as a consequence, in the folding of peptide chain of whole molecule [8,9]. Comparison of the conformational characteristics of peptide T, its active and inactive analogs allowed assessing the bioactive conformation of this peptide, to reveal the structural features necessary for its biological activity [10]. In order to characterize the bioactive conformation, the structures of the peptide T and its analogs with relative energy not higher than 5 kcal / mol were compared in pairs. A comparison of conformation profiles of molecules was carried out on the basis of an analysis of the values of the root-mean-square deviations (RMSD) of the coordinates of atoms and the interatomic distances calculated under the optimal alignment of the compared structures. Comparison of the optimal structures of peptide T with a set of optimal structures common to its active analogs revealed conformations with standard deviations in the range from 0.08 to 1.25Å. The visual inspection of superimposed pairs of conformations showed that the cyclic conformation could be considered similar to peptide T and its active analogs (4-8) peptide T and [D-Ala1]- peptide T amide and therefore was evaluated as bioactive. Table 1 shows the angles of the main chain in the biologically active conformation of the peptide T and its active analogs (4-8) peptide T and [D-Ala1]- peptide T amide. The model of bioactive conformation of [D-Ala1]- peptide T amide is also stabilized by the hydrogen bond between the Thr4 and Thr8 residues, in addition to the hydrogen bond between Thr4 and Tyr7 in the native peptide (Figure 1a). It was revealed that cyclic conformation is characterized by a much smaller dipole moment than other low-energy conformations of this molecule that can be explained if take into account that the terminal charged groups in this conformation are closer in space. In cyclic conformation, Thr4 unlike other residues with OH-group, is not localized on a surface of a molecule, it is turned in inside molecules and, it as though deforms a cycle-circle and comes nearer by side tail to N - and C-terminals parts of the peptide molecule. It leads to the

redistribution of electron density and, so to changes of charge on the atoms entering in OH-groups of side chains of Thr4, Thr8 and in the C-terminal part of the molecule, and also of charge on hydrogen atoms as the backbone and side chains of the segments of the molecule which have approached in space. The received results allows us to conclude that cyclic structure corresponds to active state of peptide T, the energetically preferred formation of the regular structure element β - turn on the its physiologically active C-terminal pentapeptide fragment is necessary for binding to the CD4 receptor.

Since the peptide T and its active analogues have similar functions, it is likely to assume that these molecules interact with the specific receptors by the same pharmacophore elements. The performed calculations and SAR studies of peptide T allowed us to construction the pharmacophore model for its interaction with the CD4 receptor (Figure 1b). The proposed model contains five areas which are occupied by pharmacophore elements marked by numbers 1-5. Important elements of this pharmacophore are the carbonyl group of the CO of the Thr4 residue, the alcoholic group CH3 in the side chain of the Thr5 residue, the amide NH2 in the side chain of the Asn6 residue, the aromatic ring of the side chain of the residue of Tyr7, the carboxyl group of the terminal Thr8 residue. Note that these atomic groups can serve, respectively, as donors and H-bond acceptors, and the remaining atoms of these residues are able to participate in hydrophobic interactions with the receptor. The relative geometric arrangement of pharmacophore groups of peptide T is shown in Å.

The represented pharmacophore model can be used to search the three-dimensional structures having similar values of the geometry of pharmacophore groups in the database.

II. Modeling of the bioactive conformation of dermorphin and of the pharmacophore for its binding to the μ -opiate receptor

It was found that the optimal structures of dermorphin (H-Tyr-DAla-Phe-Gly-Tyr-Pro-Ser-NH₂) forms compact structures, in which the physiologically active N-terminal tetrapeptid fragment of has regular structure - α -spiral or **semifolded structure**, an α - amino group and the side chains of the tyrosine and phenylalanine residues are in the identical positions in space, the residues Tyr1 and Ser7 point away from the core surface of molecule [11]. It was revealed that the distribution of charges on the atoms of the α - amino group and atoms of the side chains of tyrosine and phenylalanine reidues are similar for these structures,

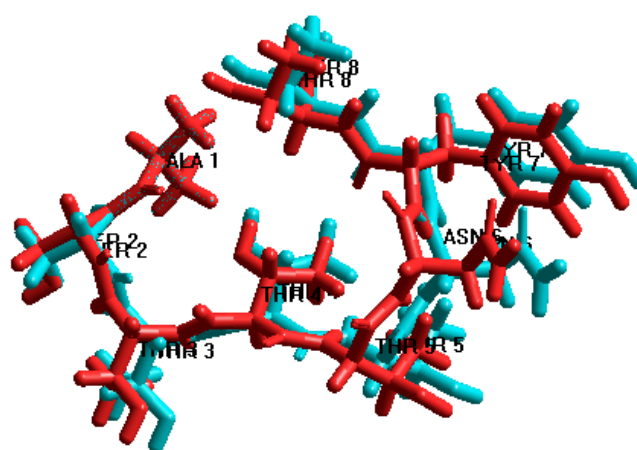
that may be correlate with their identical positions in space and ability to participate in ligand-receptor interactions.

Table 1. Backbone dihedral angles (in degrees) of proposed bioactive conformations of peptide T and its active analogues (4-8) peptide T and [D-Ala1]- peptide T amide

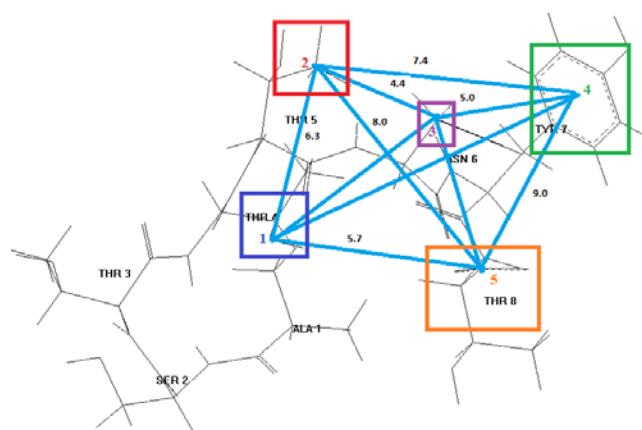
peptide T				(4-8) peptide T				[D-Ala1]- peptide T amide			
Resi- dues	ϕ	ψ	ω	Resi- dues	ϕ	ψ	ω	Resi- dues	ϕ	ψ	ω
Ala	-83	167	-173					D-Ala	157	-152	180
Ser	-68	-70	172					Ser	-52	-44	163
Thr	-102	113	180					Thr	-149	145	-175
Thr	-139	171	-178	Thr	-129	162	-173	Thr	-161	164	-170
Thr	-82	-73	-174	Thr	-84	-69	-169	Thr	-46	-48	-175
Asn	-116	-60	-171	Asn	-116	-60	-171	Asn	-178	-62	153
Tyr	-97	150	-179	Tyr	-97	150	-179	Tyr	-55	143	-164
Thr	-97	151		Thr	-100	151		Thr	-161	150	

The biologically active conformation of dermorphin was assessed by pairwise cross comparisons of the low energy conformations found for dermorphin and its tetrapeptide active analogs - strong analgesics (1-4) dermorphin and [D-Arg2]-(1-4) dermorphin, which were studied previously [12]. In order to characterize the bioactive conformation of the dermorphin, the conformation of dermorphin with a relative energy not higher than 2 kcal / mol was compared in pairs with the optimal conformations of its active analogs. The RMSD were calculated for all atoms of the main chain of four N-terminal peptide residues. Comparison of the optimal structures of dermorphin with a set of optimal structures common to its active analogs revealed conformations with standard deviations in the range from 0.09 to 1.35 Å. A visual inspection of the superimposed pairs of conformations showed that

conformations with standard deviations below 0.8 Å can be considered similar. It was found that α - amino group and the side chains of tyrosine and phenylalanine residues are in the same positions in space relative each other in similar structures of dermorphin and its active analogues. These conformations of the studied molecules were evaluated as bioactive. The dihedral angles of the proposed bioactive conformations of dermorphin and its active analogs are given in Table 2.



(a)



(b)

Figure 1. Superimposition of proposed bioactive conformations of peptide T (blue color) and its active analogue [D-Ala1] - peptide T amide (red color) (a) and the pharmacophore model for the binding of peptide T to the CD4 receptor (b)

III. Modeling of the bioactive conformations of deltorphins and of the pharmacophore for their binding to the δ -opiate receptor.

The results of the study of deltorphins (Tyr-Ala-Phe-Xaa-Val-Val-Gly-NH₂, where Xaa is Asp in deltorphin I and Glu in deltorphin II) [13] indicate that their spatial structure is characterized by conformations, in which the N- and C-terminal segments of the molecules differ on the conformational properties: Tyr-D-Ala-Phe-Asp(or Glu) sequence has folded structure close to spiral, while the Val-Val-Gly-NH₂ sequence has stretched structure, the indicated segments are close together in space due to a reverse turn at Val5 that gives compactness to these molecules. This turn is stabilized by the hydrogen bonds involving the backbone atoms. Besides, such structures are stabilized also by intensive dispersive contacts of backbone atoms. In all of them the aromatic side chains of residues Tyr1 and Phe3 have conformational mobility because of localization on surface of the peptide molecules and therefore may be in the specific orientations favorable to interaction with the δ_1 - and δ_2 - receptors. The calculations showed that in the optimal structures of both molecules Phe3 participates also in the effective interactions with Asp4 and Glu4. As can be seen from these results, the stability of spatial structure deltorphins is determined by mutual position of the aromatic side chains of residues Tyr1 and Phe3, of N-terminal amino group and charged groups of Asp or Glu residues.

The bioactive conformations of deltorphin peptides were assessed by pair wise cross comparisons of the low-energy conformations found for deltorphin I and deltorphin II. A visual inspection of the superimposed pairs of conformations showed that conformations with RMSD below 0.9 Å can be considered similar. It was found that α -amino group, and the side chains of tyrosine and phenylalanine residues are in the same positions in space relative each other in similar structures of des active analogues. These conformations of the studied molecules were evaluated as bioactive. The dihedral angles of the proposed bioactive conformations of deltorphins are given in Table 3. These conformations show common properties for both molecules. In these structures the N-terminal positive charged amino group and the negatively charged side chain atoms of residue at 4-th position are spatially close, that is accompanied by effective electrostatic contacts and formation of salt bridges between the N-protonated nitrogen atom and oxygen atoms of side chains of Asp/Glu. The superimposition of the proposed bioactive

conformations of deltorphins I and deltorphin II is shown in Figure 3a.

It was found that the bioactive conformations of deltorphins are characterized by specific distribution of electronic density, that is reflect in the values of effective charges of atoms of functional residues. The distribution of charges on the atoms of pharmacophore elements (α -amino group, the side chains of the Tyr, Phe and Asp or Glu residues) are similar that confirms their identical arrangement in space in these structures as of deltorphin I and of deltorphin II.

Table 3. Backbone dihedral angles (in degrees) of the bioactive conformations of deltorphin I and deltorphin II

		deltorphin II						
		ω	ψ	ϕ	Residues	ω	ψ	ϕ
deltorphin I	ω	180	180	-178	-173	-174	-177	180
	ψ	143	55	165	-72	-64	-63	86
	ϕ	58	93	-148	-88	-107	-99	88
	Residues	Tyr	D-Ala	Phe	Glu	Val	Val	Gly
	ω	179	178	-179	-175	180	-177	180
	ψ	142	42	163	-64	-69	-66	86
	ϕ	56	76	-146	-84	-112	103	86
Residues	Tyr	D-Ala	Phe	Asp	Val	Val	Gly	

The observed differences in the values of the charges on certain groups of atoms as of backbone and of side chains of the residues are dictated by the specifics relative position of them in each molecule. It was found that the electronic structure of these conformations characterized by significantly lower dipole moment due to the uniformity of the distribution of electron density in them. It seems that the presence of the negatively charged groups of atoms in deltorphin sequences is necessary for electrostatic attraction to the positively charged binding sites of δ -opioid receptors (Arg292) and the electrostatic repulsion from the negatively charged sites of μ -receptor. It can be assumed that the mechanism of receptor binding of deltorphin molecules is the formation of hydrogen bonds with participation of ionizable functional groups of these molecules.

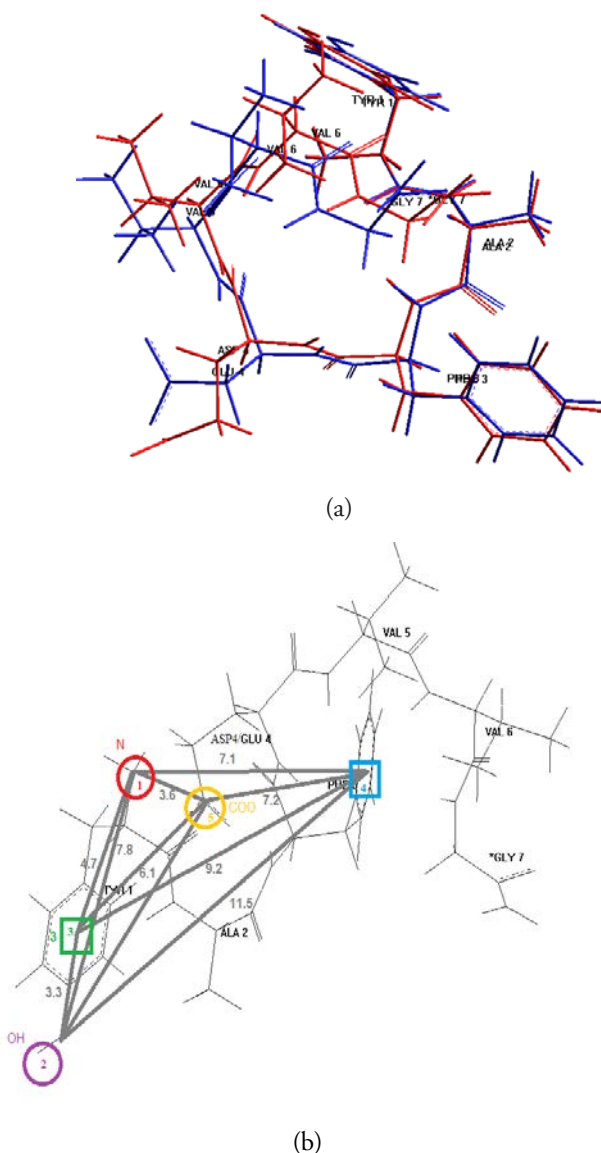


Figure 3. Superimposition of the proposed bioactive conformations of deltorphin I (red color) and deltorphin II (blue color) (a) and the pharmacophore model for their binding to the δ -receptors (b)

On the basis of the received calculation results and data of SAR studies the pharmacophore model of deltorphins for their interaction with the δ -opioid receptors was constructed (Figure 3b). The proposed model contains five areas which are occupied by pharmacophore elements marked by numbers 1-5: the α - an amino group, namely, the protonated nitrogen atom participating in electrostatic interaction with negatively charged residue of opioid receptor and in the formation of hydrogen bond with participation of protonated nitrogen atom; hydroxyl group of the side chain of residue Tyr1, participating in the transition of a charge as the donor of electronic density and in the formation of the hydrogen bond, a phenolic ring of

residue Tyr1 and an aromatic ring of residue Phe3, participating in the hydrophob interactions, a deprotonated carboxyl group of Asp4(or Glu4) participating as in electrostatic interactions and in the formation of hydrogen bond, that defines the selectivity of these ligands. The distances between the centers of the five important pharmacophore regions are given in Å

As can be seen from the presented results, the bioactive conformations of deltorphins, as of dermorphin are characterized by folded conformation of the dipeptide segment Tyr1-DAla2. Apparently, the specified minimum structural requirement is necessary for protection of the peptide bond from splitting action by enzymes in the metabolism process, that may be important for the analgesic activity of these molecules. It is expected that the represented pharmacophore models of dermorphin and deltorphin molecules can be used for search of the ligands of opioid receptors as pharmacological preparations with effective action.

4. CONCLUSION

The investigations of electronic and conformational properties of investigated biologically active molecules can appear an important basis for additional correlation of the spatial structure and structure-functional interactions of these molecules. The proposed pharmacophore models defines the presence of the similar structural elements participating in the interaction with specific receptors and may be useful in the design of new synthetic peptides and peptidomimetics.

5. REFERENCES

- Godjaye N.M., Maksumov I.S., Ismailova L.I. Program of semiempirical calculations of conformations of molecular complexes / J.Struct.Chem., 1983, v.4, pp.147-148 (in Russian)
- Akverdieva G, Godjaye N.M. Improvement of program of calculation of molecular conformation/J.Modern Technology & Engineering, 2017, v.2, No 2, pp.140-145
- Hermans J. and Ferro D. Representation of a protein molecule as a tree and application to modular computer programs which calculate and modify atomic coordinates / Biopolymers, 1971, v.10, pp.1121-1129
- IUPAC-IUB. Quantities, Units and Symbols in

- Physical Chemistry, Blackwell Scientific, Oxford 1993, p.168
5. Shaitan K.V., Saraykin S.S., Molecular dynamics method, 1999. [http:// www.moldyn.ru](http://www.moldyn.ru)
 6. Horn H. W. , Swope W. C. , Pitara J. W. et al. Development of an improved four-site water model for biomolecular simulations: TIP4P-Ew. / J. Chem. Phys. 2004, v.120, pp. 9665-9678
 7. Allinger N.L.,Yuh Y., QCPE 395, Quantum chemistry program exchange, Indiana Univ., Indiana, 1982
 8. Godjajev N.M., Akyuz S., Akverdieva G.A., A molecular mechanics conformational study of peptide T / J. Mol. Structure, 1997, v.403, pp. 95-110
 9. Akverdieva G.A., Godjajev N.M., Akyuz S., Conformational dynamics of peptide T molecule / Journal of Molecular Structure, 2002, v. 609, pp. 115-128.
 10. Akverdieva G.A., Godjajev N.M., Akyuz S. Comparative conformational analysis of peptide T analogs / Journal of Molecular Structure, 2009, v.917, pp.21-26
 11. Akverdieva G.A. Insights into bioactive conformation of dermorphin / Azerbaijan Journal of Physics, 2016,vol. XXII, No. 2, Section: En, July, pp.12-20.
 12. Akverdieva G.A., Molecular mechanics study of [D-Arg2] – dermorphin tetrapeptide analogues / 5-th International Conference on Biological Physics (ICBP), Gothenburg, Sweden, 2004, August 23-27, p.89, B05-158
 13. Akverdieva G.A. Insights into spatial structure of deltorphins / Journal of Qafqaz University, 2016, v.4, No. 1, pp.13-20

TRANSFER OF NANOPARTICLES IN A SIMPLIFIED AQUATIC FOOD CHAIN: FROM WATER PLANT ELODEA CANADENSIS TO MOLLUSCS LYMNAEA AURICULARIA

I.S.AHMADOV^{1*}, E.K.GASIMOV³, N.A. SADIQOVA², N. J. AGAYEVA²,
F.H.RZAYEV⁴, A.A. MANAFOV⁵

¹Baku State University, Nano research Laboratory, Baku, AZ1148, Z.Khalilov str.23,

²Baku State University, Department of Ecobiology, Baku, AZ1148, Z.Khalilov str.23,

³Azerbaijan Medical University, Department of Histology, Embryology and Cytology, Baku, AZ1022, Samed Vurgun str.167

⁴Azerbaijan Medical University, Electron Microscopy Laboratory, Baku, AZ1022, Samed Vurgun str.167

⁵ANAS, Institute Zoology, Laboratory of parasitology, Baku, AZ 1004, A.Abbaszastr., 1128/504

In this studies by the ESR and TEM analysis have been detected the transition of nanoparticles (Fe_3O_4 and Al) in the simple aquatic food chain which is consist from phytoplankton *Elodea Canadensis*, mollusks *Lymnaea Auricularia* and fish *Oncorhynchus mykiss Walbaum*. Nanoparticles depending on the sizes and electrical charges are adsorbed on the surface of the leaves, diffuse into the cells of the elodea and some physiological changes take place such as movement of protoplasm. According the results of these experiments were identified that nanoparticles may up taken by cells of Elodea, move along the stem and localized in the leaves. Nanoparticles pass from elodea leaves to the snail's body when they are eat leaves of elodea. Based on the results of this study it can be concluded, the nanoparticles pass from elodea to mollusks and then may transfers to the fish's body when they are eat mollusks.

PACS numbers: 43.30.+m;92.20.jf. 92.20.jq

Keywords: food chin, nanoparticles, phytoplankton, mollusks, fish

***E-mail:** ismetahmadov@mail.ru

1. INTRODUCTION

Nanotechnology constitutes a fast-expanding field and new products containing engineered nanoparticles (ENPs) are becoming more and more available. Nowadays, ENPs can be found in more than 1300 commercial products, such as novel medicines, innovative drug carriers, image contrast agents, molecular sensors, catalysts, cosmetics, and microelectronic components, fillers for plastic materials, pigments and opacifiers [1-3]. In parallel to a massive industrial preparation of ENPs and their integration into different products there is growing concern about the possible ENPs-related risks for human health and the environment. In this context, over the past decade, the evidence has grown on the eco toxicological effects of ENPs [4-7]. Nanomaterials, including nanoparticles, can fall into water basins, rivers and seas in various ways (through waste waters, industrial waters, airborne crashes, crash accidents, transportation leakage). Water ecosystems can be exposed to nanoparticles. Initially,

nanoparticles are adsorbed on the surface of phytoplankton (algae, higher water plants, etc.) in water ecosystems and even accumulate in their bodies. Although numerous nanotoxicity-oriented studies have demonstrated the potential of ENPs to induce the adverse effects on certain animals and humans, the impact on ENPs on the environment as a whole has been studied to a much lesser extent. In particular, the commercial use of ENPs raises concerns about their effects on freshwater and marine ecosystems, since many everyday products containing ENPs will finally end up there through sewage systems.

In studies it has been shown that certain ENPs, such as carbon nanotubes [8] or fullerenes [9], can induce biochemical changes in fish organisms. However, in the great majority of these studies, the top consumers in the food chain (*i.e.* fish), were exposed directly to waterborne ENPs [10]. Only quite recently, researchers started to investigate the uptake and transfer of ENPs through aquatic food chains [11,12]. In aquatic ecosystems nanoparticles may transfer from one

organisms to next through food chain. Molluscs, for example *Lymnaea auricularia* are key organisms in the simple aquatic food chain as they're eating high water plant *Elodea canadensis* on the one hand and on the other hand are being food for many fishes. Since bivalves are widely used in the monitoring of aquatic pollution, the aim of this study was to compile and analyse data concerning the ecotoxicity of ENPs using bivalve molluscs. The state of the art regarding the experimental approach, characterization, behaviour, fate, bioaccumulation, tissue and subcellular distribution and mechanisms of toxicity of ENPs in marine and freshwater bivalve molluscs is summarized to achieve a new insight into the mode of action of these nanoparticles in invertebrate organisms.

In this context, the potential of ENPs for uptake and accumulation in living organisms as well as their enhanced transfer in food chains, *i.e.* bioaccumulation and biomagnification, have become one of the most appealing problems of the modern ecotoxicology [13-15].

2. EXPERIMENTAL

In this study we have tested the hypothesis that nanoparticles (Fe_2O_3 , Fe_3O_4 , Al) are transferred through the aquatic food chain from water to the aquatic plants and then to the top consumers of the food chain, *i.e.* fish. A scheme of a typical aquatic food chain is shown in Figure. 1. Thus, the investigations were focused on the fate and potential toxic effects of nanoparticles in the selected food chains, which are typical to the freshwater aquatic environment.

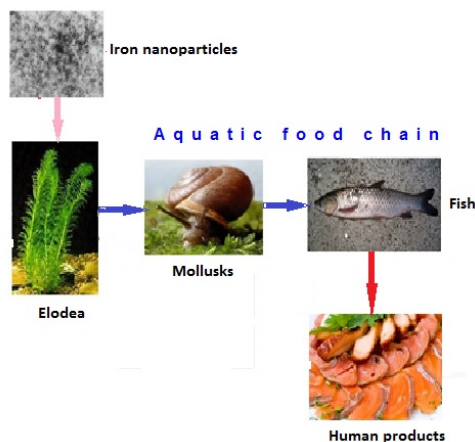


Figure 1. Schematic representation of simple aquatic food chain.

As a research object in the experiments were taken the high water plant *Elodea canadensis* from the *Hydrocharitaceae* family and molluska type *Gastropoda*. Nanoparticles Fe_3O_4 (20-30nm) and Al (18nm) were acquired from Skyspring Nanomaterials, Inc, USA, Houston TX.

To meet this objective, we designed an aquatic food chain around model aquatic plant, *Elodea canadensis*. The *Elodea c.* - first component of the food chain, easily grown in fresh and sea water gardens as a submerged, either anchored or free-floating. Water temperatures of 10-25 °C and moderate lighting is normal condition for it grown. Plant roots (rizoderms) may be anchored in the muddy bottoms of small ponds. Plants spread rapidly and can be invasive in larger bodies of water. It has stem tips grows and single specimens may reach lengths of 3 m or more. The leaves are bright green, 6-17 mm long and 1-4 mm broad. The fruit is an ovoid capsule, about 6 mm long containing several seeds that ripen underwater. The seeds are 4-5 mm long, fusiform, glabrous (round), and narrowly cylindrical.

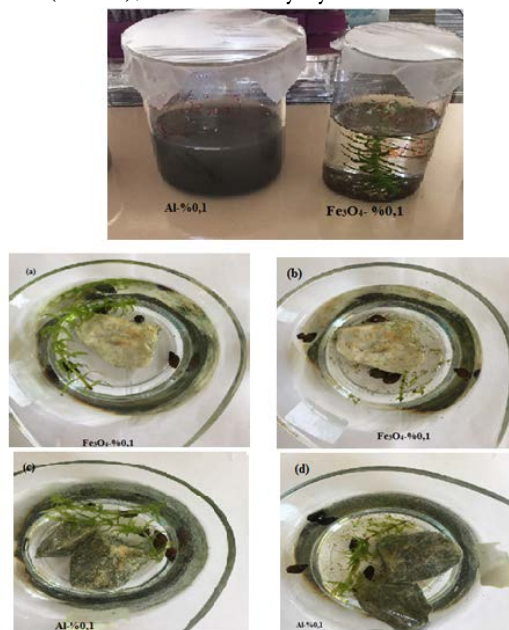


Figure 2. Exposure of *Elodea* plant in the dispersion water of nanoparticles Al and Fe_3O_4 ; a), (c) - feeding mollusks *Melanopsis praemorsa* after exposure the *Elodea* plant for 3 days in Fe_3O_4 and Al (b) nanoparticles, (d) - after 7 days

The second component of the simple food chain was the mollusks *Lymnaea auricularia*. Molluska can live on plants and boulders in water low or high-flow environments and is capable of tolerating anoxic conditions, but it tends to prefer very lentic waters in

lakes, bogs or slow rivers where there is a silt substrate. It has been found in environments with a pH from 6.0–7.1. Its average thermal preference is $\sim 19^{\circ}\text{C}$, but there is great fluctuation around this mean, depending on the photoperiod for the time of year. The body is flecked with small white spots on the back of the head and tentacles, but not on the foot. It is iteroparous, breeding biennially. It lays its eggs in clumps of 50 to 250 eggs. Eggs develop faster as temperature increases from 10°C upward, but the eggs fail to survive and develop when the water temperature reaches 36°C .

Briefly, the main goal of this work is to study the fate of nanoparticles, starting from their accumulation in aquatic soils, their transfer into and bioaccumulation/bio magnification in aquatic plants to, finally, their accumulation and possible adverse effects in the top consumers, *i.e.* fish.

The long-term goal of these experiments is to better understand the environmental behavior of nanoparticles, including their adverse effects to aquatic plants and fauna, as well as to ensure sustainable development and use of nanotechnology in environmental problems.

3. RESULTS AND DISCUSSION

The adsorption effects of nanoparticles on the plants.

Since elodea is the first component of the food chain, firstly studied the interaction of nanoparticles with this plant. For this purpose, the diffusion, adsorption, localization and movement of various nanoparticles was studied in elodea. The plants were exposed to nanoparticles accumulated in aquatic soils and to waterborne nanoparticles. This was allowing us to follow two major accumulation pathways of nanoparticles in aquatic plants: via roots and through exposure to waterborne nanoparticles. The images and videos were taken of elodea leaves by the optical microscopy which prior were carefully rinsed with tap water and subsequently exposed in dispersion solution of iron Fe_3O_4 at daylight illumination for 4 days. As shown in Fig. 3, after 4 days of exposure, could be seen marked changes in the morphology of leaves of elodea. In particular, there was no chloroplast movement in leaves. In contrast, rapid movement chloroplast could be seen in a normal leaves.

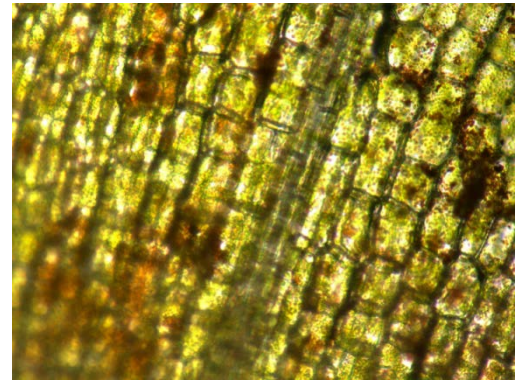


Figure 3. Effect of iron nanoparticles on the physiological state of leaves Elodea

To study the uptake, accumulation and possible biolocalization effects of nanoparticles in elodea we performed a test experiment by TEM analysis. For this purpose were prepared samples leaves of elodea exposure 4 days in solution of iron nanoparticles. In the figure 4 shows TEM pictures of cell wall, chloroplasts and mitochondria of normal elodea leaves.



Figure 4. The TEM pictures of normal elodea leaves: HD - cell wall, XL - chloroplasts, M - mitochondria

In order to confirm the diffusion of nanoparticles into the elodea cells were taken the TEM images of cell walls, chloroplasts and mitochondria. For this experiments were made samples from elodea leaves which were kept for 4 days in Fe_3O_4 nanoparticles solution. Figure 5 shows TEM images that prove the presence of Fe_2O_3 nanoparticles in the cell wall of elodea leaves (A) and mitochondria (B). TEM images, as well as distributed diagrams, show that the iron nanoparticles diffuse into the elodea cells.

Can nanoparticles pass from elodea to the snail's body when they are eat Elodea leaves ? The consumers in preferred aquatic food chain was chosen the snail (*Lymnaea auricularia*) that feed on elodea leaves. As final consumers is fish (*Oncorhynchus mykiss Walbaum*) in this food chain. Elodea is considered an aquatic macrophyte. Macrophytes are very important to the balance of these environments, because they produce oxygen – that is released in the water, and they also serve as food for many species of fish, birds, and mammals.

Besides they give shelter to small worms, as flatworms and planktonic organisms - micro-crustaceans and some types of mollusks. Snails are decomposers, so it was their job to eat the saprophytes.

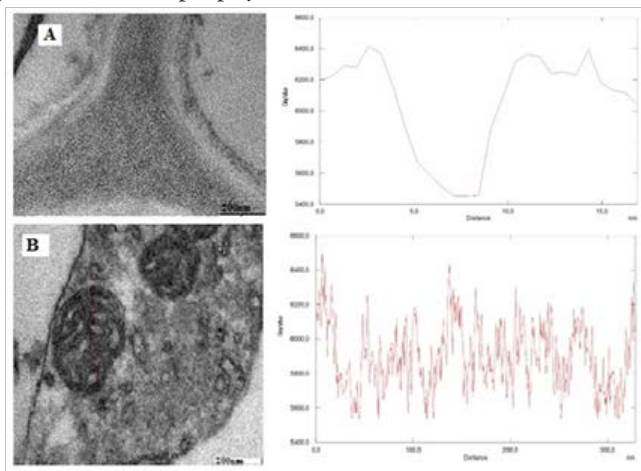


Figure 5. The TEM pictures of elodea cells exposure in iron nanoparticles solution : A-cell wall, B-mitochondria.

In order to find out the answer of these question before of the experiments the elodea was exposure in solutions of Fe_3O_4 (1mg/ml) nanoparticles for 24 hours and then allowed the molluscs to eat the leaves of this plants. In the next days we prepared experimental histological samples from different organs of molluscs. The presence of nanoparticles in the organs of molluscs we identified by two methods, firstly by the ESR signals and then by the TEM pictures of nanoparticles. The presence of nanoparticles in the organs of molluscs were identified by two methods, firstly by the ESR signals and then by the TEM pictures of nanoparticles. From the results of these experiments, we saw that EPR signal was observed in the organs of the snails feeding leaves of elodea with iron nanoparticles. In some organs, EPR signals was strong (for example, in the liver), and some have weakness. EPR signal strength has shown that iron nanoparticles are more accumulated in the liver. The results of this experiment are shown in the fig.6.

The presence of nanoparticles in the organs of molluscs was identified also by TEM microscopic methods. For this purpose we have made histological preparations and took pictures in TEM. The presence of nanoparticles in the organs of molluscs was also seeing in the TEM pictures of different organs of molluscs.

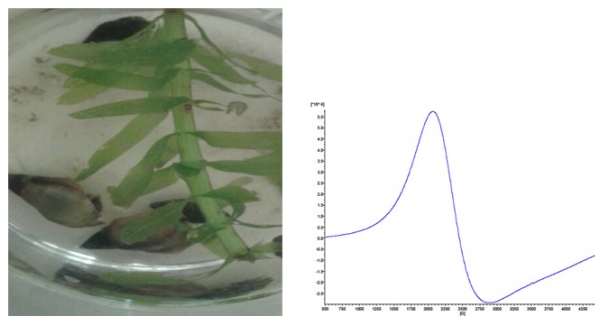


Figure 6. *Lymnaea auricularia* molluscs eating leaves of elodea (left) and ESR signal from liver of mollusks (right)

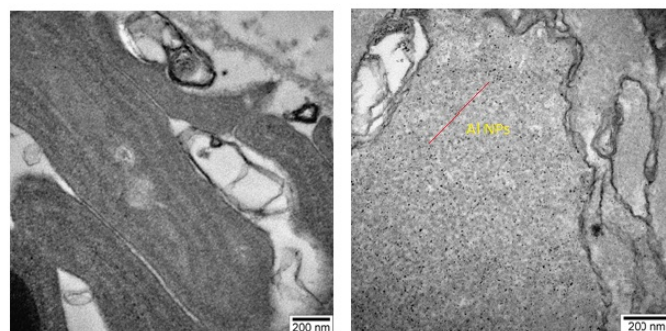


Figure 7. The TEM pictures of *Lymnaea a.* liver in normal (left) and in the liver of mollusk which are eat affected leaves with Al nanoparticles of Elodea.

For this purpose we have made histological preparations from molluscs and took pictures in TEM. In this case the elodea plant was kept in Al and iron nanoparticles solution for 4 days. Then allowed the molluscs to eat the leaves of these plants. In the next days we prepared experimental histological samples from liver of molluscs. The presence of nanoparticles in the livers of molluscs was also seeing in the TEM pictures. In the picture 7 shown the TEM picture of the livers of molluscs. The TEM picture of liver confirms the localization of aluminium nanoparticles into the cells of liver.

Nanoparticles may diffuse also into the organelle of mollusc's cells. In the picture 8 shown the TEM picture of the lysosome (A), mitochondria (B) and C-cytoplasm of liver cells of molluscs. The TEM picture of liver organelles confirms the localization of iron nanoparticles into the organelles of liver also. The experiments with aluminium nanoparticles shows that Al nanoparticles may also diffuse into the organelle of liver cells of molluscs.

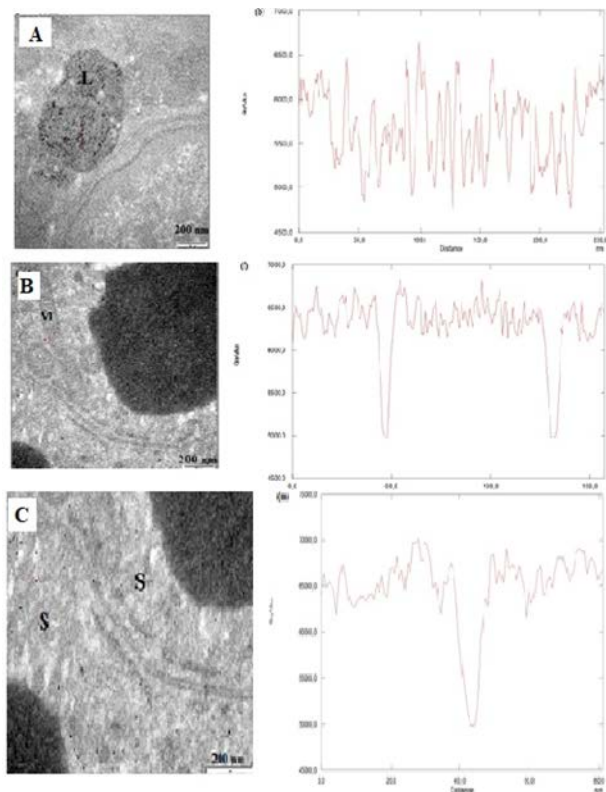


Figure 8. The TEM pictures of *Lymnaea a.* liver cell which are eat affected leaves with iron nanoparticles of elodea: A- lysosome, B – mitochondria, C- cytoplasm

4. CONCLUSION

Thus in the experiments have been detected the transition of nanoparticles from one element to another in the simple aquatic food chain which is consist from phytoplankton *Elodea Canadensis*, mollusks *Lymnaeaauricularia* and fish *Oncorhynchusmykiss Walbaum*. Nanoparticles depending on the sizes and electrical charges are adsorbed on the surface of the leaves, diffuse into the cells of the Elodea and some physiological changes take place such as movement of protoplasm. According the results of these experiments were identified that nanoparticles may up taken by cells of Elodea, move along the stem and localized in the

leaves. Nanoparticles pass from elodea leaves to the snail's body when they are eat leaves of elodea. Based on the results of this study it can be concluded, the nanoparticles pass from elodea to mollusks and then may transfers to the fish's body when they are eat mollusks.

5. REFERENCES

1. Petersen E.J.et al. /Environ. Sci. Technol., 2011, 45, 9837–9856
2. Elisa Moschini /Thesis for the degree of philosophiae doctor (ph.d), University of Milano-Bicocca, 2012, pp.155,
3. Ashok K./University of Minnesota, Minneapolis, MN, USA, Copyright © 2016 Elsevier Inc.
4. KlaineS.J. et al./Environ. Toxicol. Chem., 2008, 27, 1825–1851;
5. WiesnerM.R. et al./Environ. Sci. Technol., 2006, 40, 4336–4345;
6. NelA. et al.Science, 2006, 311, 622–627
7. Hartmann N.B.et al. /Integr Environ Assess Manag. 2010 ,Apr;6 (2):311-3.
8. Smith C.J. et al. Aquatic Toxicology 82: 94–100
9. Oberdörster E./ Environ Health Persp,2004, 112: 1058–1062
10. HouW.-C.et al./Environ. Sci.: Processes Impacts 2013, 15, 103–122.
11. Tommy Cedervall et al./PloS ONE,2012, 7, No. 2, e32254 .
12. Zhu X. et al. /Chemosphere, 2010, 79, 928–933
13. Werlin R. et al. Nat. Nanotech. 6:65-71 (2011);
14. HouW.-C.et al. /Environmental Science-Processes & Impacts 2013, 15:103-122.
15. NowackB. et al. /Environ. Toxicol. Chem. 31, 50–59 (2012)

INFLUENCE OF ADDITIVES ORGANIC AND MINERAL SUBSTANCES ON NITRIFICATION ABILITY GREY FOREST SOILS OF ACINOHUR CADASTRE REGION

K.A.HUSEYNOV*

Faculty of Ecology and Soil sciences, Baku State University, Az1148, Z.Khalilov str., 23, Baku, Azerbaijan,

The biochemical processes in soils substantially define their productive ability. The most essential indicator of fertility of the soil is biodiversity, like process nitrifications. The nitrification ability of various soils is not identical. More fertile soils have also higher nitrification ability. The suppressed course of biochemical processes in some soils (for example, podsollic) emphasizes weak activity of microorganisms in them. It is obvious that when studying productivity of soils needs to be established what nitrification ability of soils and in what way it is possible to strengthen activity of nitrifies in the soil. The last is especially important when studying a question of interaction of these or those soils with the introduced fertilizers.

PACS numbers: 91.62.Rt;92.40.Lg; 88.20.dj

Keywords: nitrification, forest soils, soil substance, grey soils, fertile soil

*E-mail: kanan.huseynov@gmail.com

1. INTRODUCTION

The biochemical processes in soils substantially define their productive ability. The most essential indicator of fertility of the soil is biodiversity, like process nitrifications.

The nitrification ability of various soils is not identical. More fertile soils have also higher nitrification ability. The suppressed course of biochemical processes in some soils (for example, podsollic) emphasizes weak activity of microorganisms in them. It is obvious that when studying productivity of soils needs to be established what nitrification ability of soils and in what way it is possible to strengthen activity of nitrifies in the soil. The last is especially important when studying a question of interaction of these or those soils with the introduced fertilizers.

We studied influence of organic and mineral substances on a nitrification ability of gray forest soils. Laboratory trials in which influence on a nitrification ability of soils of additives became clear are for this purpose made:

- a) Organic substances in the form of the crushed peat and manure and earth compost;
- b) Various salts of calcium;
- c) The mineral nitrogen brought in the form of ammonium sulfate;
- d) Various combinations of mineral substances.

The technique of carrying out experiences was as follows. The samples of soils brought to an air and dry

state were passed through a sieve with openings with a diameter of 3 mm, then the soil was humidified up to 60% of full moisture capacity and maintained in the thermostat at 25 — 30 ° on condition of full aeration within 15 — 30 days, and in some experiences — 40 days. Options of experiences were outlined according to the solution of the questions posed.

Before composting and after composting in samples of soils defined: nitrates in a water extract, nitrites, ammonia colorimetric with Nessler's reactant.

In some experiences determined also water-soluble phosphoric acid, water-soluble hummus, by pH, the easily hydrolyzed nitrogen by Tyurin and Kononova.

For experiences samples of the dark gray, gray and light gray forest soils taken in the territory of the Acinohur Cadastral region were used. All of them are characteristic representatives of these subtypes of soils and are rather in detail described in a number of works therefore the characteristic them is not provided in the present article. Mechanical structure of the soil average. Results of the made experiments are presented in table 1 - 7.

2. EXPERIMENTAL

In one of experiences influence of peat on a nitrification ability of soils was studied. The crushed peat was brought in soils in three doses: 3,1 g; 6,2 g; 9,3 g on 200 g of the soil. The research was conducted on dark gray and light gray forest soils. Experience

continued one month.

The results of a research given in table 1 show that introduction of organic substance in the form of the crushed peat enhances biological activity as dark gray, rich with a hummus, soils (10,4% of a hummus), and poor in a humus (4,0%) of light gray forest soils.

Introduction of peat at the rate of 3,1 g and especially 9,3 g on 200 g of the soil (that corresponds to 135 tons of peat on hectare) is involved by rapid development of processes of ammonification and a nitrification in these soils. So, the amount of nitrates at introduction of peat in a dose of 9,3 g increases by 200 g of the soil in the dark gray forest soil by more than 6 times in comparison with amount of nitrates in the same soil, but without peat, and in comparison with the initial soil (before experience) by 40 times, in the light gray soil respectively by more than 5 times and by 28 times.

In process of accumulation in the soil of nitrates the amount of water-soluble phosphoric acid that, apparently, is connected, with consumption by its violently developing task setters decreases. And only in the dark gray soil at a high dose of peat in the first two time the smaller decrease of water-soluble phosphoric acid is noted.

The strengthened processes of mobilization of nitric fund of soils in optimum conditions lead to sharp reduction by the end of experience of a water-soluble humus by all options. In other experience influence of manure and earth compost on a nitrification ability of gray and dark gray forest soils was studied. Samples of these soils are taken in the territory of Acinohur Cadastre region. The gray forest soil contains a humus 4,8%, dark gray — 7,1%.

The analysis of samples of compost showed very big saturation its nutritious substances - the Humus 11%, nitrogen of gross 0,6%, phosphorus of gross 0,6%, mobile phosphoric acid of 116 mg on 100 g of the soil, mobile potassium of 340 mg on 100 g of the soil, pH of a salt extract 6,8, water — 7,0 on average contain. Compost (a manure ratio to the earth 1:1) was brought at the rate of 1,8 g on 200 g of the soil that corresponds to about 15 tons on hectare. Experiment was made within 25 days. For comparison with effect of compost the option with introduction of mineral fertilizers was provided. Nitrogen was brought in the form of ammonium nitrate at the rate of 12,9 mg on 200 g of the soil, potassium in the form of chloride potassium — 11,9 mg on 200 g of the soil, phosphorus in the form of

Table 1. Impact of manure and earth compost on soil nitrification capacity

N	Soil	Options experience	Ammonia in mg on 1 kg of the soil		Nitrates in mg on 1 kg of the soil		Nitrate nitrogen in mg per 1 kg of soil after incubation	Easy hydrolysable nitrogen in mg on 1 kg of soil		Relation the nitrogen hydrolyzed to nitrogen of nitrates later incubations
			to an incubation	after an incubation	to an incubation	after an incubation		to an incubation	after an incubation	
1	Gray forest	Without fertilizers	16,5	15,6	9,6	66,6	15,0		240	16,0
2	Gray forest	Compost NPK	17,7	16,4	12,4	97,5	22,0	140	363	16,5
3			33,5	15,8	15,5	86,5	20,0		246	12,3
4			24,1	17,7	20,0	96,5	21,7		770	35,5
6	Dark gray forest	Without fertilizers	24,1	17,3	5,5	38,6	8,7	280	280	32,1
7			22,8	16,1	10,0	47,4	10,7		476	44,4
8			26,8	17,5	22,7	40,4	9,1		1316	144,6

superphosphate — 23 mg of a pas of 200 g of the soil. Results of experience are given in table 2.

From the provided data it is visible that under the

influence of manure and earth compost the nitrification ability of the explored soils, especially gray forest, sharply increased. After 25 days of incubation the greatest accumulation of nitrates is noted by option with entering into the soil of both one compost, and compost together with mineral fertilizers.

Considerably concedes on accumulation of nitrates option with introduction of one mineral fertilizer. The option "without fertilizer" differs in the smallest amount of nitrates. If to compare amount of the nitrates which are saved up after an incubation to the initial content of nitrates in the soil of each option, then it is possible to see that the content of nitrates by option "without fertilizer" after experience increased almost by 7 times, at compost introduction — almost by 8 times, and by option of "NPK" and "compost-f-NPK" only in 5,6 and 4,8 times respectively.

In the dark gray soil the same regularity, but influence of compost is shown less effectively, than on the gray forest soil. Content of the absorbed ammonia in the soil though high, but after an incubation it considerably decreases parallel to increase of nitrates.

Favorable influence of manure and earth compost on a nitrification ability of soils speaks, apparently, not only the fact that compost supplies the soil with additional amount of nutrients, but, mainly, the fact that under the influence of it the microbiological processes translating reserves of nutrients of the soil in amplify will acquire a form for plants. The last is emphasized not only data on accumulation of nitrates, but also on the maintenance of a water-soluble humus and the easily hydrolyzed nitrogen.

Mineral fertilizers to a lesser extent stimulated process of a nitrification, than compost in optimum conditions. However use of mineral fertilizers in a combination, with compost promoted the accelerated decomposition of organic substance and enrichment of soils food elements, available to plants. Mineral fertilizers, intensifying microbiological processes in the soil, accelerate processes of a mineralization of organic substance and release of the hydrolyzed nitrogen forms.

Joint introduction of compost with mineral fertilizers was studied only on the gray forest soil. The obtained data (tab. 2) show the highest content of water-soluble humus and the widest relation of the hydrolyzed nitrogen to nitrogen of nitrates by this option.

Table 2. Influence of various forms of calcium on a nitrification ability of the dark gray forest soil.

N	Options experience	Ammonia in mg on 1 kg of the soil			Nitrites in mg on 1 kg of the soil			Nitrates in mg on 1 kg of the soil					
		to an incubation	After 5 days	After 15 days	After 30 days	to an incubation	After 5 days	After 15 days	After 30 days	to an incubation	After 5 days	After 15 days	After 30 days
1	Without Ca	51.1	100.9	99.8	112.2	0.286	0.420	0.399	0.405	4.7	14.3	31.9	76.2
2	CaCO ₃		126.9	128.6	135.1		0.410	0.401	0.407		15.2	45.2	84.0
3	CaCl ₂		119.4	117.1	130.1		0.621	0.611	0.620		12.9	42.3	79.1
4	CaSO ₄		125.4	108.2	129.6		0.570	0.564	0.598		13.1	40.9	70.9

3. RESULTS AND DISCUSSION

In one experience influence of carbonic calcium on a nitrification ability of dark gray and light gray forest soils was studied. Carbonic calcium was brought at the rate of 200 mg on 200 g of the soil. In the second experience influence of various forms of calcium on nitrification ability of the dark gray forest soil was compared. Such forms of calcium were tested: CaCO₃ (it was brought at the rate of 100 mg on 100 g of the soil), CaSO₄ (it was brought at the rate of 117,5 mg on 100 g of the soil) and CaCl₂ (it was brought at the rate of 100 mg on 100 g of the soil). Results of a research are given in next tables.

In experiences very positive role of carbonic calcium in increase a nitrification of ability of soils is revealed. Introduction of CaCO₃ at the rate of 200 mg on 200 g of the soil (that corresponds to 4 tons on hectare) considerably strengthens process of a nitrification, both in dark gray, and in the light gray forest soil.

At the same time addition to the soil of carbonic calcium promotes more vigorous transition ammonium of forms of nitrogen in nitrate. Under the influence of carbonic calcium process of a mineralization of humus amplifies and there is an accumulation of its water-soluble forms. Reaction in the light gray forest soil under the influence of carbonic lime moves in the neutral party. Content of water-soluble phosphoric acid, in parallel with accumulation in the soil of nitrates, by the end of experience considerably decreases that was noticed by us and in other experiences.

These tables show that from all experienced compounds of calcium (CaCO₃, CaCl₂ and CaSO₄) the greatest effect in increase in energy of a nitrification on the dark gray forest soil is gained from carbonic calcium. Sulfate calcium even lowers intensity of accumulation of nitrates a little. The quantity of water-soluble humus after incubation considerably decreases by all options.

Experiment on clarification of influence of mineral nitrogen on a nitrification ability of soils was made in optimum conditions within 40 days. Objects of a research were gray and light gray forest soils. Nitrogen was brought in the form of ammonium sulfate. The results of experience given in tab. 5 show weak increase in nitrates under the influence of sulfate of ammonium both on gray, and on light gray forest to the soil. More considerably contents nitrogen ammonium increases in soils. Changes in the content of water-soluble phosphoric acid and water-soluble humus, under the

influence of the ammonium sulfate brought in the soil, small.

Table3. Influence of various forms of calcium on a nitrification ability of the dark gray forest soil.

N	Options experience	Phosphoric acid, water solution, in mg per 1 kg of soil				Humus water soluble in ml 0.05 p K ₂ Cr ₂ O ₇ in mg per 100 g of soil				pH water extract			
		to an incubation	After 5 days	After 15 days	After 30 days	to an incubation	After 5 days	After 15 days	After 30 days	to an incubation	After 5 days	After 15 days	After 30 days
1	Without Ca	1.5	0.88	0.85	0.83	125.9	52	24.3	20.1	7	6.8	7	7.2
2	CaCO ₃		0.86	0.82	0.8	48.8	48.8	22.4	19		6.8	7.2	7.4
3	CaCl ₂		0.84	0.8	0.75	41.6	41.6	18.4	13.8		6.4	6.8	7
4	CaSO ₄		0.82	0.76	0.7	45.6	45.6	25.6	18.2		6.2	4.8	6.8

Table 4. Effect of N,P and Ca and their combinations on nitrification ability of light gray forest soil.

Options experience	Initial Soil						The soil after composting					
	Gross hummus	The easily hydrolyzed nitrogen	The ammonia absorbed	Nitrates	Mobile phosphorus		Gross hummus	The easily hydrolyzed nitrogen	The ammonia absorbed	Nitrates	Mobile phosphorus	
			In mg per 1 kg of soil						In mg per 1 kg of soil			
1	3.10	9.52	36.9	4.8	32.9	2.89	10.08	11.4	28.7	31.2		
2	3.10	13.40	44.4	26.8	33.2	3.60	14.80	18.6	46.8	37.0		
3	3.15	9.20	29.4	6.3	39.1	3.03	10.20	9.9	28.7	37.0		
4	3.18	9.03	28.8	5.7	34.0	2.98	10.30	5.7	26.9	34.7		
5	3.20	13.10	46.8	26.6	37.0	2.99	14.40	35.4	41.3	38.0		
6	3.18	14.60	43.8	25.3	38.5	2.97	15.20	22.2	41.6	38.5		

Reaction of the environment under the influence of sulfate ammonium moves in the sour party a little.

In laboratory trial studying of influence on a nitrification ability was provided: nitrogen, phosphorus, potassium and their combinations — nitrogen + phosphorus, nitrogen + phosphorus + potassium. Nitrogen was brought in the form of ammonium nitrate at the rate of 35 mg, phosphorus in the form of superphosphate at the rate of 82 mg, potassium and a type of chloride potassium in a dose of 31 mg of 200 g of the soil. Experiment was made within 25 days on the light gray forest soil containing 3,1% of a humus. The obtained data are provided in the table. From these data it is visible that addition of nitrogen in the form of ammonium nitrate sharply increased contents in the soil easily hydrolyzed, ammonium and nitrate nitrogen. After composting the greatest accumulation of nitrates is found by options N, NP, NPK. Addition to the soil of one phosphorus (in the form of superphosphate) did not exert impact on process of a nitrification. At the same time by this option, as one would expect, the content of mobile phosphorus increases. The smallest content of nitrates in the soil after composting is observed at introduction of chloride potassium. All options with nitrogen introduction differ in the increased amount of the absorbed ammonia. After composting the content of ammonia in the soil in connection with increase of nitrates by all options is sharply reduced.

As a result of processes of disintegration of humus substances the maintenance of a gross humus in the soil after experience falls (especially on control) and the amount of the easily hydrolyzed nitrogen respectively increases.

Table 5. The influence of various forms of potassium on the course of nitrification in light gray forest soil

Options experience	Before composting		After composting	
	Ammonia in mg on 1 kg soils	Nitrates in mg on 1 kg soils	Ammonia in mg on 1 kg soils	Nitrates in mg on 1 kg soils
KCl	31.8	4.8	45.6	9.0
K ₂ CO ₃	44.4	5.1	62.4	11.5
K ₂ SO ₄	36.0	4.8	39.6	8.0

The provided data show that from all tested potassium forms the greatest accumulation of nitrates is noted at introduction of carbonic potassium and the smallest — at introduction of sulfate potassium, it completely confirms the regularity revealed by us in one

of experiences with the same forms of calcium what it is told above about.

4. CONCLUSION

In one of experiences also positive influence of joint introduction of phosphorus with potassium on process of a nitrification in the gray forest soil came to light. Under the influence of the superphosphate brought together with chloride potassium, the content of nitrates in the soil (after composting) increased from 58 mg up to 75 mg on 1 kg of the soil.

1. The conducted researches showed that entering into the soil of these or those organic and mineral substances it is possible to strengthen biochemical processes in the soil, sending them to the desirable party.

2. The greatest influence on strengthening of biological activity of soils, on increase in energy of process of a nitrification is rendered by organic substances (manure and earth compost, peat).

3. From mineral connections the ability of soils has very positive effect on nitrification carbonic calcium and also the nitrogen brought in the form of ammonium nitrate and nitrogen in combination with phosphorus and potassium.

4. In increase the nitrification of ability of soils is of great importance a form of the brought connections. From all tested calcium forms (CaCO_3 , CaCl_2 and CaSO_4) the greatest effect in accumulation of nitrates gives carbonic calcium and the smallest — sulfate calcium. The lowest accumulation of nitrates is noted also when using sulfate potassium. The nitrogen brought in the form of ammonium nitrate was also more effective in accumulation in the soil of nitrates, in comparison with sulfate ammonium.

5. REFERENCES

1. Persson T. et al. / *Plant and Soil*, 1995 .v. 168, 1, p. 55-65.
2. Jean Trap et al. / *Forest Ecology and Management*, 2009, p. 1284-1292.
3. Catherine Ste-Marie et al. / *Soil Biology and Biochemistry*, 1999, 31, p. 1579-1589.
4. Khalil M.I. et al. / *Soil Biology and Biochemistry*, 2005, v.37, p. 1507-1518.
5. Kuzyakov Y. et al. / *Soil Biology and Biochemistry*, 2000, v.32, 2000, p.1485-1498.
6. Eickenscheidt T. et al. / *Biogeosciences*, 2014, v.11, p. 2961-2976.
7. Alexander Arturovich Shpedt et al. / *J. Pharm. Sci. and Res.*, 2018, v. 10, N 4, p.870-873.
8. Kosolapova A. et al. / *Bulgarian Journal of Agricultural Science*, 2016, v. 22, N 6, p.921-926.
9. Pilar Pérez-Batallón et al. / *Ann. For. Sci.*, 2001, v.58, p. 807-818.

APPRAISAL MAPPING SOIL COVER OF THE REGION

K.A.RAHIMOVA* , G.A.HUSEYNOVA

¹Faculty of Ecology and Soil sciences, Baku State University, Az1148, Z.Khalilov str., 23, Baku, Azerbaijan

Completion of large-scale soil researches leaving of the soil card and an explanatory note to it does not give comparative ideas of quality of a soil cover of separate grounds, fields and sites. Permission of this task is helped by a appraisal or quality standard of soils. At quality standard estimated points of soils of certain sites, grounds, land use, areas are defined. On these points it is possible to compare easily the earth of various territories, to reveal a quantitative difference between them. Quality standard of soils is a basis for the differentiated solution of many organizational and economic, agro technical and zoo technical questions. Estimated points of a soil cover are established in the etalon soil region of Azerbaijan Republic on the main rating scale and correction coefficients as a result of drawing up the sheet of a appraisal of soils.

PACS numbers: 91.62.Rt;92.40.Lg; 88.20.dj**Keywords:** appraisal, maps, cadastre, forest soils.***E-mail:** konul_78_78@mail.ru

1. INTRODUCTION

The sheet of appraisal of soils gives an idea of a ratio of various soils in economy, and of sources of calculation of point taking into account internal properties of the soil, a condition of a land relief and contour. The sheet of appraisal of soils of economy (or its divisions) by all types of grounds is of the greatest practical interest. We carried out such work for all forms and grounds on the area of 55000 hectares. Sheets of appraisal of soils, certainly, increase the operational value of soil cards, but they do not give the answer to a question of a spatial arrangement of soils within this or that ground of N about quality them in a certain place.

There is a question as to show type and quality of soils in one document character of a ground the place of its arrangement. We also find the answer to this question in the card of site classes of a soil cover. The card of site classes of a soil cover represents a combination of cards of quality standard of soils of each land management contour, soil and land management with designation of point.

The card of site classes is topographical expression of the sheet of appraisal of soils with a spatial detail. For drawing up the card of site classes apply contours of grounds on the soil card, and then make an illumine colored pencils taking into account convention of the image of each combination of soils and grounds the sign of coloring.

On all soils the arable land is painted over by various shades of red color or strokes: on dark gray soils they are denser, on gray — is lighter, on light gray is even lighter, on dark-colored meadow soils — crimson color or other shading. On soils of the haymaking's or pastures which are settling down on the same kinds of soils the main is entered yellow background (from orange to light yellow), for the woods — different shades of blue and green color. In each of contours the fractional digital index the Arab signs treats: in numerator — the index of soils, in a denominator — site class (estimated point) of the soil. Illuminate the card colored pencils (but not liquid paint) in order that in case of transformation of grounds it was possible to replace one coloring another.

If the economy expands arable land at the expense of the wood on the dark gray soil, then the type of the soil in itself will not change, will change only a ground, a cultural state and site class at the expense of the amendment on forest coverage. In that case former coloring on a contour of the mastered virgin soil is erased, and other coloring representing the dark gray soil under an arable land has to be put. Thus, the card of site classes will be the peculiar operational document reflecting the nature of use of a soil cover in economy for any moment. Therefore the card of site classes of a soil cover needs not just to be made, it is necessary to conduct, note changes, messages as the diary or the operational magazine as the operational card.

The card of site classes of a soil cover will play especially important role during expansion of agricultural production to the most rational and proportional placement of grounds, especially at

expansion of an arable land. By means of the card of site classes of a soil cover the question of the sequence of land development is easier resolved under arable land, about perspective mission of certain sites for certain grounds or cultures.

Having such cards, the economy can understand quicker and more distinctly the prospect of development of primary branches, define general specialization, is more concrete carry out organizational and economic the management to complete the equipment, to develop construction of production rooms, an economic road network, economic center, cultural and community institutions, etc.

The card of site classes of a soil cover helps the soil scientist to make reasonable recommendations (mostly unique, not sample) for each economy.

At the same time from materials of appraisal of soils also recommendations about overcoming available follow shortcomings. At rational economic activity on lands of present collective farm it is possible to have profitable and highly productive agricultural enterprise.

2. EXPERIMENTAL

It can be reached by increase in site class of a soil cover various means:

1) Increase in arable land at least three times (up to 5400 hectares) due to elimination of the big area of the aspen woods and development of a part of unproductive haymaking's Π pastures;

2) Involvement in an arable land of prodigally used fertile soils of homestead fund;

3) Streamlining of an intraeconomic road network from the economic center on fields;

4) Considering proximity of the city, establishment vegetable of the dairy direction of agricultural production. Where and in what volume it is necessary to make these transformations, the card of site classes of a soil cover very well prompts.

On cespits and podsolic soils potatoes and vegetables (can well be born at the condition of application of fertilizers), lei, cereals, peas, a clover, sunflower and other high-yield forage crops. Production of grain in economy at such situation can be limited, and to increase production of vegetables and forages.

Development of economy according to this specialization will allow improving sharply living standards of toilers of economy, to increase their interest in productive use of the earth. So over time, of course,

will be.



Figure 1. Fragment of the map of appraisal classes of a soil cover (A – present.)

It is necessary to make capital expenditure of funds for land development, the device of roads, construction of production rooms and the uniform economic center, a pas for implementation of the recommendations stated above following from quality standard of a soil cover updating and acquisition of the modern equipment. It is clear, that in that case it is necessary to increase sharply and qualification of the management of economy. There is no doubt that in a few years at the correct maintaining such economy will turn into the profitable, cultural and modern enterprise. At serious intention to render the effective help to collective farm the appraisal of the recommendation following from results are the most effective, effective and correct. Otherwise there are recommendations for other economy, with other site class of soils, with other mosaic of soils on the card of site classes of a soil cover.

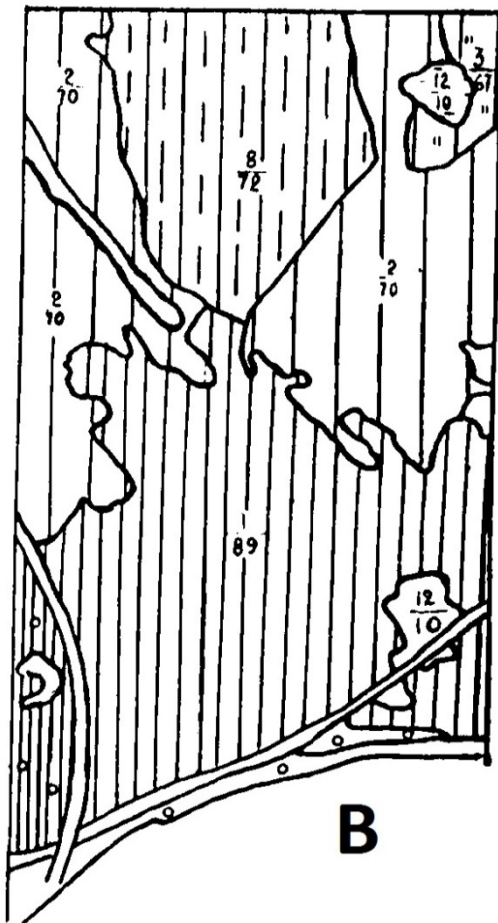


Figure 2. Fragment of the map of appraisal classes of a soil cover (B— after rational placement of grounds in the future.)

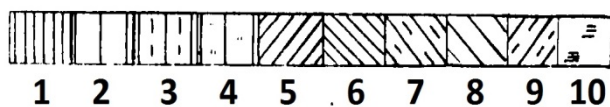


Figure 3. Fragment of the map of appraisal classes of a soil cover

1. Dark gray forest
2. Gray forest
3. Dark-colored meadow
4. Light gray forest
5. Dark gray forest
6. Dark-colored meadow
7. Dark gray forest
8. Dark-colored meadow
9. Gray forest
10. Hummus and marsh soil

Cesspits and podsollic soils make fixed assets of an arable land and virgin soil for its expansion. Under

arable lands these soils have average estimated point 42, and under the woods and pastures — 37. The estimated point of cesspits and podsollic soils of an arable land can be increased gradually systematic introduction of organic fertilizers at the rate of not less than 6 tons on hectare annually. It means that on all arable land — 520 hectares, cesspits and podsollic soils, 3120 tons of manure will be required. It would be useful to introduce in addition to it mineral fertilizers. Arable lands on the area of 724 hectares of cesspits and meadow soils are almost inaccessible for removal of manure because of big dispersion (about 200 contours) within the floodplain, extensive and remote for journey. The second way of increase in site classes of cesspits and podsollic soils of an arable land — improvement of a configuration of fields by means of coppices and forests, the device of an intraeconomic road network. Increase in site class of cesspits and podsollic soils under pastures and the woods is possible by transformation of these grounds in an arable land. At the expense of cesspits and podsollic soils from under the wood about 600 hectares located in one massif near already mastered arable lands can be mastered under an arable land. Their fertilizer would require 3600 more tons of manure.

3. RESULTS AND DISCUSSION

Soils of the second and third agro production groups cannot be practically developed under arable lands. It is difficult and inexpedient to make. It is difficult to develop these soils because of dissociation of sites swamps, lakes, because of almost annual floods covering the most part of the floodplain because of prolixity and off road terrain within the floodplain. The pas plots of the floodplain are difficult to deliver seeds, and it is even more difficult to take out harvest. Therefore on inundated lands, even at satisfactory site class of soils, the cost of products of field husbandry will be always higher, than on large massifs of cesspits and podsollic soils of a waterless valley. The area of soils of the floodplain is big, but it is not of interest to further expansion of an arable land. However partial clearings from the unproductive wood, bushes, garbage, and hummocks would allow increasing the areas of haymaking's and pastures not less than by 1000 hectares. To increase site class of soils of the second group very difficult. Here it is only possible to take measures of prevention of bogging of inundated lands by clearing a channel, dumping of flood waters from the

central floodplain on ditches through shaft in the next reservoirs.

Therefore site class of hummus and marsh soils of the floodplain it is impossible to lift over 10 points now. Thus, data of quality standard allow to establish ways of the best economic use of the existing grounds, possibilities of their transformation and ways of increase in estimated point. As a result of it becomes clear that in collective farm it can be mastered under an arable land up to 600 hectares of cespits and podsolic soils, under meadows and haymaking's — up to 1000 hectares and that for increase fertility of soils it will be required in total 6720 tons of manure in the nearest future.

Presence of the big areas of haymaking's and pastures quite provides already now necessary quantity of forages for the available cattle and allows increasing its livestock considerably. Environment is difficult, site class of local fertilizers (soils, a relief) it is low. Nevertheless at the correct specialization it is possible to have quite profitable enterprise here. For this purpose it is necessary to build economic activity counting on a combination of field husbandry and livestock production to the meat direction of cattle.

The main commodity culture of crop production on cespits and podsolic soils flax on fiber is considered. As flax can be sowed on one zero not more often than once in 7 — 8 years, therefore, the collective farm could to bring crops of this culture only to 150 hectares. Concentration of an arable land in close proximity to settlements favors to such specialization. Other cultures should be chosen, being conformed to economy — tasks of the state. To have the good predecessor for flax, it is necessary to sow a winter rye on couples fertilized by manure. L after flax on an early plough land summer grain crops and peas will yield good harvests. Under flax it is necessary for increase in marketability of field husbandry in turn to introduce mineral fertilizers on the area of 150 hectares. At the limited area of soils of the first group and also because of small number of the population in collective farm to include in a crop rotation cultures now it is premature even on the fodder purposes as and without it the nature itself reproduces many forages on soils of the second group with smaller costs of their cleaning. Specialization of livestock production on the meat direction of cattle is based that on meadows it is possible to make annually significant amount of hay, to allocate a number of convenient sites for of herds of the cattle for meat (can be even without

shepherds on island pastures). At simple measures of improvement of meadows and pastures the efficiency will easily provide them production of forages at least for 1000 heads in terms of cattle.

Types of soils, features of quality of forages, small number of working hands in collective farm dictate also a method of completing of herds on stagnation. By spring it is necessary to complete herds at the expense of the discarded live stock milk cows, young growth and also to get the cattle from local population. For the winter it is necessary to leave a minimum of uterine structure and some quantity of the cattle (young growth) taking into account a stock of forages on overexposure. On visible, such direction will require special meat breed of cattle. On dairy or even meat-and-milk direction on rough sterns under difficult local conditions to be guided it is impossible. Horse breeding could become the second not less profitable direction of meat livestock production in collective farm. To follow a way such - economic activity what follows from appraisal materials needs to render to collective farm quite certain organizational and material help. The organizational help has to include accurately developed, economically reasonable Π the approved specialization (observing constancy of the chosen direction for the long period). Material and logistical assistance will consist in granting the pas credit field husbandry mechanization, preparation of forages, acquisition of mineral fertilizers, a construction of production rooms (mainly the inexpensive yards for the cattle on overexposure). Obviously, at first it is necessary to help collective farm and shots of machine operators (on 1 — 2 - Utah). For thorough permission of a question of shots in general it is necessary to provide assignment for improvement of the settlement in the master plan of development of collective farm. In the good settlement there will be a fluidity of workers less.

4. CONCLUSION

It is necessary to concentrate the population in one well-planned center. It will also promote increase in site class of soils as fertile homestead lands will fill up the area, arable lands. It is possible to establish by more exact economic calculations also the amount of financing of collective farm for carrying out the reforms following from site class of soils. If the offered recommendations not to carry out in the next years, then the efficiency of economy at best remains on

reached low level or will raise very little. And modern economic indicators of economic activity are extremely modest.

Favorable on weather conditions for field husbandry.

The average yield of grain was 8,1 c/hectare, sena of artificial long-term herbs — 13,0 c/hectare, hay of natural haymaking's — 9,2 c/hectare. The efficiency of livestock production was expressed on 100 hectares of agricultural grounds: milk of 51 c, beef meat in lethal weight — 5,4 c/hectare.

Profound quality standard of a soil cover of all grounds of land use plays very important role in permission of many organizational and economic, agro- and zoo technical questions. It on justice will be a basis of the inventory of lands and creation of the correct economy. The card of site classes of a soil cover just is also the document, reflecting quality and production properties of each site of land use with the greatest completeness and therefore has to find recognition as the irreplaceable and obligatory document at soil researches for agriculture.

5. REFERENCES

1. Gopikrishnan.T. et al. /BCG - Boletim de Ciências Geodésicas - On-Line version, ISSN p.1982-2170
2. Yusuf Yigini et al. /Procedia Earth and Planetary sciences,2014, v.10, p. 330-338
3. G.B.Heuveilink et al. /Geoderma , 1992, v.55, v.1-2, p.1-15.
4. P.Lagacherie et al. /Geoderma, 1995,v.65, 3-4, p. 283-301.
5. William R. Effland et al. / Urban Ecosystems, 1997, v.. 1, 4, p.217-228.
6. Feng Chen et al. / Precision Agriculture, 2004, v.5, 1, p. 7-26.

IMPROVING THE PHOTOCATALYTIC ACTIVITY OF DIFFERENT MODIFICATION OF TiO₂

S.A.HASANOVA

^{*}Faculty of Ecology, Azerbaijan University of Architecture and Construction, Az1073, 5 Ayna Sultanova St., Baku, Azerbaijan,

In this study, TiO₂ and glass balls coated by N-doped TiO₂ nanoparticles were used for photocatalytic degradation of organic compounds. Laboratory experiments were carried out with industrial wastewater consisting of different contents of organic pollutants. TiO₂ having a size near to nanoparticles and the nanostructured 20 nm sized, located at the bottom. A visible lamp was used for the light irradiation. Then, the catalytic effectiveness of the coated glass balls was checked on a system of industrial interest: the reduction of the organic compounds in an industrial wastewater stream. In this case a more performing configuration of the reactor was adopted by positioning the glass balls over a wire and feeding an air stream under the wire itself, moreover a visible light. This latter result demonstrated the possibility of a strong purification of organic compounds by using the developed N-doped immobilized TiO₂ catalyst under visible light.

PACS numbers:

Keywords: Photocatalysis, Wastewater, Sol-gel, Titanium-Dioxide, NPs -TiO₂

E-mail: seynure.ibrahimova@gmail.com

1. INTRODUCTION

Environmental pollution, such as contaminated water or polluted air, has become a global issue threatening the health of mankind. Typical polluting sources are toxic organic molecules or exhausted gas compounds which are released from household waste, livestock waste and local industries. Science is thus involved in searching for new alternatives and ecologically sustainable methods for cleaning up environmental contamination. Different solutions for depollution have already been proposed: air scrubbing, adsorption, and activated carbon, etc., but some of them only remove the pollutant from one phase to another one and then require additional processes to eliminate toxic compounds. Heterogeneous photocatalysis is a potential solution that has been the object of intense research efforts since the early 1970s, when Fujishima and Honda discovered the photocatalytic splitting of water on TiO₂ electrodes. This technique can be envisaged as one of the most promising Advanced Oxidation Process (AOPs) because of its specific advantages, such as bland reaction conditions, the possibility of using molecular oxygen as oxidant species, the total mineralization of

pollutants into substances innocuous to the environment. Heterogeneous photocatalysis is based on the interaction between semiconductor materials and light. By considering that we can get 'free' light from the sun, the idea of using solar light energy as resource to clean up the environment is an ideal and extremely promising approach. Sun light, with wavelengths ranging from 10-5 to 10⁵ nm, is a clean and renewable energy source that is readily available. Before reaching the Earth's surface, a part of the solar energy is absorbed by the stratosphere, ozonosphere and other atmospheric layers. Of the solar radiation reaching the Earth, 5% is UV light, 50% is visible light and the remaining part is composed of infrared and longer wavelengths radiation (Fig. 1.1).

Approximately a 40% of the total amount of radiation arriving to Earth, mainly composed of visible, infrared, and radio energies, is constantly arriving to its surface. In particular, Ultraviolet light (UV-light), generally divided into three regions, A (315 –400 nm), B (280 – 315 nm) and C (100 – 280 nm), is responsible for most of the photochemical processes occurring in the atmosphere. While the UV-C region is mostly filtered by Earth's ozone layer, UV-A and UV-B radiations still pass and have the potential to generate photochemical processes such as the synthesis of

vitamin D in our body or the tanned skin color we get after having been exposed to sunlight.

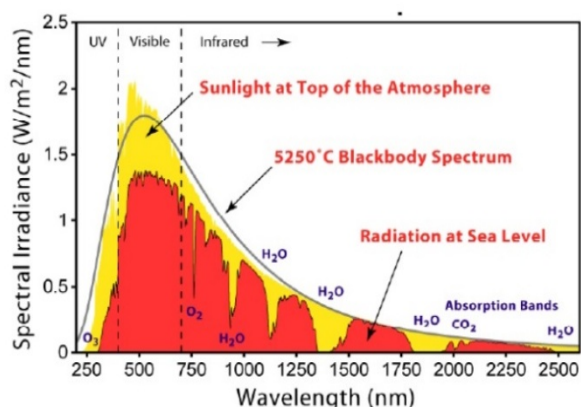


Figure 1.1 Earth's light environment (solar spectrum).

In the field of energy and environmental application of heterogeneous photocatalysis TiO₂ appears as the most active and most suitable semiconductor. In fact, TiO₂ has a high oxidation ability, its photogenerated holes being at $E_0 = 2.9 \text{ V vs. NHE at pH 0}$; moreover, it is biologically and chemically inert, photostable and cheap. In nature, TiO₂ can crystallize in the three polymorphs anatase, rutile and brookite. Anatase is thermodynamically less stable than rutile. It exhibits a shorter wavelength absorption edge and is largely recognized to be more active than rutile in oxidative detoxification reactions. Mixtures of these two polymorphs may produce intriguing effects on charge carrier transfer processes in photocatalytic applications.^{3,4} However, the following major factors limit both photocatalytic efficiency and activity of TiO₂:

- The band gap of anatase TiO₂ is 3.2 eV, *i.e.* it absorbs light in the UV region, so that only a small portion (5%) of sunlight can be used for photocatalytic processes.
- As in all semiconductors, photogenerated electron-hole couples undergo fast recombination in competition with charge transfer to adsorbed species.
- The use of slurries could limit the industrial applications of photocatalysis, theseparation of semiconductor powders after liquid phase reactions being troublesome and expensive.

2. EXPERIMENTAL

Two types of catalysts were produced: titanium oxide nanoparticles and nitrogen doped sol-gel material

to be used for the coating of glass spheres 4 mm in size. Also use magnetic titanium oxide nanoparticles and simple titanium oxide.

2.1 Materials

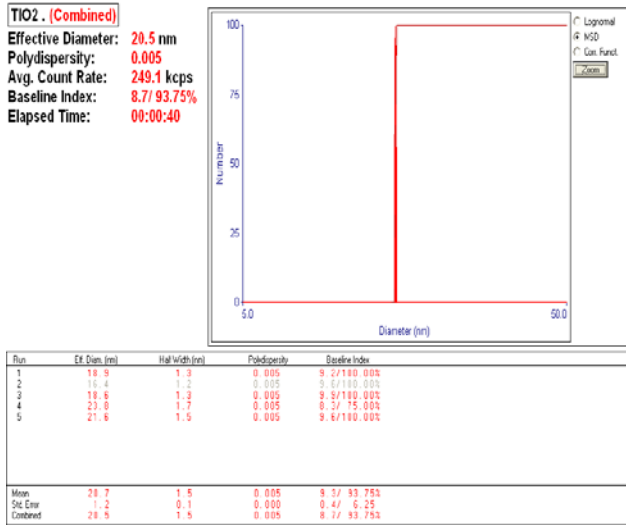
- Chemicals used in the experimental procedure in TTIP (titaniumtetraisopropoxide(Sigma-Aldrich))⁵
- Then To produce the sol-gel material, a suspension of TiO₂ NPs, produced by the above mentioned procedure, was added drop-wise by a fixed amount of hydrogen peroxide 30% b.w. . The precipitate dissolved completely by reaction with hydrogen peroxide and formed a transparent orange sol of titanium-hydrogen peroxide complex. The produced sol was added drop by drop in a cold water bath by a N-ethyl methylamine solution, previously prepared by using 97% N-ethyl methylamine solution. The color of the solution changed from orange to the yellowish. The solution was kept under stirring for 2 hours before its use for coating.
- TiO₂(Vecton)

2.2 Characterization

The size distribution of the TiO₂ NPs was determined by means of a Brookhaven Plus 90 nanosizer. A very narrow NPs distribution with an average value of 20 nm was observed, as shown in Fig.2.1.

The nature of obtained layer coating was characterized by X-ray diffraction. The X-rays diffraction of TiO₂ nanostructured layer was performed and it was ascertained that anatase was the dominant crystalline phase.

TiO₂ having a size near to nanoparticles, *i.e.* about 3 - 4 microns in size purchased from Russian CJSC "Vekton". The size distribution of the TiO₂ was determined by means of JEOL LSM 6610-LV- optical microscope and brand of MINIFLEX 600 by X-Ray Diffraction Fig.2.2 and Fig.2.3.



Measurement Parameters
 Temperature = 25.0
 Suspension = Water
 Viscosity = 0.890 cp
 Ref.Index Fluid = 1.330
 Angle = 90.00
 Wavelength = 660.0 nm
 Dust Cutoff = 30.00
 Runs Completed = 5
 Run Duration = 00:00:10
 Total Elapsed Time = 00:00:40
 Average Count Rate = 249.1 kcps
 Ref.Index Real = 2.920
 Ref.Index Imag = 2.920

Measurement Results
 TiO₂ (Combined)
 Effective Diameter: 20.5 nm
 Polydispersity: 0.005
 Baseline Index: 8.7/93.75%

Figure 2.1. Size distribution of the produced TiO₂ nanoparticles

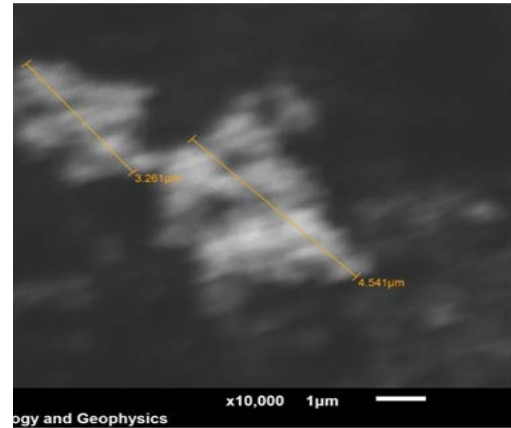


Figure 2.2. Size distribution of the produced TiO₂

Measurement Parameters

The band gap – Anatase
 Formula – TiO₂
 Weight% - 59.95% Ti,
 40.05% O
 Atomic% - 33.33% Ti,
 66.67% O
 Comp.% - 100% TiO₂

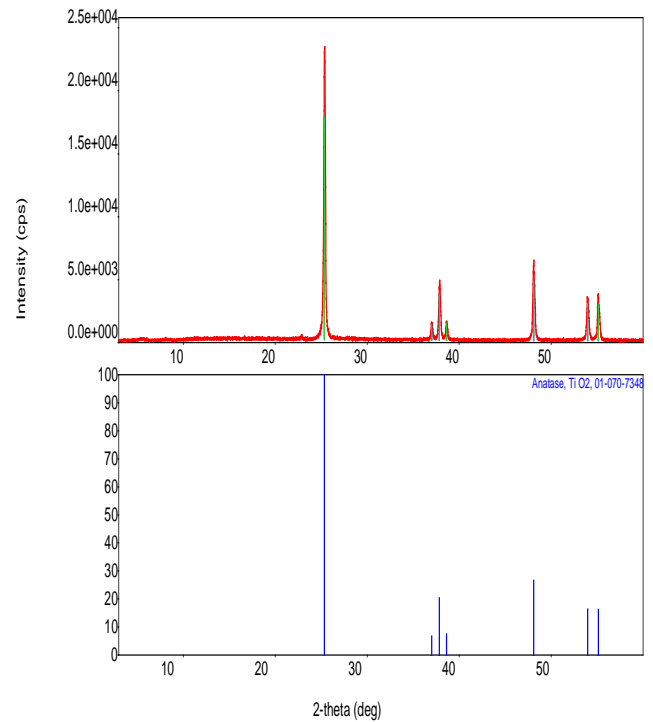


Figure 2.3. Qualitative analysis result of TiO₂

2.3 The experimental set-up

First set-up: The images of setup were prepared by using 3DMax that were shown in Figure 2.4. The image does not include a vessel, 500 ml in capacity, positioned in a cooled bath along the recycling circuit. This arrangement is required to stabilize at 30-35 °C the temperature of the solution submitted to the treatment, in order to remove the heat released by the lamp to the liquid in the reaction vessel. An UV lamp of 150 W visible lamps, alternatively, was used.

After the preparation of coated glass spheres, 20 g of coated glass spheres was put into the reaction vessel, and then around 150 ml of the waste water to be examined was used to fill the reaction vessel. During the treatment process pH must be 3.

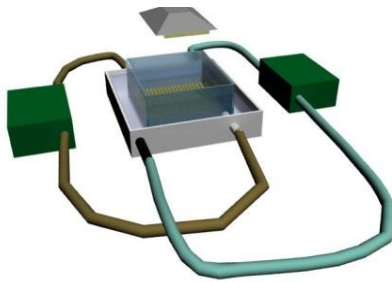


Figure 2.4. The images of the setup

Second set-up: All the process like first set-up. But we use cylindrical baker instead reactor.

3. RESULTS AND DISCUSSION

3.1 Degradation of organic compounds

The experimental data obtained by using the NPs and the coated glass spheres are reported in table 1 and 2, respectively. In fig. 3.1 the obtained results with the two kind of catalyst are compared.

Table 1. Experimental data on the organic compounds degradation by using coated glass sphere catalyst

Time [min]	0	30	60	90	120	150	180	210
Ppm	7,0	6,5	5,3	4,8	3,8	3,0	2,3	1,0

Table 2: Experimental data on the organic compounds by using 3-4 microns TiO₂

Time [min]	0	30	60	90	120	150	180	240
Ppm	8,0	7,5	6,9	6,4	5,8	5,2	4,9	4,1

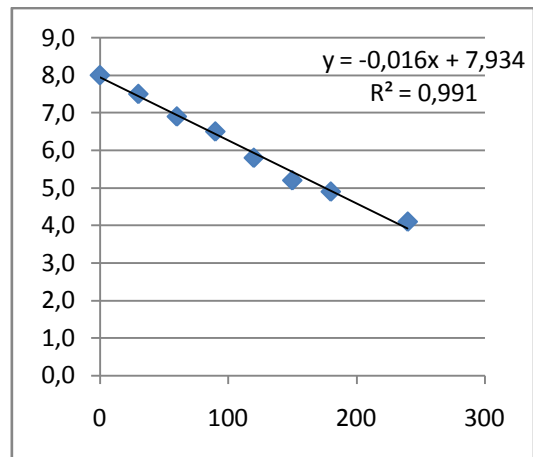
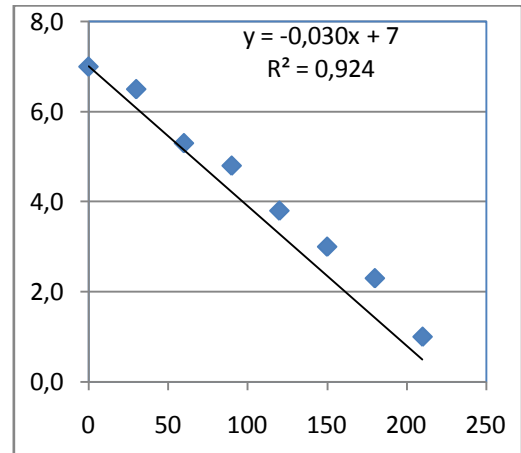


Figure 3.1. Concentration vs time curve of Table 1. and Table 2.

4. CONCLUSION

This study deals with the degradation of organic compounds by TiO₂ assisted photocatalysis. The experimental work was addressed to two objectives. The first one was to compare the effectiveness of the photocatalysis performances when titanium dioxide or a nanostructured coating layer was used. Undoped TiO₂ was used under visible light. The experiments carried out on the degradation of 8 ppm organic compounds exhibited an almost equal conversion,

around 50 %, in both the cases. Second experiments which of doped TiO_2 carried out on the degradation of 7 ppm organic compounds until 1 ppm, around 90%. This experiments also carried under visible light. The examined solution was the wastewater with a first experiments of COD value equal to 1112 mg/l and second experiments of COD value equal to 8000 mg/l. The run performed under nanoparticles titanium dioxide was very successful allowing an almost quantitative degradation of the organic compounds. This result was due to the following factors: a good N-doping of TiO_2 and a very good contact air-immobilized catalyst.

5. REFERENCES

1. Ibrahimova S., Aliyev F.G. et al. / Chemical Engineering Transactions, 200, v.47, p.199-204
2. Khalilova H.K., Hasanova S.A., Aliyev F.G. / Journal of Environmental Protection, 2018, v.9, p.691-698.
3. Marco Altomare, Gian Luca Chiarello et al / XXIV Congresso Nazionale della Società Chimica Italiana. Lecce, p.11–16 September 2011. eISBN: 978-88-8305-085-5.
4. Ruzmanova Y., Stoller M., Chianese A. / Chemical Engineering Transactions, 2013, v.32, p.2269-2274.
5. Ruzmanova Y., Ustundas M., Stoller M., Chianese A. / Chemical Engineering Transactions, 2013, v.32, p.2233-2238.
6. Stoller M., Ochando-Pulido J.M., Chianese, A., / Chemical Engineering Transactions, 2013, v.32, p.397-402.
7. Tu W., Lin Y-P, Bai R. / Sep Purif. Technol, 2013, v.115, p.180–189
8. Dozzi M. V., Chiarello G. L. and Selli E. / J. Adv. Oxid. Technol., 2010, v.13, p.305–312.



Journal of LDS

Address:

Az1148, Z.Khalilov str. 23,
Baku State University, BSU publication, Baku, Azerbaijan

E-mail: mhhuseyng@bsu.edu.az



**Published by the Baku State University and devoted to original papers
in experimental and theoretical physics, chemistry and biology**

ISSN 2308-068X